

Lawrence Berkeley National Laboratory

Recent Work

Title

THE USE OF ANTICOMMUTING INTEGRALS IN STATISTICAL MECHANICS III

Permalink

<https://escholarship.org/uc/item/04j2922x>

Author

Samuel, S.

Publication Date

1979-06-01



Lawrence Berkeley Laboratory

UNIVERSITY OF CALIFORNIA, BERKELEY, CA

Physics, Computer Science & Mathematics Division

Submitted to Annals of Physics

THE USE OF ANTICOMMUTING INTEGRALS IN
STATISTICAL MECHANICS III

Stuart Samuel

June 1979

RECEIVED
LAWRENCE
BERKELEY LABORATORY

AUG 28 1979

RECEIVED
LAWRENCE
BERKELEY LABORATORY

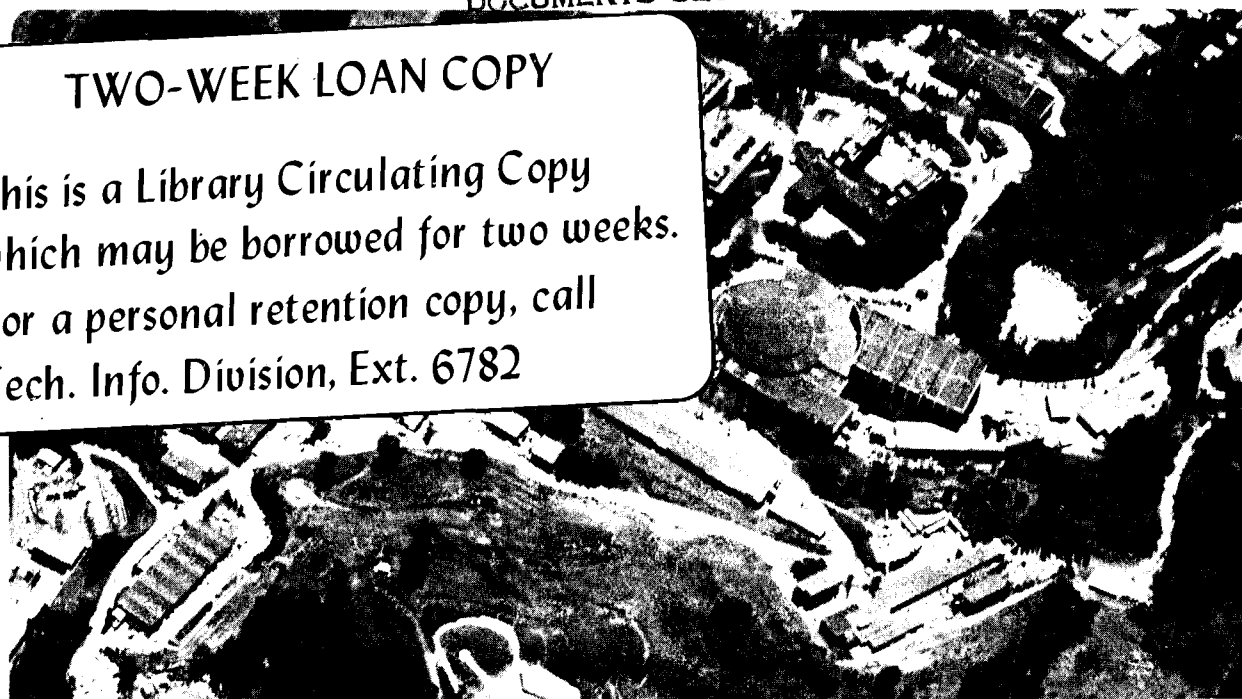
LIBRARY AND
DOCUMENTS SECTION

SEP 14 1979

LIBRARY AND
DOCUMENTS SECTION

TWO-WEEK LOAN COPY

This is a Library Circulating Copy
which may be borrowed for two weeks.
For a personal retention copy, call
Tech. Info. Division, Ext. 6782



LBL-9347-103

DISCLAIMER

This document was prepared as an account of work sponsored by the United States Government. While this document is believed to contain correct information, neither the United States Government nor any agency thereof, nor the Regents of the University of California, nor any of their employees, makes any warranty, express or implied, or assumes any legal responsibility for the accuracy, completeness, or usefulness of any information, apparatus, product, or process disclosed, or represents that its use would not infringe privately owned rights. Reference herein to any specific commercial product, process, or service by its trade name, trademark, manufacturer, or otherwise, does not necessarily constitute or imply its endorsement, recommendation, or favoring by the United States Government or any agency thereof, or the Regents of the University of California. The views and opinions of authors expressed herein do not necessarily state or reflect those of the United States Government or any agency thereof or the Regents of the University of California.

THE USE OF ANTICOMMUTING INTEGRALS IN
STATISTICAL MECHANICS III

By

Stuart Samuel*

Lawrence Berkeley Laboratory
University of California
Berkeley, California 94720

June 22, 1979

ABSTRACT

Using anticommuting variables, approximation methods are developed to attack unsolved statistical mechanics models. These include Ising models, general dimer models, polymer systems, and the general eight-vertex model. A large number of new calculational methods and results are obtained. A list of these can be found in the Introduction to which the reader is referred. Anticommuting variables appear to be a powerful approach to unsolved problems.

*"This work was supported by the High Energy Physics Division of the U.S. Department of Energy under contract No. W-7405-ENG-48. Address after September 15, 1979 is the Institute for Advanced Study, Princeton, New Jersey 08540

I. INTRODUCTION

Two previous papers^{1,2} have developed the use of anticommuting variable integrals in statistical mechanics. They showed how many models can be expressed as "fermionic" field theories. Some models, such as the two-dimensional Ising model, free-fermion ferroelectric vertex models, and planar close-packed dimer models, had quadratic actions. In this case the anticommuting variables solved the model in a page of algebra. It was trivial to extend the techniques to correlation functions. Using the methods and results in Secs. V and VI of paper II any Ising spin correlation function could be calculated. This included, for example, the product of ten spins. The anticommuting variables are powerful techniques. They will form the foundation of a large body of a large body of future work.

This paper uses the formalism in the first two. It follows their notation, conventions, techniques, and graphical transcriptions.

Most physical systems are not exactly solvable. Therefore, methods which exactly solve models but which cannot be adapted to unsolved models are not nearly as useful as those which can handle both. The anticommuting variables are in the latter class. Papers I and II showed that they can solve the solvable models with ease. This paper will show how they can generate viable approximation schemes. Where numbers are calculated, excellent accuracy is achieved. These are not crude approximation methods; they are good approximation methods.

This is just the beginning. This paper uncovers only a subset of the many possible approximation techniques available. This will certainly be an active area of future research: to establish new

techniques as well as adapting old many-body theory techniques. The numbers of models to which anticommuting variables can be applied seems limitless. This paper considers dimer and polymer systems, Ising models, and ferroelectric models in one, two, three, and more dimensions. Another area of future work will be the application to other physical systems. In short, this is just the beginning.

The method is completely new. There are other techniques in the literature with which anticommuting variables might be confused. These other techniques are different. For example, there is the operator formalism^{3,4,5} of Lieb, Schultz, and Mattis which solves the Ising model. Their basic objects are fermionic creation and destruction operators, b_i, b_i^\dagger , which satisfy canonical commutation relations, $b_i b_j^\dagger + b_j^\dagger b_i = \delta_{ij}$. The anticommuting variables η_i, η_i^\dagger , completely commute: $\eta_i \eta_j^\dagger + \eta_j^\dagger \eta_i = 0$. Unlike this paper, reference three used a transfer matrix method. The two methods are different and anticommuting variables are much more powerful. Pfaffian methods^{4,6} have also been used to solve various two dimensional models. Whenever the anticommuting variable action is quadratic, it is a Pfaffian according to Eq.(I. 2.7) and, in principle, can be solved using Pfaffian methods. The anticommuting variables are much more elegant. It is easier to handle technical problems such as minus signs, it is easier to express models in integral form, and it is easier to calculate correlation functions. The big disadvantage of Pfaffian methods, however, is their inability to handle "interacting fermionic" theories. There are few examples where Pfaffians can be used to obtain approximations to unsolved models.

This paper contains many new results. The following list of results, which might be part of the conclusion, serves to indicate the contents of this paper.

Section II. The three dimensional Ising model is expressed as an integral over anticommuting variables. In this form it is equivalent to an interacting "fermionic" field theory. This is an important result because this paper's approximation schemes become applicable to the Ising model. This section will form the foundation of future work. The higher dimensional Ising models are also written as anticommuting variable integrals.

Section III. The integral representation in Section II is adapted to the two-dimensional Ising model in magnetic field. This is also an interacting "fermionic" field theory. Presented next is a representation as a Z_2 lattice gauge theory coupled to a "fermion". The representations are again extended to higher dimensions.

Section IV. This section deals with dimer models in the abstract, that is, the most general dimer model is considered. They are expressed in anticommuting variable form and many-body field theory methods are applied. Feynman graph rules are presented. Perturbation theory turns out to be equivalent to the low temperature expansion. The self-consistent Hartree approximation is calculated. The Feynman rules are adapted so that corrections to the Hartree approximation can be calculated. These are computed to sixth order. No specific model is considered. The results of Sec. IV are valid for the most general dimer model. This is a new expansion.

Section V. The methods of Sec. IV are applied to specific dimer models. The lattices include the d-dimensional hypercubic

lattices (such as the simple quadratic and simple cubic lattices), the planar triangular, the tetrahedral, the body-centered cubic, and the face-centered cubic lattices. A special set of Feynman rules are derived for translationally invariant lattices. Embedding graphs (and their weights) are found to 5th order for close-packed lattices and to 6th order for loose-packed lattices. This allows a rapid computation of the Hartree-improved expansion to 5 or 6 orders. The method is applied to sixth order first for the two-dimensional dimer problem and then for the d -dimensional hypercubic lattices. This is for the non-isotropic case in which Boltzmann factors in different directions need not be equal. In the isotropic case, it is found that the d -dimensional hypercubic dimer problem is exactly solvable as d becomes large as long as the temperature is high enough. A $\frac{1}{d}$ expansion is presented. A similar analysis is applied to lattices with a large coordination number, q . All dimer models become exactly solvable as $q \rightarrow \infty$ and a $\frac{1}{q}$ expansion is presented. For lattices with q varying from 4 to 12, molecular freedoms are computed in the pure dimer limit. Even at such small q values results are good to several per cent. For the isotropic case, previously established low temperature expansions are combined with Hartree methods to obtain the Hartree expansion from 8 to 16 orders on six lattices. These new series expansions accurately represent the six models in the entire physical region. In the region where the approximation method is expected to be the worst, that is, at close-packing, molecular freedoms are computed to an accuracy of a fraction of a percent. Next the density and entropy are calculated. At a

density of about 90% maximum density the density and entropy are calculated to an accuracy of from 4 to 7 decimal places. At 50% density the accuracy is from 6 to 9 decimal places and at 10% density the accuracy ranges from 11 to 19 decimal places. These new series expansions are as good as any in the literature.

Section VI. This section discusses the $1/N$ expansion. This is closely related to the random phase approximation. Another new dimer expansion series is obtained. Feynman rules are developed which allows one to easily calculate the $1/N$ expansion. The expansion is computed to two loops (order $1/N$) for the d -dimensional hypercubic lattices. Next a discussion of the meaning of the $1/N$ expansion is presented. Given a dimer model, a new dimer model can be constructed called its chromodimer counterpart. They have a local $U(N)$ symmetry and are exactly solvable as $N \rightarrow \infty$. An infinite class of limiting dimer models is solved.

Section VII. For future use all the anticommuting variable correlation functions are calculated in the one-dimensional dimer model. Next, the general one-dimensional polymer system is solved. This statistical ensemble consists of dimers, trimers, quadrimers, ..., which occupy two, three, four, ... successive sites. Each species has a different Boltzmann factor so that there are an infinite number of free parameters. Grassmann integrals solve this system in three lines of algebra. The anticommuting variable correlation functions are calculated for this general system.

Section VIII. The transfer matrix elements for the two-dimensional dimer model are calculated in closed form using the results in Sec. VII. These formulas are remarkably simply.

Next, the transfer matrix elements are calculated for the two-dimensional system consisting of vertical dimers and horizontal dimers, trimers, quadrimers, etc.

Section IX. The one-dimensional dimer model is used to approach the two-dimensional dimer model. Feynman rules are developed to calculate three new expansion series to two orders, three orders, and one loop. The first of these is a power series in z_v , the Boltzmann factor for vertical dimers, whose coefficients are functions of z_h correct to all orders in z_h . The other two dimer series are of a similar structure but have a range of validity not just restricted to small z_v . Likewise, three new series expansions are obtained for the two-dimensional polymer system of Sec. VIII. Next, the two dimensional dimer model is written as an anticommuting variable integral in two additional ways. Many more (at least six) new expansions can be obtained from these but, for reasons of space, are omitted.

Section X. This formal section discusses ways of bosonizing the field theories. A simple technique using auxiliary fields is applicable to any "four-fermion" interaction. The abstract dimer model is treated as an example. A second bosonization scheme is discussed by using Feynman graph rules. Contact is made with previous approximation methods. The importance of bosonization is that it allows the use of DHN semiclassical methods^{7,8}.

Section XI. Simple rules are presented which calculate all vertex correlation functions in the free-fermion model. Several sample computations are presented.

Section XIII. Feynman graph rules are presented to do perturbation theory for the general eight vertex model. The partition function is computed to second order in a free-fermion breaking parameter. Because the free-fermion constraint can be broken in many ways it is possible to obtain many different approximation schemes each of which is different and new.

Section XIII. The Hartree-Fock equations for the general eight-vertex model are presented. They are the starting point for Hartree-Fock improved and $1/N$ expansions.

Sections XIV. This section discusses miscellaneous techniques. Among these is how explicitly doing some of the anticommuting integrals leads to interesting transformations and new approximation methods. The two-dimensional dimer model is used to illustrate this. Another result is an upper bound to the free energy of the three-dimensional close-packed dimer model.

II. THE THREE-DIMENSIONAL ISING MODEL AS AN INTERACTING FERMIONIC FIELD THEORY

This section expresses the partition function for the three-dimensional Ising model as an anticommuting variable integral over an action, that is, a lattice fermionic field theory. Unlike the two dimensional Ising model where the action was quadratic¹, the action of the three dimensional model involves quartic as well as bilinear terms. Therefore, the three dimensional model is not of the solvable free-fermion form but represents an interacting field theory.

Section III of paper I showed how any Ising model could be represented in terms of anticommuting variables using the "section rule" method. This was a brute force method that lead to awkward

unphysical actions involving products of anticommuting variables of high order. The importance of the representation of Equations (2.4)-(2.10) is that it uses at most quartic forms and is of geometrical significance. This makes it more physical than the brute force method and yields a better starting point for approximation techniques.

The partition function for the three dimensional Ising model is

$$Z = \left(\prod_{\alpha\beta\gamma} \sum_{\sigma_{\alpha\beta\gamma} = \pm 1} \right) \left[\exp \beta \sum_{\alpha\beta\gamma} \left(J_1 \sigma_{\alpha\beta\gamma} \sigma_{\alpha+1\beta\gamma} + J_2 \sigma_{\alpha\beta\gamma} \sigma_{\alpha\beta+1\gamma} + J_3 \sigma_{\alpha\beta\gamma} \sigma_{\alpha\beta\gamma+1} \right) \right] \quad (2.1)$$

The $\sigma_{\alpha\beta\gamma}$ are the spins which sit at integer-valued coordinates, α, β, γ , of a three dimensional lattice array. The J_1, J_2 , and J_3 are the nearest neighbor couplings in the x, y , and z directions. Throughout this section the numbers 1, 2, and 3 will refer to x, y , and z .

The partition function has a well-known geometrical low temperature expansion similar to the two-dimensional model except that one must sum over closed polyhedrons instead of closed polygons. Take the configuration with all spins up (that is, $\sigma_{\alpha\beta\gamma} = +1$ for all α, β, γ) whose contribution to Z is

$$f = \exp [N\beta(J_1 + J_2 + J_3)], \quad (2.2)$$

N being the total number of sites. An arbitrary configuration is obtainable from the "all spins up" minimum energy configuration by flipping spins. Draw closed polyhedrons around regions of down spin. If regions of up spin occur within regions of down spin draw polyhedrons within polyhedrons, etc. What kinds of configurations are

allowed? First, any number of non-overlapping polyhedrons can occur. They may intersect in the manner of Fig. 1a but they may not overlap as in Fig. 1b. The configuration of Fig. 1b would be drawn as in Fig. 1c. The fact that overlap is not permitted makes the use of anticommuting variables ideal. Polygons, constructed out of anticommuting variables, cannot overlap because the square of a variable is zero.

Compared to the minimum energy configuration whose Boltzmann factor is f [Eq.(2.2)], an arbitrary configuration will have a Boltzmann factor per unit face of polyhedron, representing the fact that spin flip occurs across the face. If l_1, l_2 , and l_3 , are the total number of faces pointing in the x, y , and z directions (see Fig. 2), then the Boltzmann factor is

$$f \exp [-2\beta(l_1 J_1 + l_2 J_2 + l_3 J_3)] \quad (2.3)$$

The conclusion is

$$Z_{3-d \text{ Ising}}(J_1, J_2, J_3) = f Z_{\text{closed polyhedrons}}(z_1, z_2, z_3), \quad (2.4)$$

where $Z_{\text{closed polyhedrons}}(z_1, z_2, z_3)$ is the partition function for non-overlapping but possibly intersecting polyhedrons in which the three types of faces of Fig. 2 are weighted by z_1, z_2 , and z_3 and

$$z_i \equiv \exp(-2\beta J_i) \quad (2.5)$$

In the two dimensional model, the anticommuting variable action, that generated $Z_{\text{closed polygons}}$, consisted of three pieces: A_{wall} , A_{corner} , and A_{monomer} . A_{wall} drew the sides of polygons, A_{corner} formed corners, and A_{monomer} filled unfilled sites. Similarly, in three dimensions the action consists of three pieces, A_{face} , A_{corner} , and A_{monomer} . A_{face} draws the faces of the polyhedrons and A_{corner} joins the faces together.

The expression for $Z_{\text{closed polyhedron}}$ in terms of anticommuting variables is first presented and subsequently explained.

$$Z_{\text{closed polyhedrons}}(z_1, z_2, z_3) = \int d\eta d\eta^\dagger \exp A, \quad (2.6)$$

where

$$A = A_{\text{face}} + A_{\text{corner}} + A_{\text{monomer}}, \quad (2.7)$$

$$A_{\text{face}} = \sum_{\alpha\beta\gamma} \left(z_1 n_{\alpha+\frac{1}{2}, \beta-\frac{1}{2}, \gamma-\frac{1}{2}}^{2\dagger} n_{\alpha+\frac{1}{2}, \beta+\frac{1}{2}, \gamma-\frac{1}{2}}^2 n_{\alpha+\frac{1}{2}, \beta, \gamma-\frac{1}{2}}^{3\dagger} n_{\alpha+\frac{1}{2}, \beta, \gamma+\frac{1}{2}}^3 \right. \\ \left. + z_2 n_{\alpha, \beta+\frac{1}{2}, \gamma-\frac{1}{2}}^{3\dagger} n_{\alpha, \beta+\frac{1}{2}, \gamma+\frac{1}{2}}^3 n_{\alpha-\frac{1}{2}, \beta+\frac{1}{2}, \gamma}^{1\dagger} n_{\alpha+\frac{1}{2}, \beta+\frac{1}{2}, \gamma}^1 \right. \\ \left. + z_3 n_{\alpha-\frac{1}{2}, \beta, \gamma+\frac{1}{2}}^{1\dagger} n_{\alpha+\frac{1}{2}, \beta, \gamma+\frac{1}{2}}^1 n_{\alpha-\frac{1}{2}, \beta-\frac{1}{2}, \gamma+\frac{1}{2}}^{2\dagger} n_{\alpha+\frac{1}{2}, \beta+\frac{1}{2}, \gamma+\frac{1}{2}}^2 \right), \quad (2.8)$$

$$A_{\text{corner}} = \sum_{\alpha\beta\gamma} \left[\left(n_{\alpha, \beta+\frac{1}{2}, \gamma+\frac{1}{2}}^{2\dagger} n_{\alpha, \beta+\frac{1}{2}, \gamma+\frac{1}{2}}^3 + n_{\alpha, \beta+\frac{1}{2}, \gamma+\frac{1}{2}}^{3\dagger} n_{\alpha, \beta+\frac{1}{2}, \gamma+\frac{1}{2}}^{2\dagger} \right) \right. \\ \left. + n_{\alpha, \beta+\frac{1}{2}, \gamma+\frac{1}{2}}^{3\dagger} n_{\alpha, \beta+\frac{1}{2}, \gamma+\frac{1}{2}}^2 + n_{\alpha, \beta+\frac{1}{2}, \gamma+\frac{1}{2}}^3 n_{\alpha, \beta+\frac{1}{2}, \gamma+\frac{1}{2}}^{2\dagger} \right) \\ \left. + \left(n_{\alpha+\frac{1}{2}, \beta, \gamma+\frac{1}{2}}^{1\dagger} n_{\alpha+\frac{1}{2}, \beta, \gamma+\frac{1}{2}}^3 + n_{\alpha+\frac{1}{2}, \beta, \gamma+\frac{1}{2}}^{3\dagger} n_{\alpha+\frac{1}{2}, \beta, \gamma+\frac{1}{2}}^{1\dagger} \right) \right. \\ \left. + n_{\alpha+\frac{1}{2}, \beta, \gamma+\frac{1}{2}}^{3\dagger} n_{\alpha+\frac{1}{2}, \beta, \gamma+\frac{1}{2}}^1 + n_{\alpha+\frac{1}{2}, \beta, \gamma+\frac{1}{2}}^3 n_{\alpha+\frac{1}{2}, \beta, \gamma+\frac{1}{2}}^{1\dagger} \right) \\ \left. + \left(n_{\alpha+\frac{1}{2}, \beta+\frac{1}{2}, \gamma}^{1\dagger} n_{\alpha+\frac{1}{2}, \beta+\frac{1}{2}, \gamma}^2 + n_{\alpha+\frac{1}{2}, \beta+\frac{1}{2}, \gamma}^{2\dagger} n_{\alpha+\frac{1}{2}, \beta+\frac{1}{2}, \gamma}^{1\dagger} \right) \right. \\ \left. + n_{\alpha+\frac{1}{2}, \beta+\frac{1}{2}, \gamma}^{2\dagger} n_{\alpha+\frac{1}{2}, \beta+\frac{1}{2}, \gamma}^1 + n_{\alpha+\frac{1}{2}, \beta+\frac{1}{2}, \gamma}^2 n_{\alpha+\frac{1}{2}, \beta+\frac{1}{2}, \gamma}^{1\dagger} \right) \right], \quad (2.9)$$

$$A_{\text{monomer}} = \sum_{\alpha\beta\gamma} \left[\left(n_{\alpha, \beta+\frac{1}{2}, \gamma+\frac{1}{2}}^{2\dagger} n_{\alpha, \beta+\frac{1}{2}, \gamma+\frac{1}{2}}^{2\dagger} + n_{\alpha, \beta+\frac{1}{2}, \gamma+\frac{1}{2}}^3 n_{\alpha, \beta+\frac{1}{2}, \gamma+\frac{1}{2}}^{3\dagger} \right) \right. \\ \left. + \left(n_{\alpha+\frac{1}{2}, \beta, \gamma+\frac{1}{2}}^{1\dagger} n_{\alpha+\frac{1}{2}, \beta, \gamma+\frac{1}{2}}^{1\dagger} + n_{\alpha+\frac{1}{2}, \beta, \gamma+\frac{1}{2}}^3 n_{\alpha+\frac{1}{2}, \beta, \gamma+\frac{1}{2}}^{3\dagger} \right) \right. \\ \left. + \left(n_{\alpha+\frac{1}{2}, \beta+\frac{1}{2}, \gamma}^{1\dagger} n_{\alpha+\frac{1}{2}, \beta+\frac{1}{2}, \gamma}^{1\dagger} + n_{\alpha+\frac{1}{2}, \beta+\frac{1}{2}, \gamma}^2 n_{\alpha+\frac{1}{2}, \beta+\frac{1}{2}, \gamma}^{2\dagger} \right) \right] \quad (2.10)$$

The notation needs explaining. Begin with the spatial lables. When spins, $\sigma_{\alpha\beta\gamma}$, have integer cartesian coordinates, the polyhedrons, being drawn on the dual lattice, involve half-integer coordinates. This is because faces occur between spins. Figure 3 shows a spin, σ , at (α, β, γ) and a cube of the dual lattice enclosing σ . The cube has six faces and twelve edges. The location of an edge is specified by its midpoint (as Fig. 3 illustrates). It always has two half integer coordinates and one integer coordinate. Edges can point in three directions, as shown by the three bolder lines in Fig. 3. An edge pointing in the x, y, or z direction will be called an x, y, or z edge. The anticommuting variables sit at edge midpoints. There are three types: n^1, n^2, n^3 (along with their daggered partners), which refer to anticommuting variables associated with x, y, and z directions. Coventions used in I and II are extended here: "o" and "x" indicate undaggered and daggered variables; a line in the x, y, or z direction attached to an anticommuting variable indicates whether it is of 1, 2, or 3 type; the subscripts, α, β, γ , indicate an anticommuting variable's cartesian coordinates; and arrows denote the ordering of bilinears.

Only two out of the three types of anticommuting variables occur at a particular edge midpoint. If it is an x edge, they are the other two types, namely, $\eta^2, \eta^{2\dagger}, \eta^3, \eta^{3\dagger}$. Likewise for y and z edges.

A_{face} has three terms. Each draws one of the faces of fig. 2. A_{face} involves a product of four anticommuting variables. Together they span a square unit of surface area as Fig. 4 illustrates. Figures 4(a), 4(b), and 4(c) produce the faces of Figures 2(a), 2(b), and 2(c) and correspond to the three terms (in that order) of Eq. (2.8). The anticommuting variable cartesian coordinates are easily determined by Fig. 3. The quartic terms of Fig. 4 have two arrows. These arrows determine the ordering of each of the two bilinears making up the quartic. There is never any confusion determining the ordering of anticommuting variables from figures such as Fig. 4 because bilinears commute.

The faces in the x -direction (for example) can link to form larger x -directed surface areas (Fig. 5a) but faces in two different directions cannot (Fig. 5b). A_{corner} makes this possible by using bilinear "hooks". What is needed to link the two faces in Fig. 5b is the object in Fig. 5c. It is of the form, $\eta^1 \eta^3$, and acts like a hinge. Such objects are needed at the midpoints of each of the three types edges. Thus, A_{corner} has three terms. Figure 6a shows an x edge, the possible anticommuting variables which could enter it, and the corners. The corners are exactly of the same as for the two dimensional Ising model¹. Figures 6b and 6c shows the analogous objects for y and z edges. They represent the last two terms in Eq. (2.9). Perhaps a better name for A_{corner} would

be A_{hinge} because of the manner in which the edges are joined.

Finally, monomers are needed to fill empty sites. These monomers, similar to the two dimensional case, are given in Eq. (2.10).

In short, the action in Eqs. (2.8)-(2.10), with its complicated array of indices and labels, corresponds to the simple pictures in Figures 4 and 6. One should always think in terms of these pictures.

A moment's thought reveals that the action [Eq.(2.7)] generates closed polygons of the type needed in Eq. (2.4). If faces are weighted by the appropriate Boltzmann factors [Eq.(2.5)] as done in Eq. (2.8), then, up to a minus sign, the correct weights are obtained. A minus sign might be generated because of anticommuting variable reordering. The anticommuting variables must be put in $\eta \eta^\dagger$ form. This involves anticommuting operations, each of which yields a minus factor. Fortunately, all terms are indeed positive: the quartic terms can be broken up into the product of the two bilinears. The bilinears are only able to combine with corners in a two dimensional plane. They generate planar closed polygons like the ones in the two dimensional Ising model¹. By choosing the same bilinear ordering as in the two dimensional model, all terms are guaranteed to be positive. Effectively, the minus sign problem reduces to the two dimensional case. Figure 7 illustrates this.

Equations (2.8)-(2.10) can be written in compact form as

$$A_{\text{face}} = \sum_x \sum_{\text{cyclically } i,j,k} z_i \eta_{x+v_{ij}}^{j\dagger} \eta_{x+u_{ij}}^j \eta_{x+v_{ik}}^{k\dagger} \eta_{x+u_{ik}}^k, \quad (2.11)$$

$$A_{\text{corner}} = \sum_{\vec{x}} \sum_{j < k} \left[\eta_{\vec{x}+\vec{u}_{jk}}^{j\dagger} \eta_{\vec{x}+\vec{u}_{jk}}^k + \eta_{\vec{x}+\vec{u}_{jk}}^k \eta_{\vec{x}+\vec{u}_{jk}}^{j\dagger} \right] \quad (2.12)$$

$$+ \left[\eta_{\vec{x}+\vec{u}_{jk}}^{k\dagger} \eta_{\vec{x}+\vec{u}_{jk}}^j + \eta_{\vec{x}+\vec{u}_{jk}}^j \eta_{\vec{x}+\vec{u}_{jk}}^{k\dagger} \right],$$

$$A_{\text{monomer}} = \sum_{\vec{x}} \sum_{j < k} \left(\eta_{\vec{x}+\vec{u}_{jk}}^j \eta_{\vec{x}+\vec{u}_{jk}}^{j\dagger} + \eta_{\vec{x}+\vec{u}_{jk}}^k \eta_{\vec{x}+\vec{u}_{jk}}^{k\dagger} \right), \quad (2.13)$$

where $\sum_{i,j,k}$ means letting $(i,j,k) = (1,2,3), (2,3,1)$ or $(3,1,2)$,
cyclically

where

$$\vec{x} \equiv (\alpha, \beta, \gamma), \quad (2.14)$$

and

$$\vec{u}_{ij} = \frac{1}{2} (\vec{e}_i + \vec{e}_j), \quad (2.15)$$

$$\vec{v}_{ij} = \frac{1}{2} (\vec{e}_i - \vec{e}_j). \quad (2.16)$$

The \vec{e}_i are unit vectors in the i th direction [for example, $\vec{e}_1 = (1,0,0)$].

The action in Eq. (2.7) is bilinear except for A_{face} which is a product of four anticommuting variables. If it weren't for A_{face} the three dimensional Ising model would be exactly solvable. A_{face} represents an interaction term. As written in Eq. (2.8) the four anticommuting variables which make up a plaquette in A_{face} are located on the edges of the plaquette. This interaction looks non-local in the sense that the anticommuting

variables are multiplied at different (albeit nearby) locations.

This is, however, illusory. By redefining the location of these four variables to be at the center of the plaquette a local interaction is obtained. When this is done the quadratic pieces of the action (which were previously local) will span neighboring sites and behave like an ordinary kinetic energy terms. An ordinary fermionic theory with a four point interaction is obtained.

From the above discussion, it's obvious how to extend the technique to the d -dimensional Ising model. It also is expressible as a fermionic field theory by using objects of dimension $d-1$ (the low temperature expansion). The action will consist of bilinear terms plus interacting $2(d-1)$ products of anticommuting variables:

$$A_{\text{polycomplex}} = A_{(d-1)\text{face}} + A_{\text{corner}} + A_{\text{monomer}}, \quad (2.17)$$

$$A_{(d-1)\text{face}} = \sum_{\vec{x}} \sum_{i_1, i_2, \dots, i_d \text{ cyclically}} z_{i_1} \left(\eta_{\vec{x}+\vec{v}_{i_1, i_2}}^{i_2\dagger} \eta_{\vec{x}+\vec{u}_{i_1, i_2}}^{i_2} \eta_{\vec{x}+\vec{v}_{i_1, i_2}}^{i_3\dagger} \eta_{\vec{x}+\vec{u}_{i_1, i_2}}^{i_3} \dots \times \eta_{\vec{x}+\vec{v}_{i_1, i_d}}^{i_d\dagger} \eta_{\vec{x}+\vec{u}_{i_1, i_d}}^{i_d} \right), \quad (2.18)$$

$$A_{\text{corner}} = \sum_{\vec{x}} \sum_{i < j} \left\{ \eta_{\vec{x}+\vec{u}_{ij}}^{i\dagger} \eta_{\vec{x}+\vec{u}_{ij}}^j + \eta_{\vec{x}+\vec{u}_{ij}}^j \eta_{\vec{x}+\vec{u}_{ij}}^{i\dagger} + \eta_{\vec{x}+\vec{u}_{ij}}^j \eta_{\vec{x}+\vec{u}_{ij}}^{i\dagger} + \eta_{\vec{x}+\vec{u}_{ij}}^{i\dagger} \eta_{\vec{x}+\vec{u}_{ij}}^j \right\}, \quad (2.19)$$

$$A_{\text{monomer}} = \sum_{\vec{x}} \sum_{i < j} \left\{ \eta_{\vec{x}+\vec{u}_{ij}}^i \eta_{\vec{x}+\vec{u}_{ij}}^{i\dagger} + \eta_{\vec{x}+\vec{u}_{ij}}^j \eta_{\vec{x}+\vec{u}_{ij}}^{j\dagger} \right\}, \quad (2.20)$$

with the obvious notational extensions.

III. THE TWO-DIMENSIONAL ISING MODEL IN A MAGNETIC FIELD

This section expresses the partition function for the two-dimensional Ising model in background magnetic field in two ways. The first way uses anticommuting variables only. It has quartic terms in the action and hence is an interacting fermionic field theory. The second representation is of "mixed" form: using both anticommuting variables and bosonic variables. It is, in particle physics language, a Z_2 lattice gauge theory^{9,10} coupled to a fermion. From a particle physicist's point of view this is an interesting representation: the four dimensional counterpart is a model for quark confinement.

Let H be the magnetic field. In what follows it is necessary for H to be positive (or zero).

In the $H = 0$ low temperature expansion in terms of closed polygons [Eqs. (I.3.7) and (I.3.8)], only the edges of polygons were weighted. Now, in addition to spin-spin interaction Boltzmann factors, there are magnetic field Boltzmann factors, $\exp(\beta\sigma H)$. The lowest energy configuration (with all spins up) has an extra factor of $\exp(\beta H N)$. Relative to it, each down spin must be multiplied by $\exp(-2\beta H)$. When a polygon is drawn around a region of down spin, each unit of area enclosed needs a factor of $\exp(-2\beta H)$. Thus, besides wall weights due to spin-spin interactions, there are area weight due to spin-magnetic field interactions. Summarizing, in the presence of an external magnetic field, the area of polygons must also be weighted. Thus,

$$Z_{\text{Ising}}(J_h, J_v, H) = f Z_{\text{closed polygon}}(z_h, z_v, z_A), \quad (3.1)$$

where

$$\begin{aligned} f &= \exp(\beta N H) \exp \left[\beta N (J_v + J_h) \right], \\ z_h &= \exp(-2\beta J_v), \\ z_v &= \exp(-2\beta J_h), \\ z_A &= \exp(-2\beta H), \end{aligned} \quad (3.2)$$

and N is the total number of spins. $Z_{\text{closed polygon}}(z_h, z_v, z_A)$ involves the same types of polygons as for the $H = 0$ Ising model and z_h , z_v , and z_A are the weights of each unit of horizontal wall, each unit of vertical wall, and each square unit of polygonal area.

Although the low temperature expansion is similar to the $H = 0$ case, it is convenient to do the following: Instead of drawing a square around a down spin when its amongst up spin, draw a box around it. In general, draw polyhedrons around regions of down spin in lieu of polygons. Doing this transforms the problem into the $Z_{\text{closed polyhedron}}$ type of Section II, except that the third direction is only one unit thick:

$$Z_{\text{closed polygon}}(z_v, z_h, z_A) = Z_{\text{closed polyhedron}}(z_1, z_2, z_3), \quad (3.3)$$

where $Z_{\text{closed polyhedron}}$ is given in Eq. (2.6) with Equations (2.8), (2.9), and (2.10) replaced by

$$A_{\text{face}} = \sum_{\substack{\text{over those } \gamma \\ \text{for which the} \\ \text{third coordinate} \\ \text{is } -\frac{1}{2}, 0, \text{ or } \frac{1}{2}}} \sum_{\alpha\beta} (\text{same as in Eq. (2.8)}), \quad (3.4)$$

$$A_{\text{corner}} = \sum_{\substack{\text{over those } \gamma \\ \text{for which the} \\ \text{third coordinate} \\ \text{is } -\frac{1}{2}, 0, \text{ or } \frac{1}{2}}} \sum_{\alpha\beta} (\text{same as in Eq. (2.9)}), \quad (3.5)$$

$$A_{\text{monomer}} = \sum_{\substack{\text{over those } \gamma \\ \text{for which the} \\ \text{third coordinate} \\ \text{is } -\frac{1}{2}, 0, \text{ or } \frac{1}{2}}} \sum_{\alpha\beta} (\text{same as in Eq. (2.10)}), \quad (3.6)$$

and

$$\begin{aligned} z_1 &= \exp(-2\beta J_h), \\ z_2 &= \exp(-2\beta J_v), \\ z_3 &= \exp(-\beta H). \end{aligned} \quad (3.7)$$

Notice that z_3 is the square root of z_A . This is because each unit of polyhedral area in the third direction (and hence each z_3) enters twice for each square unit of polygonal area (see Fig. 8).

In Equation (3.3) many of the quartic terms are redundant. Metaphorically, the polyhedrons can "gift wrap" regions of down spin in a simpler manner (see Fig. 9). More precisely, the faces in the y and z directions, consisting of a quartic of anticommuting variables, may be replaced by bilinears, i.e. $z_2 n_{\alpha, \beta + \frac{1}{2}, -\frac{1}{2}}^3 n_{\alpha, \beta + \frac{1}{2}, \frac{1}{2}}^3 \times$
 $n_{\alpha - \frac{1}{2}, \beta + \frac{1}{2}, 0}^1 n_{\alpha + \frac{1}{2}, \beta + \frac{1}{2}, 0}^1 \rightarrow z_2 n_{\alpha - \frac{1}{2}, \beta + \frac{1}{2}, 0}^1 n_{\alpha + \frac{1}{2}, \beta + \frac{1}{2}, 0}^1$ and

$z_3 n_{\alpha - \frac{1}{2}, \beta, \frac{1}{2}}^1 n_{\alpha + \frac{1}{2}, \beta, \frac{1}{2}}^1 \rightarrow z_3 n_{\alpha - \frac{1}{2}, \beta, \frac{1}{2}}^1 n_{\alpha + \frac{1}{2}, \beta, \frac{1}{2}}^1$ in the second and third terms of Eq.(3.4):

$$A_{\text{face}} = \sum_{\alpha\beta} \left(z_1 n_{\alpha + \frac{1}{2}, \beta - \frac{1}{2}, 0}^2 n_{\alpha + \frac{1}{2}, \beta + \frac{1}{2}, 0}^2 n_{\alpha + \frac{1}{2}, \beta, -\frac{1}{2}}^3 n_{\alpha + \frac{1}{2}, \beta, \frac{1}{2}}^3 \right. \\ \left. + z_2 n_{\alpha - \frac{1}{2}, \beta + \frac{1}{2}, 0}^1 n_{\alpha + \frac{1}{2}, \beta + \frac{1}{2}, 0}^1 \right) \quad (3.8)$$

$$+ \sum_{\gamma = \pm \frac{1}{2}} \sum_{\alpha\beta} \left(z_3 n_{\alpha - \frac{1}{2}, \beta, \gamma}^1 n_{\alpha + \frac{1}{2}, \beta, \gamma}^1 \right),$$

$$A_{\text{corner}} = \sum_{\gamma = \pm \frac{1}{2}} \sum_{\alpha\beta} \left(n_{\alpha + \frac{1}{2}, \beta, \gamma}^1 n_{\alpha + \frac{1}{2}, \beta, \gamma}^3 + n_{\alpha + \frac{1}{2}, \beta, \gamma}^3 n_{\alpha + \frac{1}{2}, \beta, \gamma}^1 \right. \\ \left. + n_{\alpha + \frac{1}{2}, \beta, \gamma}^3 n_{\alpha + \frac{1}{2}, \beta, \gamma}^1 + n_{\alpha + \frac{1}{2}, \beta, \gamma}^1 n_{\alpha + \frac{1}{2}, \beta, \gamma}^3 \right) \\ + \sum_{\alpha\beta} \left(n_{\alpha + \frac{1}{2}, \beta + \frac{1}{2}, 0}^1 n_{\alpha + \frac{1}{2}, \beta + \frac{1}{2}, 0}^2 + n_{\alpha + \frac{1}{2}, \beta + \frac{1}{2}, 0}^2 n_{\alpha + \frac{1}{2}, \beta + \frac{1}{2}, 0}^1 \right. \\ \left. + n_{\alpha + \frac{1}{2}, \beta + \frac{1}{2}, 0}^2 n_{\alpha + \frac{1}{2}, \beta + \frac{1}{2}, 0}^1 + n_{\alpha + \frac{1}{2}, \beta + \frac{1}{2}, 0}^1 n_{\alpha + \frac{1}{2}, \beta + \frac{1}{2}, 0}^2 \right), \quad (3.9)$$

$$A_{\text{monomer}} = \sum_{\gamma = \pm \frac{1}{2}} \sum_{\alpha\beta} \left(n_{\alpha + \frac{1}{2}, \beta, \gamma}^1 n_{\alpha + \frac{1}{2}, \beta, \gamma}^1 + n_{\alpha + \frac{1}{2}, \beta, \gamma}^3 n_{\alpha + \frac{1}{2}, \beta, \gamma}^3 \right) \\ + \sum_{\alpha\beta} \left(n_{\alpha + \frac{1}{2}, \beta + \frac{1}{2}, 0}^1 n_{\alpha + \frac{1}{2}, \beta + \frac{1}{2}, 0}^1 + n_{\alpha + \frac{1}{2}, \beta + \frac{1}{2}, 0}^2 n_{\alpha + \frac{1}{2}, \beta + \frac{1}{2}, 0}^2 \right). \quad (3.10)$$

It is no longer necessary to hook up z variables with y variables; hence the missing terms in Eqs. (3.9) and (3.10).

This completes the first representation in terms of anti-commuting variables. It is easy to extend the method to higher dimensions by treating the $(d-1)$ - dimensional Ising model in a background magnetic field as $Z_{\text{polycomplex}}$ for $(d-1)$ -dimensional polycomplexes in d -dimensions where the d^{th} direction is only one unit thick. In other words, the representation of the d -dimensional Ising model in Eq. (2.17) can be used to represent the $(d-1)$ dimensional Ising model in a magnetic field. This uses terms consisting of a product of $2(d-1)$ anticommuting variables.

The task of weight areas can also be done using a gauge field. Pretend, for the moment, that the polygons (or more precisely, the polygonal curves) are oriented. Think of such curves as charged particle trajectories, the orientation being associated with the direction of flow of charge. Coupling them to an abelian gauge theory (as in quantum electrodynamics) would weight the polygon's area because $1 + 1$ dimensional QED has a linear potential. Unfortunately, the curves in $Z_{\text{closed polygon}}$ (Eq. 3.1) are not oriented and this trick fails. Fortunately, the difficulty can be overcome by using a Z_2 gauge field instead of a $U(1)$ one. Being blind to the difference between positive and negative charges, a Z_2 gauge field works. The two dimensional Z_2 lattice gauge theory is defined by^{9,10}

$$Z_{Z_2} = \sum_{\substack{U_{\alpha+\frac{1}{2}\beta} = \pm 1 \\ U_{\alpha\beta+\frac{1}{2}} = \pm 1}} \exp A_{Z_2}, \quad (3.11)$$

where the Z_2 action is

$$A_{Z_2} = K \sum_{\alpha\beta} \left(U_{\alpha+\frac{1}{2}\beta} U_{\alpha+1\beta+\frac{1}{2}} U_{\alpha+\frac{1}{2}\beta+1} U_{\alpha\beta+\frac{1}{2}} \right). \quad (3.12)$$

In what follows, the spins have half integer cartesian coordinates, the gauge fields (the U 's) have one half integer coordinate and one integer coordinate, and anticommuting variables will have integer coordinates. The U 's are defined on links (see Fig. 10), anticommuting variables are defined at sites, and the spins are defined at dual sites (the centers of plaquettes). The action in Eq. (3.11) is a sum over plaquettes of the product of U 's around the plaquette (see Fig. 10). In Eq. (3.11) the U 's, like Ising spins, take on two values, ± 1 . In Eq.(3.12) K is just a coupling constant.

Use $U^2 = 1$. Expand the exponent in Eq. (3.11):

$$Z_{Z_2} = \sum_{\substack{U_{\alpha+\frac{1}{2}\beta} = \pm 1 \\ U_{\alpha\beta+\frac{1}{2}} = \pm 1}} \prod_{\alpha\beta} \left(\cosh K + \sinh K U_{\alpha+\frac{1}{2}\beta} U_{\alpha+1\beta+\frac{1}{2}} U_{\alpha+\frac{1}{2}\beta+1} U_{\alpha\beta+\frac{1}{2}} \right). \quad (3.13)$$

Next, multiply out the products. Non-zero terms occur only if each edge (of the plaquettes) occurs an even number of times. This happens only if no plaquettes occur [contributing $(4 \cosh K)^N$] or if all plaquettes occur [contributing $(4 \sinh K)^N$]. The terms contributing are the product of the first factors in Eq. (3.13) (the $\cosh K$'s) or a product of the second factors (the $\sinh K$ $UUUU$'s). For large N the second contribution is miniscule. In two dimensions the Z_2 gauge theory is trivial:

$$Z_{Z_2} = (4 \cosh K)^N. \quad (3.14)$$

An interesting correlation function is

$$\langle \prod_{\text{links of } C} (U\text{'s of each link}) \rangle. \quad (3.15)$$

In Eq. (3.15) C is a closed curve and the product is over the U 's of the links comprising C . Reasoning similar to that in obtaining Eq. (3.14) gives for Eq.(3.15)

$$\frac{\text{area of } C}{(\tanh K)}. \quad (3.16)$$

By coupling U 's to the anticommuting variables in Eq. (I.4.4) polygons can be weighted by a factor of $\tanh K$ per unit area. Set $\tanh K = \exp(-2\beta H)$, then

$$Z_{\text{Ising}}(J_h, J_v, H) = f' \sum_{\substack{U_{\alpha+1/2, \beta}^{\pm 1} \\ U_{\alpha, \beta+1/2}^{\pm 1}}} \int d\mathbf{n} d\mathbf{n}^\dagger \exp A, \quad (3.17)$$

where the action, A , is

$$A = A_{\text{wall}} + A_{\text{corner}} + A_{\text{monomer}} + A_{Z_2} \quad (3.18)$$

A_{corner} , A_{monomer} , and A_{Z_2} are the same actions as in Eq. (I.4.4) (with $a_1 = a_2 = a_3 = a_4 = b_v = b_h = 1$) and Eq. (3.11). A_{wall} is modified to

$$A_{\text{wall}} = \sum_{\alpha\beta} \left(\eta_{\alpha\beta}^{\dagger h} \eta_{\alpha+1/2, \beta}^h z_h U_{\alpha+1/2, \beta} + \eta_{\alpha\beta}^{\dagger v} \eta_{\alpha, \beta+1/2}^v z_v U_{\alpha, \beta+1/2} \right). \quad (3.19)$$

In these formulas

$$\begin{aligned} z_h &= \exp(-2\beta J_v), \\ z_v &= \exp(-2\beta J_h), \\ \tanh K &= \exp(-2\beta H), \\ f' &= \frac{\exp(N\beta H)}{(4 \cosh K)^N} \exp \beta N(J_v + J_h), \\ &= \frac{1}{(8 \sinh 2K)^{N/2}} \exp \beta N(J_v + J_h). \end{aligned} \quad (3.20)$$

Again, the method generalizes to higher dimensions. For the d -dimensional Ising model in a background magnetic field, $H > 0$,

$$Z_{\text{Ising}}(J_1, J_2, \dots, J_d, H) = f'_d Z_{\text{closed polycomplex}}(z_1, z_2, \dots, z_d, K), \quad (3.21)$$

$$Z_{\text{closed polycomplex}} = \sum_{U's=\pm 1} \int d\mathbf{n} d\mathbf{n}^\dagger \exp A.$$

The action, A , is given by Eqs. (2.18)-(2.20) with the replacement $z_{i_1} \rightarrow z_{i_1} U_{x+u_{i_1}}$ in $A_{(d-1)\text{face}}$. Furthermore, there is a U -piece which must be added to the action:

$$A_U = K \sum_x \left(\prod_{i=1}^d U_{x+u_i} \right). \quad (3.22)$$

The U 's are to be summed over ± 1 . This action is the higher dimensional analog of the Z_2 gauge field action. It has appeared in the literature before¹⁰. Wegner calls it the M_{dd-1} model. The constant K is still given in Eq. (3.20) and

$$z_i = \exp(-2\beta J_i),$$

$$\vec{u}_i = \frac{1}{2} \vec{e}_i,$$

$$r'_d = \frac{\exp(N\beta H)}{(2^d \cosh K)^N} \exp[\beta N(\sum_{i=1}^d J_i)]. \quad (3.23)$$

IV. COORDINATE SPACE PERTURBATION THEORY FOR THE GENERAL DIMER PROBLEM

This section and several following sections will deal with the dimer problem. This constitutes a whole class of problems since there are many lattices at one's disposal. The dimer problem is not only important because of its direct application to physical systems¹¹, but also because of the large number of problems which can be mapped into dimer form. This enhances their importance. The only models which have been solved are the one-dimensional dimer model and two-dimensional close-packed models. Approximation methods are therefore of interest. My purpose will be twofold: First, the anticommuting variable technique will be used to obtain new dimer series expansions. These represent new approaches to the dimer system. Secondly, in the process of obtaining the expansions, various anticommuting variable approximation techniques will be illustrated. Dimer models

are a good laboratory for testing these because of their simplicity and because of other existing approximation schemes to which they can be compared. In this sense the purpose is expository and pedagogical. The importance of these sections is that the approximation techniques are applicable to any model representable in fermionic-like field theory form (such as the models discussed in sections II and III). One merely mimics the methods illustrated here.

An extensive set of dimer references can be found in reference 12, to which the reader is referred. I would like, however, to mention the following: Previous approximation schemes fall into the following categories: First, there are those¹³ which solve exactly small finite lattices and then extrapolate to large lattices. This technique is known as the exact finite method: A close cousin is Monte Carlo¹⁴. There are also transfer matrix methods¹⁵. These give excellent numerical results. Next is the Bethe approximation¹⁶. It is of interest because of its simplicity both mathematically and physically and because of its accuracy which is reasonable. There are ways of calculating corrections to the Bethe approximation^{17,18}. Rigorous mathematical dimer results also exist^{12,19}. The importance of reference 12 should not be neglected. With reasonable assumptions Heilmann and Lieb have shown that no phase transition can occur as long as monomer Boltzmann factors are non-zero. The result is general. It is applicable to almost all dimer models. Phase transitions can only occur for pure dimer systems. Finally, there are the series expansions. The simplest is the low temperature expansion in powers of the dimer Boltzmann factor. This can be

organized into a Mayer type expansion^{20,21,22}. A great improvement is Nagle's series¹⁸. It starts with the Bethe approximation and generates a series using graphical methods. It systematically calculates corrections to the Bethe approximation, which, because it is a good starting point, guarantees an excellent series. Nagle's series is presently the best in the literature. The Hartree series developed in this section equals Nagle's in accuracy. It is a new expansion. The field theoretic Hartree method is used after expressing the dimer problem as a fermionic field theory. Since dimers cannot overlap, fermions are natural variables: roughly speaking, dimers constructed out of fermions are unable to overlap because of the Pauli principle. The perturbative techniques developed here are easily extended to other systems such as trimers or more complicated polymers. Nagle's method has also been extended to trimers²³ although more complicated polymeric systems have not been treated. A final note: reference 12 has an important implication for this paper's Hartree series (and also Nagle's series): It guarantees convergence in the entire physical region.

This section will treat the dimer problem from a general point of view: A specific example will be considered in the next section. Key results are the Hartree approximation (Eq. 4.10) and the Hartree-improved Feynman rules which generate the series in Eq.(4.18) and Figure 18.

In terms of anticommuting variables the general dimer partition function was given in Eq. (I.3.6). It is an interacting fermionic field theory with a quartic interaction term

$$V = \frac{1}{2} \sum_{\alpha\beta} z_{\alpha\beta} n_{\alpha}^{\dagger} n_{\alpha} n_{\beta}^{\dagger} n_{\beta} \quad (4.1)$$

Equation (4.1) differs from Eq. (I.3.6) in that one sums over all sites α and all sites β allowing $z_{\alpha\beta}$ to be zero if no bond exists between α and β . The factor of $\frac{1}{2}$ compensates for the double counting in Eq. (4.1) ($z_{\alpha\beta} \equiv z_{\beta\alpha}$).

The interaction, V , is pictorially depicted in Fig. 11 and is of the same form as a two-body potential in a quantized many body theory²⁴. This correspondence proves useful. The bare propagator, $G_{\alpha\beta}^0$, is determined by the quadratic piece of Eq.(I.3.6), that is, $\sum_{\alpha} n_{\alpha} n_{\alpha}^{\dagger}$. It is

$$G_{\alpha\beta}^0 \equiv \langle n_{\alpha} n_{\beta}^{\dagger} \rangle_0 = \delta_{\alpha\beta} \quad (4.2)$$

Perturbation theory is an expansion in powers of V (or $z_{\alpha\beta}$). Since $z_{\alpha\beta} = \exp(-\beta E_{\alpha\beta})$, this is the standard low temperature expansion:

$$\text{Perturbation Theory} = \text{Low Temperature Expansion.} \quad (4.3)$$

Feynman rules are similar to the usual many body theory ones²⁴. One draws all graphs using the interaction of Fig. 11. Because of the nature of the bare propagator in Eq. (4.2), fermion loops occur at a particular site. It is convenient to contract all fermion loops to a point. Figure 12 shows all the connected vacuum bubbles to third order, first in the usual way and then in the contracted form. The Feynman rules for contracted graphs are

Feynman Rules

(a) Draw all topologically distinct graphs, consisting of any number of vertices. The vertices can have one or more lines attached to them. The vertices are assigned a site index, α . The empty graph is to be included and contributes one.

(b) For each edge (Figure 13) associate a factor, $z_{\alpha\beta}$.

(c) For each vertex at α with ℓ lines emanating from it (a vertex of degree ℓ) (Fig. 14) put in a factor of $\sum_{\alpha} (-1)(\ell-1)!$.

(d) The graph may be topologically invariant under permutation of some of its vertices. Such permutations generate a symmetry group of the graph which is called the point symmetry group of the graph. Put in a factor of [order of the point symmetry group of the graph] $^{-1}$. The order of a group, G , is the number of elements in G .

(e) For each pair of vertices connected by ℓ lines (Fig. 15) put in a factor of $\frac{1}{\ell!}$.

The (-1) in rule (c) arises because the vertex was originally a fermion loop for which Feynman rules assign a minus factor. The $(\ell-1)!$ is due to the fact that ℓ lines entering a loop can be ordered in $(\ell-1)!$ ways. Figure 16 illustrates this for $\ell=4$.

If interchange of lines is considered a symmetry of a graph then rules (d) and (e) combine into one:

(de) Put in a factor of [the order of the total symmetry group of the graph] $^{-1}$.

Figure 12 shows the connected graphs through third order in $z_{\alpha\beta}$, along with the factors from rules (b), (c), (d), and (e). This illustrates how the Feynman rules work.

In rule (a) all topologically distinct graphs are to be considered including disconnected ones. It is well known in field theory that

$$Z = \sum_{\substack{\text{all graphs} \\ \text{connected or} \\ \text{disconnected}}} = \exp \sum_{\substack{\text{connected} \\ \text{graphs}}}, \quad (4.4)$$

that is, the connected graphs exponentiate. Therefore only connected graphs need be considered. Figure 12 thus gives

$$\begin{aligned} \log Z = & \frac{1}{2} \sum_{\alpha\beta} z_{\alpha\beta} - \frac{1}{2} \sum_{\alpha\beta\gamma} z_{\alpha\beta} z_{\beta\gamma} + \frac{1}{4} \sum_{\alpha\beta} z_{\alpha\beta}^2 + \frac{1}{2} \sum_{\alpha\beta\gamma\delta} z_{\alpha\beta} z_{\beta\gamma} z_{\gamma\delta} \\ & + \frac{1}{3} \sum_{\alpha\beta\gamma\delta} z_{\beta\alpha} z_{\gamma\alpha} z_{\delta\alpha} - \frac{1}{6} \sum_{\alpha\beta\gamma} z_{\alpha\beta} z_{\beta\gamma} z_{\gamma\alpha} - \sum_{\alpha\beta\gamma} z_{\alpha\beta}^2 z_{\beta\gamma} + \frac{1}{3} \sum_{\alpha\beta} z_{\alpha\beta}^3 + \dots \end{aligned} \quad (4.5)$$

Equation (4.5) is generic in character: it is the low temperature dimer expansion to third order for any dimer problem.

Just as a check, consider the simplest possible dimer problem consisting of two sites and one dimer with weight, z . The partition function is

$$1 + z = \exp(\ln(1+z)) = \exp\left(z - \frac{1}{2}z^2 + \frac{1}{3}z^3 + \dots\right). \quad (4.6)$$

The terms in Eq. (4.5), with $\alpha, \beta, \gamma, \delta = 1$ or 2 and $z_{12} = z$, give

$$\begin{aligned} z - \frac{1}{2} 2z^2 + \frac{1}{4} 2z^2 + \frac{1}{2} 2z^3 + \frac{1}{3} 2z^3 - \frac{1}{6} \cdot 0 \cdot z^3 - 2z^3 + \frac{1}{3} 2z^3 + \dots \\ = z - \frac{1}{2} z^2 + \frac{1}{3} z^3 + \dots, \end{aligned} \quad (4.7)$$

which checks.

Now that the dimer statistical system has been expressed in field theory language, standard field theory calculational methods are applicable. What has just been illustrated is simple coordinate space perturbation theory. Significant improvements can be made; for example, the self-consistent Hartree approximation.

It can be obtained by the replacement

$$\begin{aligned} \frac{1}{2} \sum_{\alpha\beta} z_{\alpha\beta} \eta_{\alpha}^{\dagger} \eta_{\alpha} \eta_{\beta}^{\dagger} \eta_{\beta} + \frac{1}{2} \sum_{\alpha\beta} z_{\alpha\beta} \left[\eta_{\alpha}^{\dagger} \langle \eta_{\beta}^{\dagger} \eta_{\beta} \rangle_{\text{H}} \right. \\ \left. + \langle \eta_{\alpha}^{\dagger} \eta_{\alpha} \rangle_{\text{H}} \eta_{\beta}^{\dagger} \eta_{\beta} - \langle \eta_{\alpha}^{\dagger} \eta_{\alpha} \rangle_{\text{H}} \langle \eta_{\beta}^{\dagger} \eta_{\beta} \rangle_{\text{H}} \right], \end{aligned} \quad (4.8)$$

where $\langle \eta_{\gamma}^{\dagger} \eta_{\gamma} \rangle_{\text{H}}$, the Hartree propagator, is determined selfconsistently:

$$\begin{aligned} \langle \eta_{\gamma}^{\dagger} \eta_{\gamma} \rangle_{\text{H}} &= \frac{\int d\eta d\eta^{\dagger} (\eta_{\gamma}^{\dagger} \eta_{\gamma}) \exp \left[\sum_{\alpha} \eta_{\alpha}^{\dagger} + \sum_{\alpha\beta} z_{\alpha\beta} \eta_{\alpha}^{\dagger} \langle \eta_{\beta}^{\dagger} \eta_{\beta} \rangle_{\text{H}} \right]}{\text{[same as numerator but without } (\eta_{\gamma}^{\dagger} \eta_{\gamma}) \text{]}} \\ &= \left[1 + \sum_{\beta} z_{\gamma\beta} \langle \eta_{\beta}^{\dagger} \eta_{\beta} \rangle_{\text{H}} \right]^{-1}. \end{aligned} \quad (4.9)$$

Equation (4.9) was obtained by calculating the propagator $\langle \eta_{\gamma}^{\dagger} \eta_{\gamma} \rangle$ with the quartic term in Eq. (4.1) replaced by Eq. (4.8).

$z_{\alpha\beta} = z_{\beta\alpha}$ was used to rewrite $\frac{1}{2} \sum_{\alpha\beta} z_{\alpha\beta} [\eta_{\alpha}^{\dagger} \langle \eta_{\beta}^{\dagger} \eta_{\beta} \rangle_{\text{H}} + \langle \eta_{\alpha}^{\dagger} \eta_{\alpha} \rangle_{\text{H}} \eta_{\beta}^{\dagger} \eta_{\beta}]$ as $\sum_{\alpha\beta} z_{\alpha\beta} \eta_{\alpha}^{\dagger} \langle \eta_{\beta}^{\dagger} \eta_{\beta} \rangle_{\text{H}}$ and the constant term $-\frac{1}{2} \sum_{\alpha\beta} z_{\alpha\beta} \langle \eta_{\alpha}^{\dagger} \eta_{\alpha} \rangle_{\text{H}} \langle \eta_{\beta}^{\dagger} \eta_{\beta} \rangle_{\text{H}}$ was cancelled from both numerator and denominator in Eq. (4.9). Equation (4.9) is a system of N ($N =$ the number of sites) simultaneous equations. They can be solved in principle. In practice, one usually has a translationally invariant lattice in which case Eq. (4.9) is simple to solve (this will be exemplified shortly).

The self-consistent Hartree approximation for Z is

$$\begin{aligned} Z_{\text{H}} &= \left[\prod_{\alpha} \left(1 + \sum_{\beta} z_{\alpha\beta} \langle \eta_{\beta}^{\dagger} \eta_{\beta} \rangle_{\text{H}} \right) \right] \times \exp \left[-\frac{1}{2} \sum_{\alpha\beta} z_{\alpha\beta} \langle \eta_{\alpha}^{\dagger} \eta_{\alpha} \rangle_{\text{H}} \langle \eta_{\beta}^{\dagger} \eta_{\beta} \rangle_{\text{H}} \right] \\ \log Z_{\text{H}} &= \sum_{\alpha} \ln \left(1 + \sum_{\beta} z_{\alpha\beta} \langle \eta_{\beta}^{\dagger} \eta_{\beta} \rangle_{\text{H}} \right) - \frac{1}{2} \sum_{\alpha\beta} z_{\alpha\beta} \langle \eta_{\alpha}^{\dagger} \eta_{\alpha} \rangle_{\text{H}} \langle \eta_{\beta}^{\dagger} \eta_{\beta} \rangle_{\text{H}}. \end{aligned} \quad (4.10)$$

Equation (4.10), the Hartree approximation to the partition function, is one of the results of this section.

As an example, apply Eq. (4.10) to the one dimensional dimer problem. The exact well known answer, obtainable from transfer matrix techniques, is

$$\Gamma \equiv \frac{1}{N} \log Z = \log \left(\frac{1}{2} + \frac{1}{2} \sqrt{1 + 4z} \right). \quad (4.11)$$

Here, Γ is the grand potential per unit site. By translational invariance, Eqs. (4.9) reduce to a single one:

$$\langle n_Y n_Y^\dagger \rangle_H = \left[1 + 2z \langle n_Y n_Y^\dagger \rangle_H \right]^{-1}, \quad (4.12)$$

or

$$\langle n_Y n_Y^\dagger \rangle_H = \frac{-1 + \sqrt{1 + 8z}}{4z}. \quad (4.13)$$

Equation (4.10) gives

$$\Gamma^H = \log \left(\frac{1}{2} + \frac{1}{2} \sqrt{1 + 8z} \right) - \frac{1}{16z} (-1 + \sqrt{1 + 8z})^2. \quad (4.14)$$

A numerical comparison of the Hartree approximation, Γ^H of Eq. (4.14), to the exact result, Γ of Eq. (4.11) is given in Table(i). The Hartree approximation is, at most, off by 8.28% for the entire range of z . The z which yields the maximum error occurs near $z = 2.31$. It is particularly good for small z and large z . It is encouraging that such a simple technique yields a reasonably accurate approximation for all z .

For the d -dimensional dimer problem on a square lattice with weights z_1, z_2, \dots, z_d , in the first, second, \dots , d^{th} directions, the Hartree approximation is Eqs. (4.13) and (4.14) with $z \rightarrow \sum_{i=1}^d z_i$:

$$\begin{aligned} \Gamma^H_{d\text{-dimensional dimer}} &= \log \left(\frac{1}{2} + \frac{1}{2} \sqrt{1 + 8 \sum_{i=1}^d z_i} \right) \\ &- \frac{1}{16 \sum_{i=1}^d z_i} \left(-1 + \sqrt{1 + 8 \sum_{i=1}^d z_i} \right)^2. \end{aligned} \quad (4.15)$$

Unfortunately, the d -dimensional dimer problem is unsolved for $d > 1$, so that comparison with the exact result is impossible.

It is common knowledge that the Hartree approximation sums up the "tadpole" vacuum bubbles. A sample tadpole graph is shown in Fig. 17. In terms of contracted graphs (that is, with fermion loops contracted to points) the tadpole graphs are the tree graphs. Knowing this allows one to compute systematically the corrections to the Hartree approximation. Let

$$g_Y = \langle n_Y n_Y^\dagger \rangle_H, \quad (4.16)$$

be the solutions to Eqs. (4.9). Then

$$\ln Z = \log Z_H + \sum G_H, \quad (4.17)$$

with Z_H given in Eq. (4.10) and $\sum G_H$ is the sum over connected Feynman graphs with rule (c) modified to

(c') allow only graphs with vertex degree ≥ 2 , i.e. graphs with one line coming into a vertex are to be excluded. For each vertex α and ℓ lines emanating (Fig. 14) from it put in a factor of

$$\sum_{\alpha} (-1) g_{\alpha}^{\ell} (\ell-1)!.$$

Feynman graph rules (a), (b), (d), and (e) remain unchanged.

Eliminating graphs of order one reduces the number of graphs to be considered. For graphs with one edge the reduction is from one graph to none, for graphs with two edges the reduction is from two to one, for graphs with three edges the reduction is from five to two. Not only is the Hartree expansion better than simple perturbation theory over an extended region of z but it is easier to

calculate. Figure 18 displays the statistical factors due to rules (c'), (d), and (e) for the graphs in G_H to sixth order in edge weight. The graphs still need to be multiplied by the g_α and $z_{\alpha\beta}$ factors of rules (b) and (c'). The terms in Fig. 18 generate a result guaranteed to be correct to order $z_{\alpha\beta}^6$ when expanded in powers of $z_{\alpha\beta}$. Thus an answer correct to z^6 for the general dimer problem has been obtained. In addition, the effects of higher order (in z) graphs have been included in the Hartree-improved expansion, so that the result can be expected to have a wider range of validity than a simple low temperature expansion. The terms in Fig. 18 to fourth order are

$$\begin{aligned} \ln Z = \ln Z_H + \frac{1}{4} \sum_{\alpha\beta} z_{\alpha\beta}^2 g_\alpha^2 g_\beta^2 - \frac{1}{6} \sum_{\alpha\beta\gamma} z_{\alpha\beta} z_{\beta\gamma} z_{\gamma\alpha} g_\alpha^2 g_\beta^2 g_\gamma^2 \\ + \frac{1}{3} \sum_{\alpha\beta} z_{\alpha\beta}^3 g_\alpha^3 g_\beta^3 - \sum_{\alpha\beta\gamma} z_{\alpha\beta}^2 z_{\beta\gamma} z_{\gamma\alpha} g_\alpha^3 g_\beta^3 g_\gamma^2 \\ - \frac{3}{4} \sum_{\alpha\beta\gamma} z_{\alpha\beta}^2 z_{\beta\gamma}^2 g_\alpha^2 g_\beta^2 g_\gamma^2 + \frac{1}{8} \sum_{\alpha\beta\gamma\delta} z_{\alpha\beta} z_{\beta\gamma} z_{\gamma\delta} z_{\delta\alpha} g_\alpha^2 g_\beta^2 g_\gamma^2 g_\delta^2 \\ + \frac{3}{4} \sum_{\alpha\beta} z_{\alpha\beta}^4 g_\alpha^4 g_\beta^4 + \dots \end{aligned} \quad (4.18)$$

The terms of fifth and sixth order can easily be written down but for reasons of space are omitted. Equation (4.18) and Fig. 18 constitute an important result in this section.

It is clear that the g_α factors can be absorbed into the $z_{\alpha\beta}$ factors: Equivalent to rules (b) and (c') are rules (c) and (b') with

(b') for each edge (Fig. 13) associate a factor of $g_\alpha z_{\alpha\beta} g_\beta$.

The Hartree improved expansion is in powers of $\omega_{\alpha\beta} \equiv g_\alpha z_{\alpha\beta} g_\beta$ in contrast to $z_{\alpha\beta}$ for simple perturbation theory. In general the factor $g_\alpha z_{\alpha\beta} g_\beta$ will be smaller than $z_{\alpha\beta}$ and for $z_{\alpha\beta}$ large it should be considerably smaller. The Hartree perturbation series represents a marked improvement over the simple low temperature one. To illustrate this consider the one dimensional dimer problem again. For large z the Hartree expansion is considerably better than the low temperature expansion and for low temperatures the Hartree expansion is just as good. Furthermore, the Hartree expansion parameter is

$$\omega = \text{Hartree expansion parameter} = \frac{(-1 + \sqrt{1 + 8z})^2}{16z}, \quad (4.19)$$

compared to z for the low temperature expansion. The factor in Eq. (4.19) is always less than z and never bigger than $\frac{1}{2}$. Therefore, ω is less than the simple perturbation theory expansion parameter. It is always bounded being guaranteed to be at most of intermediate strength. In contrast z can become arbitrarily large. The Hartree expansion parameter, ω , is given in column 5 of table (i). For d -dimensional hypercubic dimer problem the Hartree expansion parameters are

$$\omega_i = z_i \left(\frac{-1 + \sqrt{1 + 8 \frac{d}{\sum_{i=1}^d z_i} z_i}}{4 \frac{d}{\sum_{i=1}^d z_i} z_i} \right), \quad (4.20)$$

and again are guaranteed to be small or at most of intermediate magnitude. In fact, the ω_i cannot be greater than $\frac{1}{2}$ and in the isotropic case $z_1 = z_2 = \dots = z_d$, $\omega_1 = \omega_2 = \dots = \omega_d \equiv \omega \leq \frac{1}{2d}$.

It appears as if the expansion parameter, ω , becomes smaller as the dimension is increased, a point that will be discussed later.

One may also treat the combined monomer-dimer system. The action is given by

$$A(z_\alpha, z_\beta) = \sum_\alpha z_\alpha \eta_\alpha \eta_\alpha^\dagger + \frac{1}{2} \sum_{\alpha\beta} z_{\alpha\beta} \eta_\alpha \eta_\alpha^\dagger \eta_\beta \eta_\beta^\dagger, \quad (4.21)$$

which differs from A^{dimer} in that z_α , the Boltzmann factors for monomers, are not unity. By rescaling $\eta_\alpha \rightarrow \frac{1}{z_\alpha} \eta_\alpha$ (or by using simple physical reasoning) $A^{\text{dimer-monomer}}$ can be related to A^{dimer} so that $A^{\text{dimer-monomer}}$ is not any more general than A^{dimer} . However, this is not quite true. In Eq. (4.21) some of the z_α may be set equal to zero (in which case corresponding sites must be occupied by a dimer). The rescaling transformation fails. Simple perturbation theory is impossible since certain propagators blow up. Nevertheless the Hartree expansion exists because a finite Hartree propagator is generated. Thus even pure dimer systems may be treated. Equations are easily modified to account for Eq. (4.21). For example, the 1's in Eqs. (4.9) and (4.10) become z_γ and z_α . The point is that the Hartree expansion can handle the situation of having some (or all) monomer Boltzmann factors zero, whereas the usual low temperature expansions cannot.

V. DIMER MODELS (Continued)

This section tackles the dimer problems on various lattices via the methods of the last section. These models are unsolved (except in the pure dimer limit for two dimensional planar lattices²⁵). Their simplicity makes them ideal for illustrating perturbative

methods. One purpose of this section is to illustrate Feynman rules and lattice embedding effects for a concrete example. The two dimensional dimer model is treated in detail. Unlike the generic expansion [Eq. (4.5)], a specific dimer problem has lattice embedding factors for which it is useful to derive rules. Each term in Eq. (4.5) will generate several terms as the indices α, β, γ , etc. range over sites. It is useful to group these terms into a new set of diagrams and define new rules. Given an interesting model that can be translated into anticommuting variable language, the calculation of several orders of perturbation theory can be done by mimicking and generalizing the methods and rules of this section.

The second purpose of this section is to obtain new series expansions and accurately calculate physical quantities such as molecular freedoms, densities, and entropies. Models in two, three, and higher dimensions are considered. These computations test the accuracy of the Hartree expansion. It is found that it works amazingly well.

A list of the key results are the following:

(a) Feynman rules are derived for dimer models on a translational invariant lattice. Although similar to those developed in Sec. IV, there are some modifications. These rules are presented at the beginning of this section.

(b) Embedding graphs and their weights are computed in Fig. 22. Using these allows a rapid computation of the Hartree expansion to five or six orders for any dimer model.

(c) The Hartree expansion for the two-dimensional dimer model is computed to sixth order [see Eqs. (5.5), (5.6), (5.7), and

Fig. 24]. The non-isotropic case is considered in which $z_h \neq z_v$.

(d) The results in (c) are extended to the non-isotropic hypercubic dimer problem in d dimensions [see Eq. (5.11)]:

(e) The isotropic d -dimensional hypercubic dimer model is exactly solvable as $d \rightarrow \infty$ as long as z is not too small. Eq. (5.13) presents a $\frac{1}{d}$ expansion. Dimer models with a high coordination number, q , are also solvable as $q \rightarrow \infty$. Equations (5.14) and (5.15) present $\frac{1}{q}$ expansions. Molecular freedoms at close packing are computed in this $\frac{1}{q}$ limit for models with q ranging from 4 to 12 and are accurate to several percent (see Table (ii)).

(f) Gaunt's²¹ low temperature expansions are used to obtain Hartree expansions for isotropic dimer problems to orders 15, 10, 16, 12, 12, and 8 for simple quadratic, planar triangular, tetrahedral, simple cubic, body-centered cubic, and face-centered cubic lattices [see Eq.(5.16)-(5.21)].

(g) Using (f) molecular freedoms are computed in the pure dimer limit for the six lattices (see Table (iii)). Although in this region the Hartree series should work the worst, it gives good results.

(h) Using (f) the density and entropy are calculated for the six lattices (see Tables (v), (vi), (vii)) and an analysis of the numerical results are presented. Excellent accuracy is achieved ranging from .1% at high temperatures to up to 18 decimal places at low temperatures.

Consider first simple perturbation theory for the two dimensional dimer model. It is awkward and inferior compared to the Hartree improved series. With perturbation theory, however, it is

simpler to discuss the diagrammatic rules. They are then easily modified to accompany the Hartree improved series.

The Boltzmann factors for horizontal and vertical dimers are z_h and z_v . The rules for simple perturbation theory were given in the last section. To third order they involve the graphs in Fig. 12 which generate the expansion in Eq. (4.5). All terms are of the same form: constant $\times \sum_{\alpha_1 \dots \alpha_n} (\prod z\text{'s})$. By translational invariance, one of the summing indices (say α_1) may be fixed if one multiplies by N , the total number of sites. Therefore, in calculating $\frac{1}{N} \log Z$, fix one of the vertices of the graph. Each Fig. 12 graph generates several configurations due to embeddings. For example fix α to be the origin [$\alpha = (0,0)$] then the sums in column three of Fig. 12 yield several terms. Figure 19 illustrates this for graphs (a) and (b) of Fig. 12. The Fig. 12a graph results in four diagrams (Fig. 19a), while the graph in Fig. 12b results in sixteen diagrams (Fig. 19b). Notice some of the diagrams in Fig. 19 come in pairs, that is, the two diagrams have the same shape (i.e. a_1 and a_2 , a_3 and a_4 , b_1 and b_2 , etc.). This arises, in the case of Fig. 19a, because of the $\alpha \leftrightarrow \beta$ point symmetry in the graphs of Fig. 18a. If α and β are two different vertices, the symmetry maps diagrams a_1 and a_2 (and a_3 and a_4) into each other. The factor of $\frac{1}{2}$ in column 5 of Fig. 12 due to rule (d) is cancelled by the two diagrams. In general, the rule (d) factor will be cancelled among different diagrams all of the shape if all vertices have different locations. The diagrams b_{13} - b_{16} in Fig. 19 are exceptions. Under the $\alpha \leftrightarrow \gamma$ symmetry of Fig. 12b these diagrams are invariant and the group symmetry rule (d) factor is not cancelled.

It is clear what happens in general for a translationally invariant lattice. The modified rules are

Rules for a Dimer Problem on a Translationally Invariant Lattice

- (a) Draw all diagrams on the lattice with different shapes. Two graphs which are translates of each other but have the same shape are considered equivalent.
- (b) Each edge (Fig. 13) gives a factor $z_{\alpha\beta}$.
- (c) Each vertex of degree ℓ (Fig. 14) gives a factor of $(-1)^\ell(\ell-1)!$.
- (d) Treat vertices with different locations as being distinct; then there is a factor of [order of the point symmetry group of the diagram] $^{-1}$.
- (e) For each (pair of vertices with ℓ edges between them (Fig. 15)) there is a factor of $\frac{1}{\ell!}$.
- (f) $\Gamma = \frac{1}{N} \log Z = \sum_{\text{connected diagrams}} (\text{weight of diagram})$.

Figure 20 displays all diagrams to third order and their statistical factors (that is, their weights with Boltzmann factors extracted).

To third order

$$\frac{1}{N} \ln Z^{2-d \text{ dimer}} = z_h + z_v - \frac{3}{2} (z_h^2 + z_v^2) - 4z_h z_v + 16z_v z_h (z_h + z_v) + \dots \quad (5.1)$$

Consider now the Hartree-improved expansion. The Hartree propagator is $\left[\frac{-1 + \sqrt{1 + 8(z_h + z_v)}}{4(z_h + z_v)} \right]$. According to rule (b') of Section IV, for each horizontal edge, there is a factor

$$\omega_h = z_h \left(\frac{-1 + \sqrt{1 + 8(z_h + z_v)}}{4(z_h + z_v)} \right)^2, \quad (5.2)$$

and for each vertical dimer,

$$\omega_v = z_v \left(\frac{-1 + \sqrt{1 + 8(z_h + z_v)}}{4(z_h + z_v)} \right)^2. \quad (5.3)$$

The diagrammatic rules are the same as in "Rules for a Dimer Problem on a Translationally Invariant Lattice" with the above substitutions ($z_h \rightarrow \omega_h$ and $z_v \rightarrow \omega_v$) in rule (b) and diagrams with vertices of degree one are ignored. There is also a zeroth order contribution given in Eq. (4.15).

It is necessary to find all embeddings of Figure 18 graphs onto the square lattice. Fortunately, graphs with a cycle of an odd number of edges cannot be embedded and do not contribute. Only a subset of the Figure 18 graphs need be considered. Because of the large number of embeddings, it is convenient to define the concept of an "embedding graph". Many of the Figure 18 graphs have similar embeddings. An embedding graph groups these together so that they can all be embedded at once. This proves quite useful when calculating the Hartree series to sixth order. Consider, for example, the graph in box 6 of Figure 18. In summing over the four vertex locations separate out those terms where two summing indices have the same value. This results in a graph with the same summing structure as the box 5 graph of Figure 18 (see Figure 21). The embeddings of such terms from box 6 will be the same as the embeddings of box 5, and all such terms are grouped together in an "embedding graph". Box 5 of Figure 22 is the

corresponding embedding graph in this example. Its weight is the sum of the weights of contributing graphs as Figure 23 indicates.

Unfortunately, there appear to be no simple rules for calculating embedding graph weights. Figure 22 shows all embedding graphs and their weights to fifth order plus the sixth order loose-packed (those not involving cycles with an odd number of edges) ones. With embedding graphs, sum only over distinct vertex locations. For example, box 5 of Figure 22 represents the term

$$\frac{1}{[\text{point symmetry factor}]} (-1) \sum_{\substack{\alpha \neq \beta \\ \beta \neq \gamma \\ \gamma \neq \alpha}} \omega_{\alpha\beta}^2 \omega_{\beta\gamma}^2. \quad (5.4)$$

The [point symmetry factor] always goes away (basically rule (d) is operative but all vertices have different locations), and so it is omitted in Figure 22 weights. Using Figure 22 it is straightforward to calculate the Hartree expansion to sixth order:

$$\Gamma_{2\text{-d dimer}} = \log \left(\frac{1}{2} + \frac{1}{2} \sqrt{1 + 8(z_h + z_v)} \right) + \Gamma^{(1)}(\omega_h) + \Gamma^{(1)}(\omega_v) + \Gamma^{(2)}(\omega_h, \omega_v) + \dots, \quad (5.5)$$

where, for later convenience, terms of one-dimensional character are grouped into $\Gamma^{(1)}$ and terms of two-dimensional character are grouped into $\Gamma^{(2)}$:

$$\Gamma^{(1)}(\omega_h) = -\omega_h + \frac{1}{2}\omega_h^2 + \frac{2}{3}\omega_h^3 - \frac{3}{4}\omega_h^4 - \frac{6}{5}\omega_h^5 + \frac{5}{3}\omega_h^6 + \dots, \quad (5.6)$$

$$\Gamma^{(2)}(\omega_h, \omega_v) = -3\omega_h^2\omega_v^2 + 4(\omega_h\omega_v^4 + \omega_h^4\omega_v) + 4(\omega_h^2\omega_v^3 + \omega_h^3\omega_v^2) + 15(\omega_h^2\omega_v^4 + \omega_h^4\omega_v^2) + \dots. \quad (5.7)$$

A piece, $-\omega_h$, from the Hartree expansion has been regrouped into $\Gamma^{(1)}(\omega_h)$. The diagrams contributing to Eqs. (5.6) and (5.7) to fifth order are shown in Fig. 24. Sixth order graphs were omitted for reasons of space. The use of computers could extend this series to several more orders.

When expanded in powers of z_h and z_v , the low temperature expansion is recovered. Equation (5.5) will reproduce correctly terms to sixth order in z 's. Equation (5.5) will be very accurate at low temperatures. Since the Hartree expansion includes the effects of some higher order graphs, Eq. (5.5) is also expected to be good over a domain larger than the low temperature one. In fact, even though it is a modified low temperature low density expansion, the infinite temperature limit can be taken. This is because as $z_h \rightarrow \infty$ and $z_v \rightarrow \infty$, ω_h and ω_v approach constants. At infinite temperature the problem becomes the close-packed dimer model which has been solved²⁵. In the isotropic case (when $z_h = z_v = z$) the answer is

$$\Gamma^{\text{close-packed}} = \frac{1}{2} \log z + G/\pi \approx \frac{1}{2} \log z + .2916 \quad (5.8)$$

with G , Catalan's constant. The Hartree expansion in Eq.(5.5) gives

$$\Gamma \xrightarrow{z \rightarrow \infty} \frac{1}{2} \log z + .2803 \quad (5.9)$$

It is reassuring that the Hartree improved expansion is accurate in a region so far from its range of validity (low temperatures). This indicates that Eq. (5.5) is probably reasonably good over the entire range of z_h and z_v .

Having calculated the Hartree expansion to sixth order for the two-dimensional square lattice dimer model, it takes just a bit more work to obtain the Hartree expansion for the d dimensional hypercubic model to sixth order. Define

$$\begin{aligned} \Gamma^{(0)}(\{\omega_j\}) &= \log \left(\frac{1}{2} + \frac{1}{2} \sqrt{1 + 8 \sum_{i=1}^d \omega_i} \right), \\ \Gamma^{(3)}(\omega_1, \omega_2, \omega_3) &= 8(\omega_1 \omega_2^2 \omega_3^2 + \omega_1^2 \omega_2 \omega_3^2 + \omega_1^2 \omega_2^2 \omega_3) + 8\omega_1^2 \omega_2^2 \omega_3^2 \\ &- 16(\omega_1 \omega_2^2 \omega_3^3 + \omega_1 \omega_2^3 \omega_3^2 + \omega_1^2 \omega_2 \omega_3^3 + \omega_1^3 \omega_2 \omega_3^2 + \omega_1^2 \omega_2^3 \omega_3 + \omega_1^3 \omega_2^2 \omega_3) \\ &- 16 \left(\omega_1^4 \omega_2 \omega_3 + \omega_1 \omega_2^4 \omega_3 + \omega_1 \omega_2 \omega_3^4 \right), \end{aligned} \quad (5.10)$$

$$\begin{aligned} \Gamma^{(4)}(\omega_1, \omega_2, \omega_3, \omega_4) &= -32(\omega_1 \omega_2 \omega_3^2 \omega_4^2 + \omega_1 \omega_2^2 \omega_3 \omega_4^2 + \omega_1^2 \omega_2 \omega_3 \omega_4^2 \\ &+ \omega_1^2 \omega_2 \omega_3^2 \omega_4^2 + \omega_1^2 \omega_2^2 \omega_3 \omega_4^2 + \omega_1^2 \omega_2 \omega_3^2 \omega_4^2), \end{aligned}$$

where $\Gamma^{(0)}$ is the first piece of the Hartree approximation [Eq.(4.15)] and the ω_i are defined in Eq. (4.20). Then the Hartree expansion in d dimensions is

$$\begin{aligned} \Gamma(\{\omega_j\}) &= \Gamma_o(\{\omega_j\}) + \sum_{i=1}^d \Gamma^{(1)}(\omega_i) \\ &+ \sum_{i_1 < i_2}^d \Gamma^{(2)}(\omega_{i_1}, \omega_{i_2}) + \sum_{i_1 < i_2 < i_3}^d \Gamma^{(3)}(\omega_{i_1}, \omega_{i_2}, \omega_{i_3}) \\ &+ \sum_{i_1 < i_2 < i_3 < i_4}^d \Gamma^{(4)}(\omega_{i_1}, \omega_{i_2}, \omega_{i_3}, \omega_{i_4}) + \dots, \end{aligned} \quad (5.11)$$

where $\Gamma^{(1)}$ and $\Gamma^{(2)}$ are given on Eqs. (5.6) and (5.7) and the other Γ 's are given in Eq. (5.10). The superscript on the Γ 's refers to the dimension of the subspace of the imbedded diagram. Thus $\Gamma^{(n)}$ refers to those diagrams which are imbedded in an n dimension subspace of d -dimensional space.

In Sec. IV it was pointed out that, in the isotropic case, the expansion parameter, ω , gets smaller as the dimension of the lattice gets bigger. For the hypercubic lattice, $\omega = \frac{1}{2d} + 0 \left(\frac{1}{d^{3/2}} \right)$. This indicates that as d increases, the Hartree expansion works better and Eq. (5.11) will be an excellent approximation. The situation, however, is not so clear because the number of graphical embeddings increases with d . Let $d(G)$ be the dimension of the maximum space in which a graph can be embedded. A rough estimate of the number of embeddings of G is $(2d)^{d(G)} + O((2d)^{d(G)-1})$ for d large. The weight of G goes like $\left(\frac{1}{2d}\right)^b$ where b is the number of bonds, so that the total effect of G behaves like

$$\sim \frac{1}{(2d)^{(b-d(G))}}. \quad (5.12)$$

By inspection, it is found that $b - d(G) \geq 1$ for all graphs so that the effect of a graph is damped by a power of d . Graph 1 of Fig. 18 has the leading behavior, decreasing like $\frac{1}{d}$. There are many (an infinite number of) next to leading order graphs (i.e. graphs 3, 5, 6, 14, 24, etc. of Fig. 18) which behave as $\frac{1}{d^2}$. Thus as $d \rightarrow \infty$ the contribution of any given graph gets smaller. The Hartree expansion is better when d is bigger. Explicit examination of several series also seems to verify this. It appears that results in higher dimensions become more accurate.

Because of this, the hypercubic dimer model is exactly solvable in the $d \rightarrow \infty$ limit. Trivial algebra yields

$$\Gamma_{(z)}^{\text{d-dim. dimer}} \xrightarrow{d \rightarrow \infty} \frac{1}{2} \log d + \frac{1}{2} \log 2z - \frac{1}{2} + \frac{2}{(8zd)^{\frac{1}{2}}} + \left(1 - \frac{1}{z}\right) \frac{1}{8d} + \frac{1}{(8zd)^{\frac{1}{2}2d}} \left(\frac{1}{12z} - 1\right) + o\left(\frac{1}{d}\right). \quad (5.13)$$

Equation (5.13) was obtained by blindly expanding the Hartree improved series in powers of $1/d$. It is clear from Eq. (5.13) that not only must $d \gg 1$ but also $dz \gg 1$ so that z cannot be too small. Equation (5.13) is one of the interesting results in this section.

Since the Hartree approximation and graph 1 of Fig. 18 were the only inputs in Eq. (5.13), Eq. (5.13) will hold for any uniform loose-packed lattice for which the vertex degree (coordination number), q , is large. For hypercubic lattices $q = 2d$. In fact the result holds for lattices not containing a triangle so that triangle graphs

(graph 2 of Fig. 18) are absent. This triangle graph can potentially be of order $\left(\frac{1}{q}\right)$. Because $\omega \sim \frac{1}{q}$ these dimer models are exactly solvable in the $q \rightarrow \infty$ limit:

$$\Gamma_{(z)}^{\text{dimer}} \xrightarrow{q \rightarrow \infty} \frac{1}{2} \log \frac{q}{2} + \frac{1}{2} \log(2z) - \frac{1}{2} + \frac{2}{(4zq)^{\frac{1}{2}}} + \left(1 - \frac{1}{z}\right) \frac{1}{4q} + \frac{1}{(4zq)^{\frac{1}{2}q}} \left(\frac{1}{12z} - 1\right) + o\left(\frac{1}{q}\right). \quad (5.14)$$

For lattices with triangles Eq. (5.14) is valid to order $\left(\frac{1}{z}\right)$:

$$\Gamma_{(z)}^{\text{dimer, lattice with triangles}} \xrightarrow{q \rightarrow \infty} \frac{1}{z} \log \frac{q}{2} + \frac{1}{2} \log(2z) - \frac{1}{2} + \frac{2}{(4zq)^{\frac{1}{2}}} + o\left(\frac{1}{q}\right). \quad (5.15)$$

Both Eqs. (5.14) and (5.15) are only valid if $zq \gg 1$ as well as $q \gg 1$. It is interesting that dimer models are exactly solvable in this limit. In the pure dimer limit, Eqs. (5.14) and (5.15) give rough approximations for the molecular freedom. A comparison with exact and estimated molecular freedoms is presented in Table (ii) for several models. The lattices are the one dimensional (1-d), simple quadratic (sq), tetrahedral (t), simple cubic (sc), body-centered cubic (bcc), planar triangular (pt), and face-centered cubic (fcc) lattices. The latter two contain triangles and the results are not expected to be as good as lattices without triangles. The results are accurate to several per cent, even though the q value is not that large.

Gaunt²¹ has calculated low temperature expansions for several dimer models. These included both two and three dimensional systems. The expansions were for the isotropic case in which all z_i 's were equal. The low temperature expansion were computed for various lattices to these orders: the simple quadratic lattice to 15 orders, the planar triangle lattice to 10 orders, the tetrahedral lattice to 16 orders, the simple cubic lattice to 12 orders, the body-centered cubic lattice to 12 orders, and the face-centered cubic lattice to 8 orders. When expanded in powers of z the Hartree expansion to order n is guaranteed to reproduce the low temperature expansion to order n . Hence n orders of low temperature expansion uniquely determine n orders of Hartree expansion and Gaunt's series can be used to obtain the Hartree series to many orders. The Hartree series in the isotropic case has been calculated this way for the abovementioned lattices. The results are

$$\begin{aligned} \Gamma^{\text{sq}}(\omega) = & \log\left(\frac{1}{1-4\omega}\right) - 2\omega + \omega^2 + \frac{1}{3}\omega^3 - 4\frac{2}{3}\omega^4 + 13\frac{3}{5}\omega^5 \\ & + 33\frac{1}{3}\omega^6 - 106\frac{2}{7}\omega^7 + 273\frac{3}{4}\omega^8 + 1432\frac{4}{9}\omega^9 - 2816\frac{4}{5}\omega^{10} \\ & + 6197\frac{9}{11}\omega^{11} + 63602\omega^{12} - 93974\frac{2}{13}\omega^{13} - 446\frac{6}{7}\omega^{14} \\ & + 2667238\frac{14}{15}\omega^{15} + \dots, \end{aligned} \quad (5.16)$$

$$\begin{aligned} \Gamma^{\text{pt}}(\omega) = & \log\left(\frac{1}{1-6\omega}\right) - 3\omega + 1\frac{1}{2}\omega^2 - 23\frac{1}{4}\omega^4 + 92\frac{2}{5}\omega^5 \\ & - 8\omega^6 - 1743\frac{3}{7}\omega^7 + 8202\frac{3}{8}\omega^8 - 1478\omega^9 - 196618\frac{1}{5}\omega^{10} + \dots, \end{aligned} \quad (5.17)$$

$$\begin{aligned} \Gamma^{\text{t}}(\omega) = & \log\left(\frac{1}{1-4\omega}\right) - 2\omega + \omega^2 + \frac{1}{3}\omega^3 - \frac{5}{2}\omega^4 + \frac{3}{5}\omega^5 \\ & + 21\frac{1}{3}\omega^6 - 66\frac{2}{7}\omega^7 + 186\frac{1}{4}\omega^8 + 472\frac{4}{9}\omega^9 - 2744\frac{4}{5}\omega^{10} \\ & + 4493\frac{9}{11}\omega^{11} + 19074\frac{2}{3}\omega^{12} - 91614\frac{2}{13}\omega^{13} + 192537\frac{1}{7}\omega^{14} \\ & + 952636\frac{4}{15}\omega^{15} - 3910844\frac{7}{8}\omega^{16} + \dots, \end{aligned} \quad (5.18)$$

$$\begin{aligned} \Gamma^{\text{sc}}(\omega) = & \log\left(\frac{1}{1-6\omega}\right) - 3\omega + \frac{1}{2}\omega^2 + 2\omega^3 - 11\frac{1}{4}\omega^4 + 68\frac{2}{5}\omega^5 \\ & - 41\omega^6 - 279\frac{3}{7}\omega^7 + 5688\frac{3}{8}\omega^8 - 12695\frac{1}{3}\omega^9 + 10999\frac{4}{5}\omega^{10} \\ & + 543356\frac{8}{11}\omega^{11} - 2067458\frac{1}{2}\omega^{12} + \dots, \end{aligned} \quad (5.19)$$

$$\begin{aligned} \Gamma^{\text{bcc}}(\omega) = & \log\left(\frac{1}{1-8\omega}\right) - 4\omega + 2\omega^2 + \frac{2}{3}\omega^3 - 15\omega^4 + 235\frac{1}{5}\omega^5 \\ & - 645\frac{1}{3}\omega^6 + 1979\frac{3}{7}\omega^7 + 30390\frac{1}{2}\omega^8 - 189343\frac{1}{9}\omega^9 + 1370054\frac{2}{5}\omega^{10} \\ & + 1393387\frac{7}{11}\omega^{11} - 35573416\omega^{12} + \dots, \end{aligned} \quad (5.20)$$

$$\begin{aligned} \Gamma^{\text{fcc}}(\omega) = & \log\left(\frac{1}{1-12\omega}\right) - 6\omega + 3\omega^2 - 4\omega^3 - 79\frac{1}{2}\omega^4 + 1192\frac{4}{5}\omega^5 \\ & - 10232\omega^6 + 48353\frac{1}{7}\omega^7 + 166814\frac{1}{4}\omega^8 + \dots, \end{aligned} \quad (5.21)$$

where ω is defined in terms of z and the coordination number, q , by

$$\omega = z \left(\frac{-1 + \sqrt{1 + 4qz}}{2qz} \right)^2, \quad (5.22)$$

or

$$z = \frac{\omega}{(1 - q\omega)^2} \quad (5.23)$$

The coordination numbers of the various lattices can be found in Table (ii).

By taking $z \rightarrow \infty$ and using the truncated series in Eqs. (5.16)-(5.21) the molecular freedoms at close packing can be calculated. These along with a comparison to other methods are shown in Table (iii). Rough error estimates are also included. As expected more accuracy is obtained for models with larger q 's. As an indication of what is obtainable "by hand" (that is, without the use of computers) sixth order computations are also shown. Even at this order molecular freedoms are correct to 1% or 2% for lattices with small q and to less than 1% for lattices with larger q . At maximum order results are correct to within .1% for large q lattices and within $\frac{1}{2}\%$ for the low q lattices with the exception of the simple quadratic lattice where the error persists at 1%.

For the hypercubic models in dimensions one, two, and three, Table (iv) shows the molecular freedom estimates order by order as calculated by the Hartree series and, for comparative reasons, by Nagle's series extended by Gaunt. The Bethe approximation (order one in Nagle's series), being more physical, is a better starting point than the Hartree approximation (order one in the Hartree series) although after a few orders both methods approach exact or estimated molecular freedoms in a similar manner.

The dimer density, ρ , normalized so that at close-packing $\rho = \frac{1}{q}$, is

$$\rho = \frac{2}{q} z \frac{d\Gamma}{dz} \quad (5.24)$$

The quantity $\frac{q}{2}\rho$ is the number of dimers per site, whereas ρ is the number of dimers per bond. The entropy, S , and molecular freedom, ϕ , are

$$\begin{aligned} S &= -\rho \ln z + \frac{2}{q} \Gamma, \\ \phi &= \exp(qS). \end{aligned} \quad (5.25)$$

Tables (v), (vi), and (vii) show the numerical values of ρ and S as a function of $\frac{\omega}{\omega_{\max}}$ (ω is the Hartree expansion parameter [Eq. (5.22)] and

$$\omega_{\max} \equiv \frac{1}{q}, \quad (5.26)$$

is the maximum physical value of ω). These numerical values were computed from the truncated series in Eqs. (5.16)-(5.21). The subscripts on ρ and S in tables (v), (vi), and (vii) indicate the orders at which the series were truncated.

Notice that lattices with the same coordination number (table (v) and table (vi)) have almost identical entropies and almost identical densities. Only at extremely high temperatures do they begin to deviate for different models. Mathematically the reason for this is simple: Models have a universal (as far as q is concerned) Hartree expansion to order ω^2 :

$$\Gamma_{(\omega)}^q = \log \left(\frac{1}{1-q\omega} \right) - \frac{q}{2} \omega + \frac{q}{4} \omega^2 + (\text{non-universal}). \quad (5.27)$$

Because the Hartree series at second order is already a good approximation models with the same q have almost identical properties. Furthermore in higher orders, they will have many identical Feynman graphs. In fact for lattices without triangles subgraphs, Eq.(5.27) is universal to third order

$$\Gamma_{(\omega)}^q = \log \left(\frac{1}{1-q\omega} \right) - \frac{q}{2} \omega + \frac{q}{4} \omega^2 + \frac{q}{3} \omega^3 + (\text{non-universal}). \quad (5.28)$$

Next, notice that ω is a good approximation to the density, ρ . For the simple quadratic and tetrahedral lattices, for the planar triangular simple cubic, and body-centered cubic lattices and for the face-centered cubic lattice, ρ and ω never differ by more than about 5%, 3%, and 1%. The reason for this is simple: Equation (5.24) implies the

$$\rho = \left\langle z \prod_{\vec{x}} \prod_{\vec{x}'} \eta_{\vec{x}} \eta_{\vec{x}'}^\dagger \right\rangle, \quad (5.29)$$

where \vec{x} and \vec{x}' are nearest neighbors. In the Hartree approximation

$$\rho \approx z \left(\left\langle \prod_{\vec{x}} \eta_{\vec{x}} \right\rangle_H \right)^2 \equiv \omega. \quad (5.30)$$

In other words, ω is the Hartree approximation to the density. From this point of view the Hartree series has a more physical flavor: it is an expansion in a parameter which is approximately the density.

Tables (iii), (v), (vi), and (vii) have error estimates. The uncertainty is in the last two figures, so that, for example, the sq lattice at $\omega = .225$ has $\rho_{15} = .22998 \pm .00020$. These errors are set to the contribution of the last order. Doing this works only when the numerical coefficient of the maximum power of ω is not unnaturally small. This turns out to be the case for all the models considered. Since the Hartree series seem to converge this is a rough but reasonable measure of the error. As a check, the exactly solvable one dimensional dimer model can be used. Its Hartree expansion to 16th order is

$$\begin{aligned}
\Gamma(\omega)^{1-d} = & \log\left(\frac{1}{1-2\omega}\right) - \omega + \frac{1}{2}\omega^2 + \frac{2}{3}\omega^3 - \frac{3}{4}\omega^4 - \frac{1}{5}\omega^5 \\
& + \frac{1}{3}\omega^6 + \frac{2}{7}\omega^7 - \frac{4}{8}\omega^8 - \frac{7}{9}\omega^9 + \frac{12}{5}\omega^{10} + \frac{22}{11}\omega^{11} \\
& - 38\frac{1}{2}\omega^{12} - 71\frac{1}{13}\omega^{13} + 122\frac{4}{7}\omega^{14} + 228\frac{4}{5}\omega^{15} - 402\frac{3}{16}\omega^{16} + \dots
\end{aligned} \quad (5.31)$$

Table (viii) displays the approximated ρ_{16} , the exact ρ , the approximated S_{16} , and the exact S . The same error estimate method was used. As can be seen the exact results always fall within the "error bar" region. In fact estimated errors are roughly 5 times actual errors. For the one dimensional model this is a conservative method of estimating errors.

Tables (v), (vi), and (vii) show excellent accuracy. In 90% of the physical region (as measured by ω) the density and entropy are at least computed to .1% for all models. For the bcc and fcc lattices the minimal accuracy is about 5 decimal places. It is only for dense systems (i.e. 90% maximal dimer density) that errors are even of the above stated size. For example, at 10% maximal dimer density results for the six models are accurate to an estimated 17, 18, 11, 14, 14, and 11 decimal places. As expected at low dimer densities best accuracy is achieved for those models for which the series has been computed to the most orders whereas at high densities best accuracy occurs for models with the highest q .

VI. THE 1/N EXPANSION

This section develops another expansion method: the 1/N expansion (N is not to be identified with the total number of sites). In recent years 1/N expansions have been popular in particle physics²⁶. Like the Hartree-improved perturbation series, they are

semi-perturbative in the sense that they include the effects of higher order graphs. In many body theory the 1/N expansion is similar to the "ring approximation" or the "random phase approximation"²⁴. Throughout this paper I will use the terminology "1/N expansion" rather than "ring approximation" or "random phase approximation".

This section is organized as follows: A brief introduction to the 1/N method is presented. The method is then applied to the two-dimensional dimer model. This calculation, carried out to second order, is illustrative. The 1/N expansion is applicable to any dimer model and can be generalized to any fermionic-like system. Next 1/N Feynman rules are given. This is a useful set of graphical rules. Finally the meaning of 1/N is explained. Given any dimer model in any dimension or on any lattice, a modified dimer model with a local $U(N)$ symmetry can be constructed. As $N \rightarrow \infty$ these models become exactly solvable. This is one of the important results of this section: a whole class of (limiting) dimer problems is solved.

Sections IV and V showed how to calculate corrections to the Hartree approximation by considering the Hartree-improved graphs of Fig. 18. That method expands in the number of graph edges; box 1 of Fig. 18 is of second order, box 6 of Fig. 18 is of fourth order. The expansion parameters, $\omega_{\alpha\beta} = g_{\alpha} z_{\alpha\beta} g_{\beta}$, are given in Eq. (4.20) for dimer models in d -dimensions. Another expansion is the 1/N expansion. Its zeroth order is also the Hartree approximation. It also allows one to systematically calculate corrections to the Hartree approximation. Instead of expanding in powers of graph edge, it expands

in the number of graphical loops (in particle physics loop expansions are called semi-classical or \hbar (Planck's constant) expansions). Boxes 1, 2, 6, etc. in Fig. 18 have one loop, boxes 3, 4, 5, 11, etc. have two loops, and so on. First order in $1/N$ sums all the one loop graphs, second order sums all two loop graphs, etc. After first order the effect of the $1/N$ expansion is to eliminate all graphs with vertices of degree two. Instead a "superpropagator", $G_{\alpha\alpha'}^S$, (see Fig. 25) is used which includes all vertices of degree two. $G_{\alpha\alpha'}^S$ is a sum over all graphs of the type in Fig. 25 which go from α to α' . In terms of the superpropagator, denoted by a bolder line, the one loop graphs are represented as in Fig. 26 and the two loop graphs as in Fig. 27.

The $1/N$ expansion will be illustrated for the two-dimensional dimer model. The method, of course, can be applied to any dimer problem. The imbedding of Fig. 26 graphs into the two-dimensional lattice is related to finding all closed random walks. Such a problem has been considered by Temperley²⁷. His method will be used here. Consider $[\exp(ip_x) + \exp(-ip_x) + \exp(ip_y) + \exp(-ip_y)]^M = [\exp(ip_x) + \exp(-ip_x) + \exp(ip_y) + \exp(-ip_y)] \cdots [\exp(ip_x) + \exp(-ip_x) + \exp(ip_y) + \exp(-ip_y)]$. Multiplying out the brackets is equivalent to choosing a term from each bracket, multiplying the chosen factors, and summing over all choices. Associate choosing $\exp(ip_x)$ with taking a step in the $+x$ direction. Likewise associate $\exp(-ip_x)$, $\exp(ip_y)$, and $\exp(-ip_y)$ with taking steps in the $-x$, $+y$, and $-y$ directions. Then each term in the above expansion is associated with a random walk M steps long. The coefficient of $\exp(inp_x + ilp_y)$ in $[2 \cos p_x + 2 \cos p_y]^M$ is

the number of walks from $(0,0)$ to (n,ℓ) in an M step process. Call this number $C_{n,\ell}^M$; then

$$C_{n,\ell}^M = \int_{-\pi}^{\pi} \frac{dp_x}{2\pi} \int_{-\pi}^{\pi} \frac{dp_y}{2\pi} \exp(-ip_x n - ip_y \ell) [2 \cos p_x + 2 \cos p_y]^M. \quad (6.1)$$

In the Feynman graphs of Fig. 25 horizontal sides are weighted by ω_h and vertical sides by ω_v . In addition there is a (-1) for each vertex. The superpropagator sums these weighted walks and also sums over M . Therefore,

$$G_{n,\ell}^S = \sum_{M=1}^{\infty} (-1)^{M+1} \int_{-\pi}^{\pi} \frac{dp_x}{2\pi} \int_{-\pi}^{\pi} \frac{dp_y}{2\pi} \exp(-ip_x n - ip_y \ell) [2\omega_h \cos p_x + 2\omega_v \cos p_y]^M \\ = \int_{-\pi}^{\pi} \frac{dp_x}{2\pi} \int_{-\pi}^{\pi} \frac{dp_y}{2\pi} \frac{\exp(-ip_x n - ip_y \ell) (2\omega_h \cos p_x + 2\omega_v \cos p_y)}{(1 + 2\omega_h \cos p_x + 2\omega_v \cos p_y)} \quad (6.2)$$

Now the one loop graphs of Fig. 26 can be summed. For a loop with M vertices, rule (d) of Sec. IV gives a factor of $\frac{1}{2M}$. The contribution of one loop graphs, $\Sigma^{(1)}$, is

$$\Sigma^{(1)} = N \sum_{M=1}^{\infty} \frac{(-1)^M}{2M} \int_{-\pi}^{\pi} \frac{dp_x}{2\pi} \int_{-\pi}^{\pi} \frac{dp_y}{2\pi} (2\omega_h \cos p_x + 2\omega_v \cos p_y)^M \\ = N (-) \int_{-\pi}^{\pi} \frac{dp_x}{2\pi} \int_{-\pi}^{\pi} \frac{dp_y}{2\pi} \ln(1 + 2\omega_h \cos p_x + 2\omega_v \cos p_y), \quad (6.3)$$

where N is the total number of sites, so that the contribution to Γ is

$$\Gamma^{(1)} = - \int_{-\pi}^{\pi} \frac{dp_x}{2\pi} \int_{-\pi}^{\pi} \frac{dp_y}{2\pi} \ln(1 + 2\omega_h \cos p_x + 2\omega_v \cos p_y). \quad (6.4)$$

For the d -dimensional hypercubic dimer problem the result would be

$$\Gamma_{d\text{-dimensions}}^{(1)} = - \int \frac{d^d p}{(2\pi)^d} \ln \left(1 + \sum_{i=1}^d 2\omega_i \cos p_i \right). \quad (6.5)$$

Because $\omega_i < \frac{1}{2}$ for finite temperature, the argument of the logarithm cannot vanish and $\Gamma^{(1)}$ is analytic in the temperature. The only possible non-analyticity can occur for $\omega_i \rightarrow \frac{1}{2}$, that is, the pure dimer limit. In this approximation the absence of a phase transition except possibly in a pure dimer limit is in complete accord with reference 12.

For graphs with two or more loops, a set of $1/N$ Feynman rules are easily derived. Perhaps the graphs should be called "supergraphs" since they use superpropagators.

$\frac{1}{N}$ Feynman Rules For Supergraphs

(a) Draw all topologically distinct graphs consisting of any number of vertices. Vertices must have at least three lines attached to them (vertex degree ≥ 3). Tadpoles (see Fig. 28) are allowed.

(b) For each edge between (α, β) and (α', β') associate a factor of G^S where G^S is given in Eq. (6.2).
 $\alpha \sim \alpha, \beta \sim \beta$

(c) For a vertex at (α, β) with ℓ lines emanating from it (see Fig. 14), put in a factor of $(-1) \sum_{\alpha\beta} (\ell-1)!$.

(d) Put in a factor of [the order of the point symmetry group of graph] $^{-1}$.

(e) For each pair of vertices with ℓ degenerate edges between them (see Fig. 15) put in a factor of $\frac{1}{\ell!}$.

(f) For a vertex with ℓ tadpoles (see Fig. 28), put in a factor of $\frac{1}{2^{\ell} \ell!}$.

(g) $\Gamma = \Gamma^H + \Gamma^{(1)} + \sum_{\text{connected graphs}} (\text{weight of graph})$ where Γ^H is the Hartree approximation (Eq. (4.15)) and $\Gamma^{(1)}$ is the one loop contribution (Eq. (6.4)).

The graphs in Fig. 27 respectively give a two loop contribution of

$$\Gamma^{(2)} = - \frac{3}{4} [G_{od}^S]^2 + \frac{1}{2} [G_{oo}^S]^2 \sum_{\alpha\beta} G_{\alpha\beta}^S + \frac{1}{3} \sum_{\alpha\beta} [G_{\alpha\beta}^S]^3. \quad (6.6)$$

There are also momentum space Feynman rules: The statistical factors in rules (a), (c), (d), (e), and (f) remain the same. In rule (c) one no longer sums over a vertex's coordinates, instead one assigns loop momentum in the standard manner²⁴. There is a factor of $\int_{-\pi}^{\pi} \frac{d^d p}{(2\pi)^d}$ for each loop momentum. The momentum of a particular line is determined by the total loop momenta flowing in the line. For an edge with momentum \vec{p} there is a factor of

$$G^S(\vec{p}) = \frac{+ 2\omega_h \cos p_x + 2\omega_v \cos p_y}{1 + 2\omega_h \cos p_x + 2\omega_v \cos p_y} \quad (6.7)$$

$$= - \frac{1}{1 + 2\omega_h \cos p_x + 2\omega_v \cos p_y} + 1.$$

In momentum space Eq. (6.6) becomes

$$\begin{aligned}
\Gamma^{(2)} = & -\frac{3}{4} \left[\int \frac{d^2 p}{(2\pi)^2} G^S(p) \right]^2 \\
& + \frac{1}{2} \left(\frac{-2\omega_h - 2\omega_v}{1 + 2\omega_h + 2\omega_v} \right) \left[\int \frac{d^2 p}{(2\pi)^2} G^S(p) \right]^2 \\
& + \frac{1}{3} \int \frac{d^2 p_1}{(2\pi)^2} \int \frac{d^2 p_2}{(2\pi)^2} G^S(p_1) G^S(p_2) G^S(p_1 + p_2).
\end{aligned} \tag{6.8}$$

It's not too difficult to find the relevant graphs to several orders in loop number. When the $1/N$ expansion is calculated to order (n) and re-expressed in terms of z (or ω), it is guaranteed to reproduce the first $(n+1)$ terms in the low temperature z (or Hartree-improved ω) expansion. Since the Hartree-improved series works well, the $1/N$ expansion, which includes higher order Hartree-improved graphs, may produce an even better series. The drawback is that the result is in integral form (as exemplified in Eq.(6.8)). Although it's easy to write down a graph's contribution in integral form, the integrals themselves are cumbersome to do analytically (the first two terms in Eq. (6.8) can be related to complete elliptic integrals). This means that numerical comparisons are not possible unless numerical integration is performed. Such an undertaking is not attempted here.

What is the expansion parameter in the $1/N$ expansion?

The answer is $1/N$. What is N ? The answer for the two-dimensional dimer model is $N = 1$.

In general, N represents some internal symmetry index. In particle physics it could be the N in $U(N)$, $O(N)$, or $SU(N)$. N might be the number of colors or flavors in a modern theory of strong

interactions (quantum chromodynamics) or of weak and electromagnetic interactions (quantum flavodynamics). Take the two dimensional dimer model consisting of monomers and dimers. Introduce an internal symmetry by having different types of monomers, say N types. One could color them with N different colors. Allow dimers (which are just pairs of monomers) to have colored monomer endpoints. There would be N^2 different types of dimers. The corresponding anti-commuting variable action is

$$\begin{aligned}
A^{2-d} \text{ chromodimer}(z_h, z_v, N) = & \sum_{\alpha\beta} \left[\sum_{i=1}^N \eta_{\alpha\beta}^i \eta_{\alpha\beta}^{i\dagger} + \right. \\
& \left. + \sum_{i=1}^N \sum_{j=1}^N \left(\frac{z_h}{N} \eta_{\alpha\beta}^i \eta_{\alpha\beta}^{i\dagger} \eta_{\alpha+1\beta}^j \eta_{\alpha+1\beta}^{j\dagger} + \frac{z_v}{N} \eta_{\alpha\beta}^i \eta_{\alpha\beta}^{i\dagger} \eta_{\alpha\beta+1}^j \eta_{\alpha\beta+1}^{j\dagger} \right) \right].
\end{aligned} \tag{6.9}$$

The indices i and j label different colors. The action in Eq.(6.9) is invariant under local $U(N)$ transformations: $\eta_{\alpha\beta}^i \rightarrow \sum_j U_{\alpha\beta}^{ij} \eta_{\alpha\beta}^j$ and $\eta_{\alpha\beta}^{i\dagger} \rightarrow \sum_j (U^\dagger)_{\alpha\beta}^{ij} \eta_{\alpha\beta}^{j\dagger}$ for $N \times N$ unitary matrices $U_{\alpha\beta}$. The subscript on U indicates that these unitary matrices may vary from site to site.

The factor of $1/N$ in z_h/N (or z_v/N) in Eq. (6.9) is put in for convenience, since z_h (or z_v) can be varied independently of N . More precisely, it is indicative of the limit to be considered: N is to become large while z_h and z_v remain fixed. The Feynman graphs in simple perturbation theory for this chromodimer model are exactly the same as for the normal ($N = 1$) dimer models (those graphs typified in Fig. 20). The weights of graphs are also the same except that fermion loops now come in N colors. This means that each fermion

loop gives an extra factor of N . Each bond gives a factor of z_h/N or z_v/N because of the $\frac{1}{N}$ factors in Eq. (6.9). The N dependence of graphs is easily determined: For tree graphs (such as in Fig. 17) the contribution is N times the corresponding normal ($N=1$) dimer model contribution; for one loop graphs (Fig. 26), the contribution is exactly the same; and for two loop graphs the contribution is $1/N$ times the corresponding $N=1$ dimer model contribution. Thus, if the loop expansion in the dimer model is

$$\Gamma^{\text{dimer}} = \sum_{n=0}^{\infty} \Gamma^{(n)}, \quad (6.10)$$

with the superscript (n) being the number of loops, then

$$\Gamma^{\text{chromodimer}} = \sum_{n=0}^{\infty} \frac{1}{N^{n-1}} \Gamma^{(n)}. \quad (6.11)$$

Graphs with many loops contribute less as $N \rightarrow \infty$. Equation (6.11) explains why the $1/N$ expansion is called the $1/N$ expansion.

In conclusion

$$\begin{aligned} & \Gamma^{\text{2-d chromodimer}}(z_h, z_v, N) \xrightarrow{N \rightarrow \infty} \\ & N \log \left(\frac{1}{2} + \frac{1}{2} \sqrt{1 + 8(z_h + z_v)} \right) \\ & - \frac{N}{16(z_v + z_h)} \left(-1 + \sqrt{1 + 8(z_v + z_h)} \right) \\ & - \int_{-\pi}^{\pi} \frac{dp_x}{2\pi} \int_{-\pi}^{\pi} \frac{dp_y}{2\pi} \ln(1 + 2\omega_h \cos p_x + 2\omega_v \cos p_y) \\ & + o\left(\frac{1}{N}\right), \end{aligned} \quad (6.12)$$

and the large N limit of the model is exactly solved. For N very large the Hartree approximation (times N) is the answer. When N is large but finite the $1/N$ Feynman rules systematically calculate corrections. This is not the first time a model has been found solvable in an " N goes to infinity" limit. There is the spherical model²⁸, whose structure and solution are similar to that of Eq.(6.12).

The large N method, of course, is applicable to any dimer model. The Hartree approximation is the zero loop approximation. The one loop contribution, $\Gamma^{(1)}$, is the sum over all closed random walks weighted by the $\omega_{\alpha\beta}$ factors and a $\frac{(-1)^M}{2^M}$ for an M -step walk. The superpropagator, $G_{\alpha\alpha}^S$, is determined by summing over all random walks going from site α to site α weighted by $(-1)^{M+1}$ and $\omega_{\alpha\beta}$ factors. The Feynman rules are identical to those given above except for each edge (see Fig. 13) one uses $G_{\alpha\beta}^S$. A chromodimer model can be constructed from any dimer model. In such a model loops are suppressed by $1/N$ factors. The chromodimer analog of Eqs.(I.3.6) and (4.1) is described by the anticommuting action

$$A = \sum_{\alpha} \sum_{i=1}^N \eta_{\alpha}^i \eta_{\alpha}^{i\dagger} + \frac{1}{2} \sum_{\alpha\beta} \sum_{i=1}^N \sum_{j=1}^N \frac{z_{\alpha\beta}}{N} \eta_{\alpha}^i \eta_{\alpha}^{i\dagger} \eta_{\beta}^j \eta_{\beta}^{j\dagger}. \quad (6.13)$$

It is the same dimer model with N different colored monomers at each site. The models in Eq.(6.13) are all exactly solvable as $N \rightarrow \infty$. The result is N times the Hartree approximation given in Eqs. (4.9) and (4.10). Thus, given any dimer model its "chromo" version can be constructed and exactly solved in the $N \rightarrow \infty$ limit. An infinite class of (limiting) dimer models has been solved.

VII. THE ONE-DIMENSIONAL DIMER AND MULTIPOLYMER SYSTEMS

This section will solve the one-dimensional dimer problem via the anticommuting variable method. Since it is trivially solvable by transfermatrix (as well as other) methods, why solve it again using anticommuting variables? The answer is as follows: every exactly solvable model is a starting point for attacking unsolved problems via perturbative and/or other techniques. It is important to find as many models solvable via anticommuting variables as possible. These can be the base for approximations as will be demonstrated.

The formulas developed in this section will be used in subsequent sections. Given a solvable model (i.e. a quadratic action) all anticommuting variable correlation functions can be calculated. If ordinary correlation functions can be related to anticommuting variable ones then all correlation functions are calculable [this happens, for example, with the Ising model (see II)] and the model is completely solved. Everything possible can, in principle, be calculated. This section will calculate the anticommuting variable correlation functions. These formulas are valuable.

It happens that the same trick which solves the one-dimensional dimer model can solve the more complicated system consisting simultaneously of dimers, trimers, quadrimers, etc. This very general system again can be the starting point for approximating other unsolvable systems.

The main results are the one-dimensional dimer anticommuting variable correlation functions in Eq. (7.7), the one-dimensional multipolymer solution in Eq. (7.14), and its corresponding anticommuting variable correlation functions in Eq. (7.15).

The one-dimensional dimer action is

$$A^{1-d \text{ dimer}}(z) = \sum_{\alpha} (\eta_{\alpha} \eta_{\alpha}^{\dagger} + z \eta_{\alpha} \eta_{\alpha+1}^{\dagger} \eta_{\alpha+1}^{\dagger}). \quad (7.1)$$

Suppose $z \eta_{\alpha} \eta_{\alpha+1}^{\dagger} \eta_{\alpha+1}^{\dagger}$ is replaced by $z^{\frac{1}{2}} (\eta_{\alpha} \eta_{\alpha+1}^{\dagger} + \eta_{\alpha}^{\dagger} \eta_{\alpha+1})$. Then $\exp z^{\frac{1}{2}} (\eta_{\alpha} \eta_{\alpha+1}^{\dagger} + \eta_{\alpha}^{\dagger} \eta_{\alpha+1}) = 1 + z^{\frac{1}{2}} (\eta_{\alpha} \eta_{\alpha+1}^{\dagger} + \eta_{\alpha}^{\dagger} \eta_{\alpha+1}) + z (\eta_{\alpha} \eta_{\alpha+1}^{\dagger} \eta_{\alpha+1}^{\dagger})$ contains the wanted "1" term and the wanted $z \eta_{\alpha} \eta_{\alpha+1}^{\dagger} \eta_{\alpha+1}^{\dagger}$ term in $\exp(z \eta_{\alpha} \eta_{\alpha+1}^{\dagger} \eta_{\alpha+1}^{\dagger})$. What about the unwanted terms $z^{\frac{1}{2}} \eta_{\alpha} \eta_{\alpha+1}^{\dagger}$ and $z^{\frac{1}{2}} \eta_{\alpha}^{\dagger} \eta_{\alpha+1}$? They do not contribute. If they are used x's and o's cannot fill all anticommuting variable sites as Fig. 29 illustrates. There is always a leftover "o" and "x" at the end of a string of \otimes 's. They might contribute if periodic boundary conditions are used: they could "loop around" the entire line. For $z < 1$ these configurations carry negligible weight. In any case they are washed out in the thermodynamic limit. One may take

$$A^{1-d \text{ dimer}}(z) = \sum_{\alpha} \left[\eta_{\alpha} \eta_{\alpha}^{\dagger} + z^{\frac{1}{2}} (\eta_{\alpha} \eta_{\alpha+1}^{\dagger} + \eta_{\alpha}^{\dagger} \eta_{\alpha+1}) \right], \quad (7.2)$$

which in momentum space is

$$A^{1-d \text{ dimer}}(z) = \sum_s \left[a_s a_s^{\dagger} + z^{\frac{1}{2}} a_s a_s^{\dagger} \left(\exp\left(\frac{-2\pi i s}{2N+1}\right) - \exp\left(\frac{2\pi i s}{2N+1}\right) \right) \right]. \quad (7.3)$$

The thermodynamic limit may be taken and results in a grand potential per unit site of

$$\Gamma(z) = \int_{-\pi}^{\pi} \frac{dp_x}{2\pi} \ln[1 - 2iz^{\frac{1}{2}} \sin p_x] \quad (7.4)$$

$$= \ln[\frac{1}{2} + \frac{1}{2} \sqrt{1 + 4z}],$$

which is the known answer.

From the above discussion it's clear that one could break up $zn_{\alpha}^{\dagger} n_{\alpha+1}^{\dagger} n_{\alpha+1}$ as $c_1 n_{\alpha}^{\dagger} n_{\alpha+1}^{\dagger} + c_2 n_{\alpha}^{\dagger} n_{\alpha+1}$ as long as c_1 and c_2 satisfy $c_1 c_2 = z$ (one could even allow the c_i 's to be position dependent: $zn_{\alpha}^{\dagger} n_{\alpha+1}^{\dagger} n_{\alpha+1} + c_1^{\alpha+\frac{1}{2}} n_{\alpha}^{\dagger} n_{\alpha+1}^{\dagger} + c_2^{\alpha+\frac{1}{2}} n_{\alpha}^{\dagger} n_{\alpha+1}$ as long as $c_1^{\alpha+\frac{1}{2}} c_2^{\alpha+\frac{1}{2}} = z$). This replacement leads to

$$\Gamma(z) = \int_{-\pi}^{\pi} \frac{dp_x}{2\pi} \ln[1 + c_1 \exp(-ip_x) - c_2 \exp(ip_x)], \quad (7.5)$$

which, by inspection, is the same result as in Eq. (7.4).

Let us now calculate the anticommuting variable correlation functions. These depend on the way the dimer is broken up. The symmetric case $c_1 = c_2 = z^{\frac{1}{2}}$ will be used. Of course, physical correlations (such as dimer density) do not depend on the breakup procedure. Using the methods in I and II

$$\langle a_s a_s^{\dagger} \rangle = \frac{1}{1 - 2iz^{\frac{1}{2}} \sin p_x}, \quad (7.6)$$

so that

$$g_{\beta-\alpha}(z) \equiv \langle n_{\alpha}^{\dagger} n_{\beta}^{\dagger} \rangle = \int_{-\pi}^{\pi} \frac{dp_x}{2\pi} \frac{\exp[-ip_x(\beta-\alpha)]}{(1 - 2iz^{\frac{1}{2}} \sin p_x)}$$

$$= \begin{cases} \frac{1}{\sqrt{1+4z}} \left(\frac{-1 + \sqrt{1+4z}}{2z^{\frac{1}{2}}} \right)^{|\beta-\alpha|}, & \text{for } \beta-\alpha \geq 0 \\ & \text{or } \beta-\alpha \text{ even} \\ \frac{-1}{\sqrt{1+4z}} \left(\frac{-1 + \sqrt{1+4z}}{2z^{\frac{1}{2}}} \right)^{|\beta-\alpha|}, & \text{for } \beta-\alpha \text{ odd and negative.} \end{cases} \quad (7.7)$$

The g 's satisfy $g_n(z) = (-1)^n g_n(z)$. Also

$$\langle n_{\alpha}^{\dagger} n_{\alpha+n}^{\dagger} \rangle = z^{n/2} \langle n_{\alpha}^{\dagger} n_{\alpha+1}^{\dagger} n_{\alpha+1}^{\dagger} \cdots n_{\alpha+n}^{\dagger} n_{\alpha+n}^{\dagger} \rangle, \quad (7.8)$$

for $n \geq 0$, since the terms $z^{\frac{1}{2}} n_{\beta+1}^{\dagger}$, for $\beta = \alpha, \alpha+1, \dots, \alpha+n-1$, in the action of Eq. (7.2) must be used to fill the "x" at α and the "o" at $\alpha+n$.

Everything is now calculable. For example, the probability that there is a dimer between α and $\alpha+1$ (that is at $\alpha + \frac{1}{2}$) is

$$\langle z n_{\alpha}^{\dagger} n_{\alpha+1}^{\dagger} n_{\alpha+1}^{\dagger} \rangle = z \langle n_{\alpha}^{\dagger} n_{\alpha+1}^{\dagger} \rangle = z g_1(z), \quad (7.9)$$

which is the dimer density (normalized to $\frac{1}{2}$ for close-packing).

Equation (7.8) was used in Eq.(7.9) and $g_1(z)$ is given in Eq.(7.7).

The probability of having two dimers, one at $\alpha + \frac{1}{2}$ and one at $\alpha + n + \frac{1}{2}$ is

$$\begin{aligned}
& \langle (z \eta_{\alpha} \eta_{\alpha}^{\dagger} \eta_{\alpha+1} \eta_{\alpha+1}^{\dagger}) (z \eta_{\alpha+n} \eta_{\alpha+n}^{\dagger} \eta_{\alpha+n+1} \eta_{\alpha+n+1}^{\dagger}) \rangle \\
&= z^2 \langle \eta_{\alpha} \eta_{\alpha+1}^{\dagger} \eta_{\alpha+n} \eta_{\alpha+n+1}^{\dagger} \rangle \quad (7.10) \\
&= z^2 [g_1(z) g_1(z) - g_{1+n}(z) g_{1-n}(z)].
\end{aligned}$$

The analog of Eq.(7.8) was used in Eq. (7.10). Equation (II.6.5) was also used. The probability that no dimer covers α is

$$\langle \eta_{\alpha} \eta_{\alpha}^{\dagger} \rangle = g_0(z). \quad (7.11)$$

Everything is trivially calculable.

The above trick of breaking up $\eta_{\alpha} \eta_{\alpha+1}^{\dagger} \eta_{\alpha+1} \eta_{\alpha+2}^{\dagger}$ works for the more complicated system of dimers, trimer, quadrimers, etc. By a trimer I mean a triatomic molecule which can occupy three sites in a row (see Fig. 30), by an n -mer I mean a polymer occupying n sites in a row. The multipolymer system consists simultaneously of dimers, trimers, ..., and n -mers which can be absorbed on the one-dimensional lattice. Each different n -mer can have a different Boltzmann factor. The corresponding anticommuting variable action is

$$\begin{aligned}
A^{1-d} \text{ multipolymer}(z_2, z_3, \dots) = \sum_{\alpha} [& \eta_{\alpha} \eta_{\alpha}^{\dagger} + z_2 \eta_{\alpha} \eta_{\alpha+1}^{\dagger} \eta_{\alpha+1} \eta_{\alpha+1}^{\dagger} \\
& + z_3 \eta_{\alpha} \eta_{\alpha+1}^{\dagger} \eta_{\alpha+1} \eta_{\alpha+2}^{\dagger} \eta_{\alpha+2} \eta_{\alpha+2}^{\dagger} + \dots] , \quad (7.12)
\end{aligned}$$

and z_2, z_3, \dots etc. are the Boltzmann factors for dimers, trimers, etc.

One may replace Eq. (7.12) with

$$A^{1-d} \text{ multipolymer}(z_2, z_3, \dots) = \sum_{\alpha} [\eta_{\alpha} \eta_{\alpha}^{\dagger} + \eta_{\alpha}^{\dagger} \eta_{\alpha+1} + \sum_{\ell=2} z_{\ell} \eta_{\alpha} \eta_{\alpha+\ell-1}^{\dagger}], \quad (7.13)$$

because the extra terms do not contribute. This leads to a grand potential per unit site of

$$\Gamma^{1-d} \text{ multipolymer}(z_2, z_3, \dots) = \int_{-\pi}^{\pi} \frac{dp_x}{2\pi} \ln [1 - \exp(ip_x) + \sum_{\ell=2} z_{\ell} \exp(-ip_x \ell)]. \quad (7.14)$$

The anticommuting variable correlations are easily calculated:

$$\begin{aligned}
g_{\beta-\alpha}(z_2, z_3, \dots) &\equiv \langle \eta_{\alpha} \eta_{\beta}^{\dagger} \rangle \\
&= \int_{-\pi}^{\pi} \frac{dp_x}{2\pi} \frac{\exp(-i(\beta-\alpha)p_x)}{[1 - \exp(ip_x) + \sum_{\ell=2} z_{\ell} \exp(-ip_x \ell)]}. \quad (7.15)
\end{aligned}$$

Unlike the dimer case I have no closed forms for Eqs. (7.14) and (7.15).

The generalization of Eq.(7.8) for $\langle \eta_{\alpha} \eta_{\alpha+n}^{\dagger} \rangle$ with $n > 0$ is

$$\langle \eta_{\alpha} \eta_{\alpha+n}^{\dagger} \rangle = \langle \eta_{\alpha} \eta_{\alpha}^{\dagger} \eta_{\alpha+1} \eta_{\alpha+1}^{\dagger} \dots \eta_{\alpha+n} \eta_{\alpha+n}^{\dagger} \rangle, \quad (n \geq 0). \quad (7.16)$$

All physical quantities are determined by the $g_{\beta-\alpha}$. The multipolymer system is completely solved.

Although quite general, this system is not the most general multipolymer system. One could also include dimers (or other polymers) whose atoms are spaced two or more units apart. This would be the most

general system. Unfortunately the trick used above fails and there is no simple solution method.

VIII. TRANSFER MATRIX ELEMENTS FOR THE TWO DIMENSIONAL DIMER MODEL.

This section will calculate the transfer matrix elements of the two-dimensional dimer problem. This is done in the limit of N_h , the number of horizontal sites (or vertical columns), going to infinity. For the pure dimer case, the transfer matrix is diagonalizable and the eigenvalues have been calculated²⁹. For the general model of monomers and dimers much less is known. Lieb¹⁵ has written down the form of the transfer matrix. Baxter¹⁵ and Runnels¹⁵ have used this transfer matrix formalism to estimate the partition function. These methods seem to give excellent numerical results. In this section the transfer matrix elements will be explicitly computed. The answer is relatively simple and in closed form. These results should be useful in variational computations like those of Baxter and Runnels. Their simplicity beckon an attempt at the exact solution. Perhaps somebody with enough ingenuity can utilize them to solve the general two-dimensional dimer model. Such a formidable undertaking is not attempted in this work. The important equations are Eqs.(8.4) and (8.5). One can also calculate the transfer matrix for the two dimensional multipolymer system consisting of vertical dimers and horizontal n-mers. In the vertical direction there are only dimers, whereas in the horizontal direction there can be dimers, trimers, quadrimers, etc. The important equations are the same ones, Eqs. (8.4) and (8.5), except that Z^{1-d} and g_{ij} are different functions.

This paragraph reviews the definition of the transfer matrix, T , for the two-dimensional dimer problem. The square lattice consists of alternating rows of vertical bonds and horizontal bonds. Roughly speaking, the transfer matrix propagates a configuration of vertical dimers in a row of vertical bonds to another configuration of vertical dimers in the successive row of vertical bonds by summing over all horizontal dimer configurations in the interpolating row of horizontal bonds. Consider the $\beta = -\frac{1}{2}$ row of vertical bonds (see Fig. 31). The initial state, $|s\rangle$, specifies the location of vertical dimers in this row. For example, the configuration in Fig. 31 is $|2,3,4,8\rangle$ meaning that there are vertical dimers at $(2, -\frac{1}{2})$, $(3, -\frac{1}{2})$, $(4, -\frac{1}{2})$, and $(8, -\frac{1}{2})$ (the midpoints of dimers are being used to specify their locations). The order of the numbers in $|2,3,4,8\rangle$ is unimportant, i.e. $|2,8,3,4\rangle = |2,3,4,8\rangle$. The final state, $\langle s'|$, specifies the location of vertical dimers in the $\beta = \frac{1}{2}$ row. In Fig. 31 $\langle s'| = \langle 1,7|$. The transfer matrix element $\langle s'|T|s\rangle$ is the sum over all configurations of horizontal dimers and monomers in the $\beta=0$ row, compatible with the fact that some sites are covered by the dimers in $\langle s'|$ and $|s\rangle$. Of course, if $\langle s'|$ and $|s\rangle$ have a common dimer location, $\langle s'|T|s\rangle = 0$ (for example, $\langle 1,3|T|3\rangle = 0$). If $|s\rangle = |s_1, s_2, \dots, s_\ell\rangle$ and $\langle s'| = \langle s'_1, s'_2, \dots, s'_m|$ with s_i and s'_i integers specifying dimer locations then $\langle s'|T|s\rangle$ is the one-dimensional dimer partition function with sites s_1 through s_ℓ and s'_1 through s'_m covered by monomers. Define $N_\alpha = n_\alpha n'_\alpha$. Then in terms of anticommuting variables

$$\langle s' | T | s \rangle = z_v^{\left(\frac{\ell+m}{2}\right)} z^{1-d} \text{dimer}(z_h) \quad (8.1)$$

$$\times \langle (N_{s'_1} N_{s'_2} \dots N_{s'_m}) (N_{s_1} N_{s_2} \dots N_{s_\ell}) \rangle \text{ 1-d dimer.}$$

A factor of $z_v^{\left(\frac{\ell+m}{2}\right)}$ (the square root of the vertical dimer Boltzmann factors in the two rows of vertical bonds) has been included in the definition of T for convenience. With periodic boundary conditions in the vertical direction,

$$z^{2-d} \text{dimer}(z_h, z_v) = \text{trace}(T^M), \quad (8.2)$$

for a lattice of M rows.

Because transfer matrix elements depend only on the sites covered in the horizontal $\beta = 0$ row, the following symmetry relations hold

$$\begin{aligned} \langle s'_1, s'_2, \dots, s'_m | T | s_1, s_2, \dots, s_\ell \rangle &= \\ &= \langle s'_1, s'_2, \dots, \hat{s}'_k, \dots, s'_m | T | s'_k, s_1, s_2, \dots, s_\ell \rangle = \quad (8.3) \\ &= \langle s'_1, s'_2, \dots, s'_m, s_j | T | s_1, s_2, \dots, \hat{s}_j, \dots, s_\ell \rangle \\ &= \langle \Omega | T | s'_1, s'_2, \dots, s'_m, s_1, s_2, \dots, s_\ell \rangle, \end{aligned}$$

where a circumflex over a position index indicates the absence of that index and the "vacuum" state, Ω , is the one with no dimers.

Equation (8.3) means that integer dimer location indices can be moved from one side of T to the other side.

Using Eq. (II.6.5) in conjunction with Eq. (7.7), Eq. (8.1) can be re-expressed as a determinant of an $(\ell+m) \times (\ell+m)$ matrix. It is useful, however, to make use of the simplifying relation in Eq.(7.8). The set $\{s'_1, \dots, s'_m, s_1, \dots, s_\ell\}$ indicates which sites are already covered in the $\beta = 0$ horizontal row. Arrange these numbers in increasing order and define a new set of ordered pairs $\{(t_1, u_1), (t_2, u_2), \dots, (t_n, u_n)\}$ with $t_1 \leq u_1 < t_2 \leq u_2 < \dots < t_n \leq u_n$. The pairs (t_i, u_i) mean that sites t_i through u_i are covered. In the example of Fig. 31, $s = \{2, 3, 4, 8\}$ and $s' = \{1, 7\}$ yields the (t, u) representation, $\{(1, 4), (7, 8)\}$ meaning that vertical dimers cover sites $(1, 0)$, $(2, 0)$, $(3, 0)$, $(4, 0)$, $(7, 0)$, and $(8, 0)$. The states $|s\rangle$ and $\langle s'|$ uniquely determine the (t, u) pairs. Using Eq. (7.8) the $\langle s' | T | s \rangle$ matrix element is

$$\begin{aligned} \langle s' | T | s \rangle &= z_v^{\left(\frac{\ell+m}{2}\right)} z^{1-d} \text{dimer}(z_h) \\ &\times \langle \hat{n}_{t_1} \hat{n}_{u_1}^\dagger \hat{n}_{t_2} \hat{n}_{u_2}^\dagger \dots \hat{n}_{t_n} \hat{n}_{u_n}^\dagger \rangle \quad (8.4) \\ &= z_v^{\left(\frac{\ell+m}{2}\right)} z^{1-d} \text{dimer}(z_h) \det(M), \end{aligned}$$

where

$$M_{ij} = g_{u_j - t_i}(z_h), \quad (8.5)$$

and the g 's are given in Eq.(7.7). For example, the transfer matrix element in Fig. 31 is

$$z_v^3 \left(\frac{1}{2} + \frac{1}{2} \sqrt{1 + 4z_h} \right)^{N_h} \{g_3(z_h)g_1(z_h) - g_7(z_h)g_{-3}(z_h)\}, \quad (8.6)$$

for rows of N_h sites. The relatively simple structure of the transfer matrix elements should be useful in variational calculations like Baxter's and Runnels' and may even open the door to an exact solution.

In the same manner one can handle the two dimensional multipolymer system consisting of vertical dimers and horizontal polymers. The horizontal polymers are n -mers occupying n consecutive sites in the horizontal direction. In the vertical direction only dimers are allowed so that there is a horizontal-vertical asymmetry. The discussion proceeds as above except that the expressions "horizontal dimers" and "1-d dimer" are replaced by "horizontal polymers" and "1-d polymer". All the above equations are still valid if the $g_{u_j-t_i}(z_h)$ of Eq.(8.5) are replaced by the $g_{u_j-t_i}(z_2, z_3, \dots)$ in Eq.(7.15) and if $Z^{1-d} \text{ dimer}(z_h)$ is replaced by $Z^{1-d} \text{ multipolymer}(z_2, z_3, \dots) = \exp[N_h \Gamma^{1-d} \text{ multipolymer}(z_2, z_3, \dots)]$ with $\Gamma^{1-d} \text{ multipolymer}$ given in Eq.(7.14).

IX. THE ONE-DIMENSIONAL APPROACH TO THE TWO-DIMENSIONAL DIMER MODEL

This section reconsiders the two-dimensional dimer model. The Sec. VII results for the one-dimensional dimer problem are used to attack the two-dimensional problem. Section VII displayed the trivial nature of the one-dimensional dimer model: the partition function and all correlation functions were easily calculated. These calculations can be used to approach the two-dimensional model. Suppose, for example, that $z_v \approx 0$. Then the two-dimensional model would become many one-dimensional models. When $z_v \neq 0$, a

perturbative expansion in powers of z_v is possible. The form of this expansion is $\frac{1}{N} \ln Z(z_h, z_v) = \sum_{\ell} c_{\ell}(z_h) z_v^{\ell}$, a power series in z_v but correct to all orders in z_h .

After writing down the Feynman graph rules, three new expansion series are obtained. They are the simple perturbative expansion [Eq.(9.9)], the Hartree-improved expansion [Eq.(9.23)], and the $1/N$ approximation [Eq.(9.28)]. These three series are the main results in this section. They work best for small z_v , however the latter two probably work reasonably well for all values of z_v .

The dimer model has no phase transitions¹². All the approximation methods developed here show no evidence for such a phase transition.

Also presented are several other approaches to the two-dimensional model along with the corresponding anticommuting variable actions. It is straightforward to develop new approximations using these actions, however such an analysis is not carried out. This paper has already presented good approximations. It would be overdoing it to present more. So, for reasons of space they are omitted.

The results of this section are easily adapted to the two-dimensional polymer system considered in Sec. VIII. This is presented at the end.

Apply the dimer "breakup" trick (used in Sec. VII to solve the one-dimensional problem) to each horizontal row of dimers. The trick cannot simultaneously be done with vertical dimers because extra

configurations (of closed loops) not in the partition function are generated. The resulting anticommuting variable action becomes

$$A^{2-d} \text{ dimer}(z_h, z_v) = \sum_{\alpha\beta} \{ n_{\alpha\beta} n_{\alpha\beta}^\dagger + z_h^{\frac{1}{2}} n_{\alpha\beta} n_{\alpha+1\beta}^\dagger + n_{\alpha\beta}^\dagger n_{\alpha+1\beta} \} \\ + z_v n_{\alpha\beta} n_{\alpha\beta}^\dagger n_{\alpha\beta+1} n_{\alpha\beta+1}^\dagger \}. \quad (9.1)$$

The free propagator is

$$g_{\alpha'\alpha}^{2-d}{}_{\beta'\beta}(z_h, z_v) \equiv \langle n_{\alpha\beta} n_{\alpha'\beta'}^\dagger \rangle_{z_v} = 0 \quad (9.2) \\ = \delta_{\beta\beta'} g_{\alpha'\alpha}^{1-d}(z_h),$$

and $g_{\alpha'\alpha}^{1-d}$ is given in Eq. (7.7):

$$g_{\alpha'\alpha}^{1-d}(z_h) = \int \frac{dp_x}{2\pi} G(p_x) \exp[-i(\alpha' - \alpha)p_x], \quad (9.3)$$

$$G(p_x) = \frac{1}{1 - 2iz_h^{\frac{1}{2}} \sin p_x}.$$

A set of Feynman graph rules is easily derived. They are similar to those in Sec.V under the heading "Rules for a Dimer Problem on a Translationally Invariant Lattice", except that fermion loops are now non-local and cannot be shrunk to a point. This causes rule (c) to be modified.

Feynman Rules for the Action in Equation (9.1)

(a) Draw all diagrams on the square lattice using the "dotted-line" interaction in Fig. 32 and "horizontal" oriented fermion loops (solid lines) (see Figs. 33, 34, and 35 for examples).

(b) Each Fig. 32 interaction gives a factor of z_v , and there is a sum, \sum_{α} , over the x-coordinate of the interaction.

(c) Each fermion propagator from (α, β) to (α', β) (Fig. 13) gives a factor of $g_{\alpha'\alpha}^{1-d}(z_h)$.

(d) For each fermion loop there is a (-1) .

(e) Shrink fermion loops to points. Treat the points in different rows as being distinguishable. There is a factor of [the order of the point symmetry group of the diagram] $^{-1}$. Diagrams in Figs. 34b and 34c have a factor of $\frac{1}{2}$ from this rule, but Fig. 34d does not.

(f) Two fermion loops with ℓ interactions between them (Fig. 36) have a factor of $\frac{1}{\ell!}$. Figures 34a and 35 have factors of $\frac{1}{2!}$ and $\frac{1}{3!}$ from this rule.

(g) If ℓ interactions (dotted lines) are attached to a fermion loop all $(\ell-1)!$ possible orderings must be considered. They no longer contribute equally as in Fig. 16, that is, all the possibilities on the right hand side of Fig. 16 must be considered separately.

(h) $\frac{1}{N} \log Z(z_h, z_v) \equiv \Gamma^{2-d} \text{ dimer}(z_h, z_v) = \Gamma^{(0)}(z_h) + \sum_{\text{connected diagrams}} (\text{weight of diagram}),$ where $\Gamma^{(0)}(z_h)$ is

$$\Gamma^{(0)}(z_h) = \Gamma^{1-d} \text{ dimer}(z_h), \quad (9.4)$$

and $\Gamma^{1-d} \text{ dimer}$ is given in Eq. (7.4).

Momentum space Feynman rules can also be derived. Because the propagator in Eq. (9.2) has a simple $\beta\beta'$ structure, it is

convenient to Fourier transform in x-coordinates only. The statistical factors remain the same as above. Loop momentum are assigned in the standard way²⁴. Rule (c) becomes

(c') for each fermion propagator with momentum, p_x , flowing in the direction of an arrowed line (see Fig. 37) there is a factor of $G(p_x)$ (given in Eq.(9.3)). No longer sum over the x-coordinate of the interaction as in rule (b). Instead assign a factor of $\int_{-\pi}^{\pi} \frac{dk}{2\pi} x$ for each loop momentum.

In first order perturbation theory there is one graph (Fig.33).

In momentum space the contribution is

$$z_v \left(\int_{-\pi}^{\pi} \frac{dk}{2\pi} G(k) \right)^2 = \frac{z_v}{1+4z_h} = \Gamma^{(1)}(z_h, z_v), \quad (9.5)$$

where Eq. (7.7) has been used.

There are four second order graphs (Fig. 34). Figures 34b and 34c have the same weight and Fig. 34d has twice the weight of Fig. 34b. Hence

$$\Gamma^{(2)}(z_h, z_v) = 4\Gamma^{(b)}(z_h, z_v) + \Gamma^{(a)}(z_h, z_v), \quad (9.6)$$

where, in momentum space,

$$\Gamma^{(b)} = \left(-\frac{1}{2}\right) z_v^2 \left[\int_{-\pi}^{\pi} \frac{dk}{2\pi} G(k) \right]^2 \left[\int_{-\pi}^{\pi} \frac{dk}{2\pi} G(k)G(k) \right], \quad (9.7)$$

$$\Gamma^{(a)} = \frac{1}{2} z_v^2 \int_{-\pi}^{\pi} \frac{dk_1}{2\pi} \int_{-\pi}^{\pi} \frac{dk_2}{2\pi} \int_{-\pi}^{\pi} \frac{dk_3}{2\pi} \left[G(k_1)G(k_2 + k_1)G(k_3 - k_2)G(k_3) \right].$$

The loop momentum assignment for $\Gamma^{(a)}$ is shown in Fig. 38.

$\Gamma^{(b)}$ and $\Gamma^{(a)}$ can be explicitly calculated:

$$\Gamma^{(b)}(z_h, z_v) = - \left(\frac{z_v}{1+4z_h} \right)^2 \left[\frac{(1+\sqrt{1+4z_h})}{(1+\sqrt{1+4z_h})^2 + 4z_h} \right],$$

$$\Gamma^{(a)}(z_h, z_v) = \frac{1}{2} \left(\frac{z_v}{1+4z_h} \right)^2 \left[\frac{(1+\sqrt{1+4z_h})^4 + 16z_h^2}{(1+\sqrt{1+4z_h})^4 - 16z_h^2} \right]. \quad (9.8)$$

This concludes the calculation to second order for the two-dimensional dimer model treated as a perturbation of one-dimensional dimer models:

$$\Gamma^{2-d \text{ dimer}}(z_h, z_v) = \Gamma^{(0)} + \Gamma^{(1)} + \Gamma^{(2)} + \dots, \quad (9.9)$$

with $\Gamma^{(0)}$, $\Gamma^{(1)}$, and $\Gamma^{(2)}$ given in Eqs. (9.4), (9.5), and (9.6).

Equation (9.9) is an expansion in powers of z_v but exact to all orders in z_h .

Now consider the Hartree treatment of Eq. (9.1). It replaces

$$z_v n_{\alpha\beta} n_{\alpha\beta}^{\dagger} n_{\alpha\beta+1} n_{\alpha\beta+1}^{\dagger} + z_v \langle n_{\alpha\beta} n_{\alpha\beta}^{\dagger} \rangle_H n_{\alpha\beta+1} n_{\alpha\beta+1}^{\dagger} \quad (9.10)$$

$$+ z_v n_{\alpha\beta} n_{\alpha\beta}^{\dagger} \langle n_{\alpha\beta+1} n_{\alpha\beta+1}^{\dagger} \rangle_H - z_v \langle n_{\alpha\beta} n_{\alpha\beta}^{\dagger} \rangle_H \langle n_{\alpha\beta+1} n_{\alpha\beta+1}^{\dagger} \rangle_H$$

and determines $m \equiv \langle n_{\alpha\beta} n_{\alpha\beta}^{\dagger} \rangle_H$ self-consistently. Substituting (9.10) into Eq.(9.1) gives

$$m = \frac{1}{1+2z_v m} g_0^{1-d} \left(\frac{z_h}{(1+2z_v m)^2} \right) \quad (9.11)$$

with g_0 given in Eq. (7.7). This leads to a fourth order polynomial equation for m :

$$4z_v^2 m^4 + 4z_v m^3 + (1 + 4z_h)m^2 - 1 = 0. \quad (9.12)$$

Numerically Eq. (9.12) was found to have a unique positive root so that m is determined unambiguously. Equation (9.12) can be solved using standard (messy) formulas for a fourth order equation.

The effective anticommuting variable action becomes

$$A^{\text{eff. 2-d dimer}}(z_h, z_v) = \sum_{\alpha\beta} \left[\eta_{\alpha\beta} \eta_{\alpha\beta}^\dagger (1 + 2z_v m) - z_v m^2 + z_v \eta_{\alpha\beta} \eta_{\alpha\beta}^\dagger \eta_{\alpha+1\beta} \eta_{\alpha+1\beta}^\dagger + z_h \left(\eta_{\alpha\beta} \eta_{\alpha+1\beta}^\dagger + \eta_{\alpha\beta}^\dagger \eta_{\alpha+1\beta} \right) \right]. \quad (9.13)$$

The normal ordering symbol $::$ means "do not take (self-interaction) Wick contractions within the colons". Rescaling anticommuting variables by a factor of $1/\sqrt{1 + 2z_v m}$ yields

$$Z^{2\text{-d dimer}}(z_h, z_v) = (1 + 2z_v m)^N \exp(-z_v m^2 N) \int d\eta d\eta^\dagger \exp(A^{\text{Hartree}}), \quad (9.14)$$

where N is the total number of sites and A^{Hartree} is the action for generating the Hartree improved perturbation series:

$$A^{\text{Hartree}}(z_h, z_v) = \sum_{\alpha\beta} \left\{ \eta_{\alpha\beta} \eta_{\alpha\beta}^\dagger + \xi_h \left[\eta_{\alpha\beta} \eta_{\alpha+1\beta}^\dagger + \eta_{\alpha\beta}^\dagger \eta_{\alpha+1\beta} \right] + \xi_v \left[\eta_{\alpha\beta} \eta_{\alpha\beta}^\dagger \eta_{\alpha\beta+1} \eta_{\alpha\beta+1}^\dagger \right] \right\} \quad (9.15)$$

with

$$\xi_h = z_h / c^2,$$

$$\xi_v = z_v / c^2, \quad (9.16)$$

$$c = 1 + 2z_v m.$$

From Eq. (9.14) the Hartree approximation, Γ^H , is

$$\Gamma^H(z_h, z_v) = \ln(1 + z_v m) - z_v m^2. \quad (9.17)$$

Equations (9.17) and (9.12) summarize the Hartree approximation in the one-dimensional approach to the two-dimensional dimer problem. Γ^H includes the effects of diagrams in Fig. 33, 34b, 34c, and 34d as well as higher order ones of the structure indicated in Fig. 17.

Next consider the Hartree-improved perturbation expansion. The calculation will be done to third order in ξ_v . The action in Eq. (9.15) is almost of the same form as in Eq. (9.1) except that $z_h \rightarrow \xi_h$, $z_v \rightarrow \xi_v$, and there is normal ordering. The Feynman rules used above are still valid with the replacements

$$\begin{aligned} z_h &\rightarrow \xi_h, \\ z_v &\rightarrow \xi_v. \end{aligned} \quad (9.18)$$

In addition, normal ordering means that graphs with a fermion loop connected to a single interaction dotted line are to be ignored. The first term in the Hartree-improved series is the second order (in ξ_v) graph shown in Fig. 34a. The contribution is the same as

before (Eq. 9.8) when the Eq.(9.18) substitutions are made;

$$\Gamma^{(2)}(z_h, z_v) = \frac{1}{2} \left(\frac{z_v}{c^2 + 4z_h} \right)^2 \left[\frac{(c + \sqrt{c^2 + 4z_h})^4 + 16z_h^2}{(c + \sqrt{c^2 + 4z_h})^4 - 16z_h^2} \right] \quad (9.19)$$

In third order there are four graphs (see Fig. 35). It turns out that all four have the same weight. In coordinate space the contribution is

$$\begin{aligned} \Gamma^{(3)}(z_h, z_v) &= \sum_{n,m} (\xi_v)^3 \frac{4}{3!} \left[g_m(\xi_h) g_n(\xi_h) g_{m-n}(\xi_h) \right]^2 \\ &= \frac{2}{3} \left(\frac{z_v}{c^2 + 4z_h} \right)^3 \sum_{n,m} a^{2|m|} a^{2|n|} a^{2|m-n|}, \end{aligned} \quad (9.20)$$

where Eq. (7.7) has been used and

$$a = \frac{-c + \sqrt{c^2 + 4z_h}}{2z_h^{1/2}} = \frac{2z_h^{1/2}}{c + \sqrt{c^2 + 4z_h}} \quad (9.21)$$

Equation(9.20) yields

$$\Gamma^{(3)}(z_h, z_v) = \frac{2}{3} \left(\frac{z_v}{c^2 + 4z_h} \right)^3 \left[\frac{1 + 4a^4 + a^8}{(1 - a^4)^2} \right] \quad (9.22)$$

This completes the calculation of the Hartree-improved series to third order in ξ_v :

$$\Gamma^{\text{Hartree exp.}}(z_h, z_v) = \Gamma^H(z_h, z_v) + \Gamma^{(2)}(z_h, z_v) + \Gamma^{(3)}(z_h, z_v) + \dots, \quad (9.23)$$

where the Γ 's are given in Eqs. (9.17), (9.19), and (9.22). The

constants, ξ_h , ξ_v , c , a , and m are determined by Eqs. (9.16), (9.21), and (9.12). Like Eq. (9.9), Eq. (9.23) produces a series correct to all powers in z_h . Of course, Eq. (9.23) will produce a series with a much better z_v behavior since higher order (in z_v) effects are taken into account.

Finally, consider the $1/N$ expansion approach. The one loop correction will be calculated. The zeroth order contribution is Γ^H and is given in Eq. (9.17). The one loop contribution involves summing the graphs of Fig. 39. Graphs with an odd number of fermion loops give zero. For a graph with M fermion loops, there is a statistical factor of $(-1)^M/2M$ from rules (d) and (e), a factor of ξ_v^M , a factor of c_o^M , the number of closed one-dimensional random walks of M steps (which is the embedding factor in the vertical direction) and a factor of $\sum_{\alpha_2 \dots \alpha_M} g_{\alpha_2 - \alpha_1}^2 g_{\alpha_3 - \alpha_2}^2 \dots g_{\alpha_M - \alpha_{M-1}}^2 g_{\alpha_1 - \alpha_M}^2$ for the propagators:

$$\Gamma^{\text{1-loop}}(z_h, z_v) = \sum_{M=1}^{\infty} \frac{(-1)^M}{2M} \xi_v^M c_o^M \sum_{\alpha_2 \dots \alpha_M} \left[g_{\alpha_2 - \alpha_1}^2 g_{\alpha_3 - \alpha_2}^2 \dots g_{\alpha_1 - \alpha_M}^2 \right] \quad (9.24)$$

Using the same method as in section VI

$$c_o^M = \int \frac{dp_y}{2\pi} (2\cos p_y)^M, \quad (9.25)$$

and Fourier decomposition of the propagator factor gives

$$\xi_v^M \sum_{\alpha_2 \dots \alpha_M} \left[g_{\alpha_2 - \alpha_1}^2 \dots g_{\alpha_1 - \alpha_M}^2 \right] = \left(\frac{z_v}{c^2 + 4z_h} \right)^M \int \frac{dp_x}{2\pi} \left(\frac{1 - a^4}{1 + a^4 - 2a^2 \cos p_x} \right)^M, \quad (9.26)$$

leading to the final result

$$\Gamma^{1\text{-loop}}(z_h, z_v) = -\frac{1}{2} \int \frac{dp_x}{2\pi} \int \frac{dp_y}{2\pi} \ln \left[1 - \left(\frac{z_v}{c^2 + 4z_h} \right) (2 \cos p_y) \left(\frac{1 - a^4}{1 + a^4 - 2a^2 \cos p_x} \right) \right], \quad (9.27)$$

where c and a are given in Eqs. (9.16) and (9.21). The $1/N$ expansion gives

$$\Gamma^{1/N \text{ exp.}}(z_h, z_v) = \Gamma^H(z_h, z_v) + \Gamma^{1\text{-loop}}(z_h, z_v) + \dots, \quad (9.28)$$

with Γ^H given in Eq. (9.17) and $\Gamma^{1\text{-loop}}$ given in Eq. (9.27).

Higher order corrections are easily calculated.

A phase transition (or non-analyticity) could occur if the argument in the logarithm in Eq. (9.27) vanishes. It would first happen in the integration region near $p_y = 0, p_x = 0$. The condition for a phase transition is

$$1 = \left(\frac{z_v}{c^2 + 4z_h} \right) (2) \left(\frac{1 + a^2}{1 - a^2} \right). \quad (9.29)$$

Condition (9.29) when combined with the definitions of $m, c,$ and a [Eqs. (9.12), (9.16), and (9.21)] implies

$$\left(-z_h + \sqrt{z_h^2 + z_v^2} \right) \left[\left(\frac{-z_h + \sqrt{z_h^2 + z_v^2}}{2} \right)^{\frac{1}{2}} + 1 + 4z_h \right] = 0. \quad (9.30)$$

For $z_h, z_v > 0$ Eq. (9.30) cannot be satisfied; hence condition (9.29) cannot be met and no phase transition occurs in the $1/N$ approximation. The two previous approximations in this section [Eqs. (9.9) and (9.23)] are also analytic functions of z_h and z_v and hence also predict

no phase transition. Thus the three methods in this section as well as the ones in Secs. V and VI all predict no phase transition in the two-dimensional dimer model in complete agreement with reference 12.

The action in Eq. (9.1) can be modified so that successive terms in Eq. (9.28) get multiplied by factors of $1/N$. This is done in the same manner as in Sec. VI. The modified action is

$$A = \sum_{\alpha\beta} \sum_{i=1}^N \left[\eta_{\alpha\beta}^i \eta_{\alpha\beta}^{i\dagger} + z_h \eta_{\alpha\beta}^i \eta_{\alpha\beta}^{i\dagger} \eta_{\alpha+1\beta}^i \eta_{\alpha+1\beta}^{i\dagger} + \frac{z_v}{N} \sum_j \eta_{\alpha\beta}^i \eta_{\alpha\beta}^{i\dagger} \eta_{\alpha\beta+1}^j \eta_{\alpha\beta+1}^{j\dagger} \right]. \quad (9.31)$$

Equation (9.31) generates the series

$$\Gamma_N(z_h, z_v) = N \Gamma^H(z_h, z_v) + \Gamma^{1\text{-loop}}(z_h, z_v) + \frac{1}{N} \Gamma^{2\text{-loop}}(z_h, z_v) + \dots, \quad (9.32)$$

where $\Gamma^H, \Gamma^{1\text{-loop}},$ etc. are the same quantities as in Eq. (9.28).

There are other ways to attack the two-dimensional dimer model. First, the method of this section can be applied along diagonals as in Fig. 40 instead of horizontal rows. The corresponding anticommuting variable action would be

$$A^{2\text{-d dimer}}(z_h, z_v) = \sum_{\substack{\text{even} \\ \text{sites}}} \left[z_v \eta_{\alpha\beta} \eta_{\alpha\beta}^\dagger \eta_{\alpha\beta+1} \eta_{\alpha\beta+1}^\dagger + z_h^{\frac{1}{2}} (\eta_{\alpha\beta} \eta_{\alpha+1\beta}^\dagger + \eta_{\alpha\beta}^\dagger \eta_{\alpha+1\beta}) \right] \\ + \sum_{\substack{\text{odd} \\ \text{sites}}} \left[z_h \eta_{\alpha\beta} \eta_{\alpha\beta}^\dagger \eta_{\alpha+1\beta} \eta_{\alpha+1\beta}^\dagger + z_v^{\frac{1}{2}} (\eta_{\alpha\beta} \eta_{\alpha\beta+1}^\dagger + \eta_{\alpha\beta}^\dagger \eta_{\alpha\beta+1}) \right], \quad (9.33)$$

where an even site, (α, β) , means $\alpha + \beta =$ an even integer and an odd site, (α, β) , means $\alpha + \beta =$ an odd integer. This "staircase"

approximation, unlike the horizontal breakup, generates an expansion series symmetric in z_h and z_v (as should be the case).

A second approach is the following: Break up both horizontal and vertical dimers:

$$z_h n_{\alpha\beta} n_{\alpha\beta}^\dagger n_{\alpha+1\beta} n_{\alpha+1\beta}^\dagger \rightarrow z_h^{\frac{1}{2}} (n_{\alpha\beta} n_{\alpha+1\beta}^\dagger + n_{\alpha\beta}^\dagger n_{\alpha+1\beta}), \quad (9.34)$$

$$z_v n_{\alpha\beta} n_{\alpha\beta}^\dagger n_{\alpha\beta+1} n_{\alpha\beta+1}^\dagger \rightarrow z_v^{\frac{1}{2}} (n_{\alpha\beta} n_{\alpha\beta+1}^\dagger + n_{\alpha\beta}^\dagger n_{\alpha\beta+1}).$$

In this case (closed loop) configurations will be generated which are not contained in the partition function (see Fig. 41 for example). They must involve the eight corners of Fig. 42. By adding terms to the action to cancel these corners, the unwanted configurations can be eliminated. The corresponding action is

$$\begin{aligned} A^{2-d} \text{ dimer}(z_h, z_v) = & \sum_{\alpha\beta} \{ n_{\alpha\beta} n_{\alpha\beta}^\dagger + z_h^{\frac{1}{2}} (n_{\alpha\beta} n_{\alpha+1\beta}^\dagger + n_{\alpha\beta}^\dagger n_{\alpha+1\beta}) \\ & + z_v^{\frac{1}{2}} (n_{\alpha\beta} n_{\alpha\beta+1}^\dagger + n_{\alpha\beta}^\dagger n_{\alpha\beta+1}) - (z_h z_v)^{\frac{1}{2}} n_{\alpha\beta} n_{\alpha\beta}^\dagger [n_{\alpha+1\beta}^\dagger n_{\alpha\beta+1} \\ & + n_{\alpha\beta+1}^\dagger n_{\alpha-1\beta} + n_{\alpha\beta+1} n_{\alpha+1\beta}^\dagger + n_{\alpha+1\beta} n_{\alpha\beta+1}^\dagger + n_{\alpha\beta-1\beta}^\dagger \\ & + n_{\alpha-1\beta} n_{\alpha\beta-1}^\dagger + n_{\alpha+1\beta}^\dagger n_{\alpha\beta-1} + n_{\alpha\beta-1}^\dagger n_{\alpha+1\beta}] \}. \quad (9.35) \end{aligned}$$

The "cancelling" corners are the last eight terms in Eq. (9.33).

When integrated, the action in either Eq. (9.33) or Eq. (9.35)

generates the two-dimensional dimer partition function. One could

apply the same scenario of approximation schemes to obtain even more series expansion. This is not done for reasons of space. These two representations (along with previous ones) show that the anti-commuting variable method offers many avenues of attack. It is up to one's ingenuity to find the best approximation in the region of interest.

So far, the approximation methods work best for small z_h or z_v (although some are still very good for large z_h and z_v). Is there an approach which works best for large z_h and z_v ? The answer is affirmative since as $z_h \rightarrow \infty$ and $z_v \rightarrow \infty$ the dimer model becomes the pure dimer problem which can be solved by the anticommuting variable method²⁵. One needs to calculate monomer-monomer correlation functions in the pure dimer problem. This is easy to do using anticommuting variables. Actually, this has already been done in reference 30. Reference 30 shows how pfaffian perturbation theory works in simple cases, and calculates monomer-monomer correlations. In principle all monomer correlations (i.e. a product of many monomers) are calculable using the method of reference 30. The anticommuting variable approach reproduces the results of reference 30 with much labor saved. Most of these results follow immediately or in a few lines of algebra.

The methods of this section can be adapted to the two-dimensional multipolymer system discussed in Sec. VIII. Roughly speaking, one merely replaces the word "dimer" by "multipolymer" and uses the anticommuting variable correlation function in Eq.(7.15) instead of Eq. (7.7). For example, g^{1-d} in Eq. (9.2) is replaced

by the g in Eq. (7.15). This corresponds to replacing the $G(p_x)$ in Eq. (9.3) with

$$G^{\text{multi}}(p_x) = [1 - \exp(ip_x) + \sum_{\ell=2} z_\ell \exp(-ip_x(\ell-1))]^{-1}. \quad (9.36)$$

The right hand side of Eq. (9.4) is replaced by Γ^{1-d} multipolymer (z_2, z_3, \dots) [Eq.(7.14)]. To obtain the perturbation series for the two-dimensional multipolymer system replace the $G(p_x)$ [Eq.(9.3)] by $G^{\text{multi}}(p_x)$ [Eq.(9.36)] in Eqs.(9.5), (9.6), (9.7), and (9.9). Equation (9.11) determines the Hartree factor, m^{multi} , if the g_0 in Eq. (7.15) is used. Equations (9.13) through (9.17), which give the Hartree approximation, are valid if m^{multi} is used. The Hartree propagator in momentum space is

$$G_H^{\text{multi}}(p_x) = [1 - c^{-1} \exp(ip_x) + \sum_{\ell=2} \xi_\ell^{\frac{1}{2}} \exp(-ip_x(\ell-1))]^{-1}, \quad (9.37)$$

where

$$\xi_\ell = z_\ell / c^2, \quad (9.38)$$

$$c = 1 + 2z_v m^{\text{multi}}.$$

Then $\Gamma^{(1)}$ and $\Gamma^{(2)}$ of the Hartree series are the same as simple perturbation theory [Eqs. (9.5), (9.5), and (9.7)] if $z_v \rightarrow \xi_v$ and $G^{\text{multi}}(p_x)$ is used. It is straightforward to compute several orders of the Hartree series. It is also straightforward to obtain the $1/N$ expansion.

SECTION X BOSONIZATIONS

This section considers bosonizations of the anticommuting variable actions. This means that the anticommuting actions are rewritten in terms of commuting (boson) fields. Bosonization can lead to new insights and new methods, although none are developed here. The analysis is carried out for formal purposes and so no numerical calculations are presented. Instead, contact is made with previous approximation methods such as perturbation theory, the Hartree approximation, etc. Much insight is gained into the perturbative techniques discussed in Secs. IV and VI. The dimer model in its complete generality is treated, although the methods are applicable, in principle, to any anticommuting variable action. Because the whole class of dimer models is being considered all at once, this section is abstract in character.

In two dimensions there is a direct way of establishing a fermion-boson correspondence. A summary and review with references can be found in reference 31. In higher dimensions it is not possible to rewrite fermion operators directly in terms of bosonic ones and vice versa. It is, however, possible to find bosonic actions which reproduce the partition function (and correlation functions). A common way to do this is by the use of auxiliary scalar fields.³² This section applies the auxiliary field method to the abstract dimer problem. The result is Eq. (10.6). What then follows is a description of how the Hartree approximation, the Hartree-improved series, and $1/N$ expansion are recovered from the bosonic action. In addition, a second bosonization scheme is discovered. It is based on Feynman graph rules. A boson action is found which exactly

reproduces the Feynman graphs (of Sec. IV) and their weights. This boson action is presented in Eq. (10.16). The Hartree and $1/N$ theory are also easily recovered [Eqs. (10.17) through (10.25)].

The importance of the auxiliary field method (and other bosonizations) is that it allows semi-classical methods to be used. In a series of papers^{7,8} Dashen, Hasslacher, and Neveu developed the semi-classical method for bosonic field theories. For fermionic fields it was necessary to first bosonize the system⁸. In this way semiclassical techniques become (indirectly) applicable to fermionic systems. Thus the auxiliary field method is important because it allows semi-classical methods to be used.

For the dimer problem, the semi-classical method recovers the Hartree approximation. Calculating successive orders of quantum corrections generates the $1/N$ expansion. For most dimer models, its accuracy explains why the partition function is well approximated by the saddle point and a few orders of quantum corrections: the partition function receives its contribution from a "deep well" in function space.

This bosonization method, which will be called the auxiliary field method, works for a field theory whose interaction term is a product of four anticommuting variables (or fermionic fields). It introduces an auxiliary boson field to linearize the fermionic degrees of freedom. This trick is sometimes useful⁸. The method is used here formally so that no numerical results are obtained. The purpose is to make the reader aware of the auxiliary field method.

Take the general dimer interaction term, $\frac{1}{2} \sum_{\alpha\beta} z_{\alpha\beta} \eta_{\alpha}^{\dagger} \eta_{\beta}^{\dagger}$, and rewrite it as

$$\exp\left(\frac{1}{2} \sum_{\alpha\beta} z_{\alpha\beta} \eta_{\alpha}^{\dagger} \eta_{\beta}^{\dagger}\right) = \prod_{\alpha\beta} \int_{-\infty}^{\infty} \frac{dA_{\alpha\beta}}{\sqrt{2\pi}} \exp\left[-\frac{1}{2} \sum_{\alpha\beta} A_{\alpha\beta}^2 + \sum_{\alpha\beta} \sqrt{\frac{z_{\alpha\beta}}{2}} A_{\alpha\beta} (\eta_{\alpha}^{\dagger} + \eta_{\beta}^{\dagger})\right]. \quad (10.1)$$

Recall that α and β label vertices. Thus $A_{\alpha\beta}$ represents a "bond" variable between vertices α and β . For convenience $A_{\alpha\beta}$ has been chosen to be different from $A_{\beta\alpha}$. Those $A_{\alpha\beta}$ for which $z_{\alpha\beta} = 0$ may be ignored (or integrated to yield a multiplicative factor of 1). Equation (10.1) is true because Gaussian integration over the A 's still works for sources such as η_{α}^{\dagger} .

Integrate over the anticommuting variables in Eqs.(4.1) and (1.3.6) to get

$$\prod_{\alpha} \left[1 + \sum_{\beta} \sqrt{\frac{z_{\alpha\beta}}{2}} (A_{\alpha\beta} + A_{\beta\alpha}) \right]. \quad (10.2)$$

The bosonized action is

$$A^{\text{dimer}} = -\frac{1}{2} \sum_{\alpha\beta} A_{\alpha\beta}^2 + \sum_{\alpha} \ln \left[1 + \sum_{\beta} \sqrt{\frac{z_{\alpha\beta}}{2}} (A_{\alpha\beta} + A_{\beta\alpha}) \right]. \quad (10.3)$$

This effective action involves arbitrary powers of A 's (when the logarithm is expanded) and is not so aesthetic. It is easy to verify directly that $\exp(A^{\text{dimer}})$ when integrated over the $A_{\alpha\beta}$'s generates the partition function.

Equation (10.1) relies on the identity $(\eta_\alpha \eta_\alpha^\dagger)^2 = 0$. It is useful to explicitly cancel this factor by using two auxiliary fields $A_{\alpha\beta}^{(1)}$ and $A_{\alpha\beta}^{(2)}$. These two can be grouped into one complex field, $A_{\alpha\beta}$:

$$A_{\alpha\beta} = \frac{A_{\alpha\beta}^{(1)} + i A_{\alpha\beta}^{(2)}}{\sqrt{2}} \quad (10.4)$$

$$A_{\alpha\beta}^* = \frac{A_{\alpha\beta}^{(1)} - i A_{\alpha\beta}^{(2)}}{\sqrt{2}}$$

In terms of these variables the action which yields the dimer potential is

$$- \sum_{\alpha\beta} (A_{\alpha\beta} A_{\alpha\beta}^*) + \sum_{\alpha\beta} \sqrt{\frac{z_{\alpha\beta}}{2}} (A_{\alpha\beta} \eta_\alpha \eta_\alpha^\dagger + A_{\alpha\beta}^* \eta_\beta \eta_\beta^\dagger) \quad (10.5)$$

and leads to the bosonic representation of

$$Z^{\text{dimer}} = \left(\prod_{\alpha\beta} \int \frac{1}{2\pi} dA_{\alpha\beta} dA_{\alpha\beta}^* \right) \exp \left[- \sum_{\alpha\beta} A_{\alpha\beta} A_{\alpha\beta}^* + \sum_{\alpha} \ln \left[1 + \sum_{\beta} \sqrt{\frac{z_{\alpha\beta}}{2}} (A_{\alpha\beta} + A_{\beta\alpha}^*) \right] \right] \quad (10.6)$$

The Hartree approximation of Sec. IV becomes the semiclassical approximation in the auxiliary field representation. The integrals in Eq.(10.6) can be approximated by their saddle points. The equations of motion are

$$A_{\alpha\beta}^{*cl} = \frac{\sqrt{\frac{z_{\alpha\beta}}{2}}}{1 + \sum_{\gamma} \sqrt{\frac{z_{\gamma\beta}}{2}} (A_{\gamma\beta}^{cl} + A_{\beta\gamma}^{*cl})} \quad (10.7)$$

$$A_{\alpha\beta}^{cl} = \frac{\sqrt{\frac{z_{\alpha\beta}}{2}}}{1 + \sum_{\gamma} \sqrt{\frac{z_{\gamma\beta}}{2}} (A_{\beta\gamma}^{cl} + A_{\gamma\beta}^{*cl})}$$

where A^{cl} denotes the classical field, that is, the saddle point solutions. Equations (10.7) imply

$$A_{\alpha\beta}^{cl*} = A_{\beta\alpha}^{cl} \quad (10.8)$$

One then concludes that the functions $A_{\alpha\beta}^{cl} \equiv A_{\alpha\beta}^{cl} \sqrt{\frac{2}{z_{\alpha\beta}}}$ are independent of α (that is, $A_{\alpha\beta}^{cl} = A_{\alpha'\beta}^{cl}$). Call these g_β :

$$g_\beta \equiv A_{\alpha\beta}^{cl} = A_{\alpha'\beta}^{cl} = A_{\alpha\beta}^{cl} \sqrt{\frac{2}{z_{\alpha\beta}}} \quad (10.9)$$

The g 's satisfy the same Hartree equations as in Sec. IV [Eqs. (4.9) and (4.16)]:

$$g = \frac{1}{1 + \sum_{\gamma} z_{\gamma\beta} g_\gamma} \quad (10.10)$$

In fact this is not surprising since in the mixed representation of Eq. (10.5) the classical equation of motion for $A_{\alpha\beta}$ is

$$A_{\alpha\beta}^{cl} = \sqrt{\frac{z_{\alpha\beta}}{2}} \eta_\alpha \eta_\alpha^\dagger \quad (10.11)$$

The classical value of A is just the Hartree expectation $\langle \eta \eta^\dagger \rangle_H$.
The saddle point contribution (to $\ln Z$) in Eq. (10.6) is

$$-\frac{1}{2} \sum_{\alpha\beta} g_\alpha z_{\alpha\beta} g_\beta + \sum_\alpha \ln(1 + \sum_\beta z_{\alpha\beta} g_\beta), \quad (10.12)$$

which is the same as the Hartree approximation in Eq. (4.10).

The advantage of using complex fields as in Eq. (10.5) is that no new auxiliary fields need be introduced when the N colored modified version is introduced. As discussed in Sec. VI given any dimer model a modified "chromo" model can be constructed with a local $U(N)$ symmetry. The coupling between auxiliary fields and fermions becomes

$$\sum_{\alpha\beta} \sum_{i=1}^N \sqrt{\frac{z_{\alpha\beta}}{2N}} (A_{\alpha\beta} n_\alpha^i n_\alpha^{i\dagger} + A_{\alpha\beta}^* n_\beta^i n_\beta^{i\dagger}) \quad (10.13)$$

Integrating over anticommuting variables and rescaling the A 's yields

$$Z^{\text{chromodimer}} = \left(\prod_{\alpha\beta} \int \frac{dA_{\alpha\beta}}{(2\pi)} dA_{\alpha\beta}^* \right) \exp \left[-N(A^{N=1}) \right], \quad (10.14)$$

where $A^{N=1}$ is the same action as in Eq. (10.6). The point in deriving Eq. (10.14) is to show that $1/N$ plays the role of \hbar . On general grounds³³, a loop expansion in the A 's will generate the $1/N$ expansion. This is, of course, what was noted in Sec. VI: that the $1/N$ expansion is an expansion in interaction loops after fermion loops have been shrunk to points. The dotted interaction line in Fig. 11 may be identified with A .

The second bosonization method is similar to the auxiliary field method except that the boson fields are defined at vertices

rather than on bonds. In Sec. IV Feynman rules were given for contracted diagrams (that is, fermion loops contracted to points). Can a functional integral over a scalar field be found which reproduces these rules? The answer is yes. Define a matrix, G , whose elements are $z_{\alpha\beta}$: $G_{\alpha\beta} = z_{\alpha\beta}$. Let H be the inverse of G , so that

$$z_{\alpha\beta} H_{\beta\gamma} = H_{\alpha\beta} z_{\beta\gamma} = \delta_{\alpha\gamma},$$

$$GH = HG = 1, \quad (10.15)$$

$$G_{\alpha\beta} = z_{\alpha\beta}.$$

Then

$$Z^{\text{dimer}} = \mathcal{N} \prod_\alpha \int \frac{d\phi_\alpha}{\sqrt{2\pi}} \exp \left[-\frac{1}{2} \phi_\alpha H_{\alpha\beta} \phi_\beta + \sum_\alpha \sum_{\ell=1}^{\infty} (-1) \frac{1}{\ell} \phi_\alpha^\ell \right], \quad (10.16)$$

works, where $\mathcal{N} = (\det G)^{-\frac{1}{2}}$. The term $(-1) \frac{1}{\ell} \phi_\alpha^\ell$ produces the correct combinatorial factor of $(-1)(\ell-1)!$ in rule (c) of Sec. IV. The second term in Eq. (10.16) is $\sum_\alpha \ln(1-\phi_\alpha)$. Rewriting $\exp\left[\sum_\alpha \ln(1-\phi_\alpha)\right]$ as $\prod_\alpha (1-\phi_\alpha)$, it is not hard to verify directly that Eq. (10.16) produces the dimer partition function.

The Hartree approximation is recovered through the equations of motion and evaluating Eq. (10.16) at the saddle point. The stationary point of Eq. (10.16) is

$$\sum_{\beta} H_{\alpha\beta} \phi_{\beta}^{c\ell} = \left(\frac{-1}{1 - \phi_{\alpha}^{c\ell}} \right). \quad (10.17)$$

Setting $\phi_{\alpha}^{c\ell} = -\sum_{\beta} z_{\alpha\beta} g_{\beta}$ and using Eq.(10.15) transforms (10.17) into

$$g_{\beta} = \frac{1}{1 + \sum_{\alpha} z_{\beta\alpha} g_{\alpha}}, \quad (10.18)$$

which is again the Hartree equations [Eq. (4.9)]. The saddle point contribution again yields the Hartree approximation [Eq. (4.10) or Eq. (10.12)].

For the chromodimer modified problem a factor of N multiplies the action in Eq. (10.16) and $\int \frac{d\phi_{\alpha}}{\sqrt{2\pi}}$ becomes $\int \sqrt{\frac{N}{2\pi}} d\phi_{\alpha}$. Again $1/N$ plays the role of λ and the loop expansion of Eq.(10.16) generates the $1/N$ expansion.

Now shift ϕ_{α} by the classical solution, $\phi_{\alpha}^{c\ell}$. As should be the case terms linear in ϕ are absent from this shifted action:

$$A_{\text{dimer}}^{\text{shifted}} = -\frac{1}{2} \sum_{\alpha\beta} \phi_{\alpha} H_{\alpha\beta} \phi_{\beta} - \sum_{\alpha} \sum_{\ell=2}^{\infty} \frac{(g_{\alpha} \phi_{\alpha})^{\ell}}{\ell} + \left[-\frac{1}{2} \phi_{\alpha}^{c\ell} H_{\alpha\beta} \phi_{\beta}^{c\ell} + \sum_{\alpha} \ln(1 - \phi_{\alpha}^{c\ell}) \right]. \quad (10.19)$$

The last term [in brackets] in Eq. (10.19) is the Hartree approximation.

This shifted action generates the Hartree improved series for the dimer model. The Feynman rules for this scalar field theory are precisely the same as the Hartree improved rules of Sec. IV. The $1/N$ superpropagator is obtained from the quadratic piece of $A_{\text{dimer}}^{\text{shifted}}$:

$$A_{\text{dimer}}^{1/N} = -\frac{1}{2} \sum_{\alpha\beta} \phi_{\alpha} \left[H_{\alpha\beta} + g_{\alpha}^2 \delta_{\alpha\beta} \right] \phi_{\beta} - \sum_{\alpha} \sum_{\ell=3}^{\infty} \frac{(g_{\alpha} \phi_{\alpha})^{\ell}}{\ell} + \left[\text{Hartree Approx.} \right]. \quad (10.20)$$

It is the inverse of this quadratic piece:

$$G_{\alpha\beta}^S = \left([H + g^2]^{-1} \right)_{\alpha\beta}, \quad (10.21)$$

where g^2 denotes the multiplication matrix $(g^2 v)_{\alpha} = g_{\alpha}^2 v_{\alpha}$ (α not summed) for vectors, v . Is $G_{\alpha\beta}^S$ the sum over all random walks from α to β weighted by $z_{\alpha\beta}$ factors and a $(-1)^{\text{number of steps}}$? Yes. Multiply the identity $G^S(H + g^2) = 1$ by G (Eq. 10.15) from the right:

$$G^S(1 + g^2 G) = G,$$

$$G^S = G - Gg^2G + Gg^2Gg^2G - Gg^2Gg^2Gg^2G + \dots, \quad (10.22)$$

or in indexed notation

$$G_{\alpha\alpha'}^S = z_{\alpha\alpha'} - \sum_{\beta} z_{\alpha\beta} g_{\beta}^2 z_{\beta\alpha'} + \sum_{\beta\gamma} z_{\alpha\beta} g_{\beta}^2 z_{\beta\gamma} g_{\gamma}^2 z_{\gamma\alpha'} - \dots, \quad (10.23)$$

which is exactly the series depicted in Fig. 25.

The first $1/N$ correction to the Hartree approximation, the one loop correction, is obtained by dropping $\sum_{\alpha} \sum_{\ell=3}^{\infty} \frac{(g_{\alpha} \phi_{\alpha})^{\ell}}{\ell}$ and doing the quadratic integration:

$$\left[\det (G^S)^{-1} G \right]^{-\frac{1}{2}} = \exp \left(-\frac{1}{2} \text{tr} \ln [(G^S)^{-1} G] \right). \quad (10.24)$$

The factor of G in Eq. (10.24) comes from \mathcal{N} in Eq. (10.16).

Upon using (10.15) and (10.21), Eq. (10.24) becomes

$$\Gamma^{(1)} = -\frac{1}{2} \text{tr} \ln (1 + g^2 G)$$

$$= \sum_{\alpha\beta} \frac{1}{4} g_{\alpha}^2 z_{\alpha\beta} g_{\beta}^2 - \frac{1}{6} \sum_{\alpha\beta\gamma} g_{\alpha}^2 z_{\alpha\beta} g_{\beta}^2 z_{\beta\gamma} g_{\gamma}^2 z_{\gamma\alpha} + \dots, \quad (10.25)$$

which is exactly the terms in Fig. 25.

Summarizing, the bosonic actions in Eqs. (10.16), (10.19), and (10.20) with the Hartree self-consistent equations [Eq. (10.13)] respectively generate simple perturbation theory, the Hartree improved series, and the $1/N$ expansion.

XI. THE FREE-FERMION EIGHT VERTEX MODEL CORRELATION FUNCTIONS

Once a model is solved via the anticommuting variable method, it is straightforward to compute anticommuting variable correlation functions. It is then possible (in practically all cases) to compute physical correlation functions. This was demonstrated for the Ising model in Sec. VI of II.

This section calculates all the vertex correlation functions for the free-fermion model described by Eq. (I.4.3) and Fig. I.11 of paper I. It is just a simple extension of the methods used in II. The answer is expressed in terms of a Pfaffian of (in general) a large matrix. A few simple examples are worked out [see Eqs. (11.2), (11.4), (11.14), (11.16), and (11.25)]. The main result is a set of computational rules. By blindly following them, all vertex correlation functions can be calculated.

In Sec. VI of II Ising model spin correlation functions were calculated. It is just as easy to calculate vertex correlation functions in the free-fermion model [Eq. (I.4.3) and Fig. I.11].

Equations (II.5.18) - (II.5.27) are all that's needed.

Let

$$B_{\alpha+\frac{1}{2}\beta} = z_h \eta_{\alpha\beta}^{\dagger h} \eta_{\alpha+1\beta}^h, \quad (11.1)$$

$$B_{\alpha\beta+\frac{1}{2}} = z_v \eta_{\alpha\beta}^{\dagger v} \eta_{\alpha\beta+1}^v.$$

$B_{\alpha+\frac{1}{2}\beta}$ represents the operator which produces a unit of horizontal wall between (α, β) and $(\alpha+1, \beta)$. Likewise $B_{\alpha\beta+\frac{1}{2}}$ produces a unit of vertical wall between (α, β) and $(\alpha, \beta+1)$. If B's are inserted in the integral of Eq. (I.4.3) then walls must occur where B's operate. A closed polygon partition function with constraints that walls be in certain places is obtained. Hence

$$\langle B_{\alpha+\frac{1}{2}\beta} \rangle = \text{the probability that a wall occurs at } (\alpha+\frac{1}{2}, \beta)$$

$$= z_h \langle \eta_{\alpha\beta}^{\dagger h} \eta_{\alpha+1\beta}^h \rangle,$$

$$\langle B_{\alpha\beta+\frac{1}{2}} \rangle = \text{the probability that a wall occurs at } (\alpha, \beta+\frac{1}{2})$$

$$= z_v \langle \eta_{\alpha\beta}^{\dagger v} \eta_{\alpha\beta+1}^v \rangle. \quad (11.2)$$

Because Eqs. (II.5.8) and (II.5.9) have computed these anticommuting variable correlations, these probabilities are explicitly known. In general

$$\langle B_{\alpha_1\beta_1} B_{\alpha_2\beta_2} \dots B_{\alpha_m\beta_m} \rangle = \text{the probability that walls}$$

$$\text{simultaneously occur at } (\alpha_1, \beta_1), (\alpha_2, \beta_2), \dots, (\alpha_m, \beta_m). \quad (11.3)$$

In Eq. (11.3) one of the indices α_i or β_i is half integer.

To calculate (11.3) insert the definitions in Eq. (11.1) factor out the z_h 's and z_v 's to obtain the expectation value of a product of $2m$ η 's. Use Eq. (II. 6.3) to express this as a Pfaffian of a matrix M . The elements of M are the anticommuting variable correlations given in Eqs. (II.5.18)-(II.5.27). The answer is just a $2m$ by $2m$ dimensional Pfaffian (or an $2m$ by $2m$ determinant since $(\text{Pf } M)^2 = \det M$). For example, the probability that horizontal walls simultaneously occur at $(\alpha + \frac{1}{2}, \beta)$ and $(\alpha' + \frac{1}{2}, \beta')$ is

$$\langle B_{\alpha+\frac{1}{2}\beta} B_{\alpha'+\frac{1}{2}\beta'} \rangle = z_h^2 \left[\langle \eta_{\alpha\beta}^{h\dagger} \eta_{\alpha+1\beta}^h \rangle \langle \eta_{\alpha'\beta'}^{h\dagger} \eta_{\alpha'+1\beta'}^h \rangle \right. \\ \left. + \langle \eta_{\alpha\beta}^{h\dagger} \eta_{\alpha'+1\beta'}^h \rangle \langle \eta_{\alpha+1\beta}^h \eta_{\alpha'\beta'}^{h\dagger} \rangle - \langle \eta_{\alpha\beta}^{h\dagger} \eta_{\alpha'\beta'}^{h\dagger} \rangle \langle \eta_{\alpha+1\beta}^h \eta_{\alpha'+1\beta'}^h \rangle \right]. \quad (11.4)$$

The quantities on the right hand side of Eq.(11.4) are given in Eqs. (II.5.18), (II. 5.22), and (II. 5.25).

A different set of questions can be asked, such as what is the probability that one of the configurations in Fig. I.11 occurs at (α, β) . Define

$$\theta_{\alpha\beta}^{(a)} = (b_h b_v - a_1 a_3 - a_2 a_4) \eta_{\alpha\beta}^h \eta_{\alpha\beta}^{h\dagger} \eta_{\alpha\beta}^v \eta_{\alpha\beta}^{v\dagger}, \quad (11.5)$$

$$o_{\alpha\beta}^{(b)} = b_h \eta_{\alpha\beta}^h \eta_{\alpha\beta}^{h\dagger} (1 - b_v \eta_{\alpha\beta}^v \eta_{\alpha\beta}^{v\dagger}), \quad (11.6)$$

$$o_{\alpha\beta}^{(c)} = b_v \eta_{\alpha\beta}^v \eta_{\alpha\beta}^{v\dagger} (1 - b_h \eta_{\alpha\beta}^h \eta_{\alpha\beta}^{h\dagger}), \quad (11.7)$$

$$o_{\alpha\beta}^{(d)} = a_1 \eta_{\alpha\beta}^{h\dagger} \eta_{\alpha\beta}^v (1 - a_3 \eta_{\alpha\beta}^v \eta_{\alpha\beta}^{h\dagger}), \quad (11.8)$$

$$o_{\alpha\beta}^{(e)} = a_2 \eta_{\alpha\beta}^v \eta_{\alpha\beta}^{h\dagger} (1 - a_4 \eta_{\alpha\beta}^h \eta_{\alpha\beta}^v), \quad (11.9)$$

$$o_{\alpha\beta}^{(f)} = a_3 \eta_{\alpha\beta}^v \eta_{\alpha\beta}^h (1 - a_1 \eta_{\alpha\beta}^h \eta_{\alpha\beta}^v), \quad (11.10)$$

$$o_{\alpha\beta}^{(g)} = a_4 \eta_{\alpha\beta}^h \eta_{\alpha\beta}^v (1 - a_2 \eta_{\alpha\beta}^h \eta_{\alpha\beta}^v), \quad (11.11)$$

$$o_{\alpha\beta}^{(h)} = 1 - \sum_{(j)=(a)}^{(g)} o_{\alpha\beta}^{(j)} = (1 - b_h \eta_{\alpha\beta}^h \eta_{\alpha\beta}^{h\dagger}) (1 - b_v \eta_{\alpha\beta}^v \eta_{\alpha\beta}^{v\dagger}) \\ \times (1 - a_1 \eta_{\alpha\beta}^{h\dagger} \eta_{\alpha\beta}^v) (1 - a_2 \eta_{\alpha\beta}^v \eta_{\alpha\beta}^{h\dagger}) (1 - a_3 \eta_{\alpha\beta}^v \eta_{\alpha\beta}^h) (1 - a_4 \eta_{\alpha\beta}^h \eta_{\alpha\beta}^v). \quad (11.12)$$

In Eq. (11.12) the sum lets j be "a" through "g". The superscripts (a), (b), ..., (h) refer to the configurations in Fig I.11, i.e. $o_{\alpha\beta}^{(a)}$ should be associated with Fig. I.11a. The probability that configuration (a) occurs at (α, β) is

$$\langle o_{\alpha\beta}^{(a)} \rangle = \text{Prob. that conf. (a) occurs at } (\alpha, \beta). \quad (11.13)$$

The reason for this is simple: when $o_{\alpha\beta}^{(a)}$ operates all the anti-commuting variables are used up; no walls can enter the (α, β) site so that nothing can happen (which is exactly what is depicted in Fig I.11a). The factor of $(b_h b_v - a_1 a_3 - a_2 a_4)$ assures that this site has the appropriate weight of configuration (a).

A similar conclusion is reached for the other $0_{\alpha\beta}$'s. The probability in Eq. (11.13) is easily calculated

$$\begin{aligned} \langle 0_{\alpha\beta}^{(a)} \rangle &= (b_h b_v - a_1 a_3 - a_2 a_4) \left[\langle \eta_{\alpha\beta}^h \eta_{\alpha\beta}^{h\dagger} \rangle \langle \eta_{\alpha\beta}^v \eta_{\alpha\beta}^{v\dagger} \rangle \right. \\ &\quad \left. - \langle \eta_{\alpha\beta}^h \eta_{\alpha\beta}^v \rangle \langle \eta_{\alpha\beta}^{h\dagger} \eta_{\alpha\beta}^{v\dagger} \rangle + \langle \eta_{\alpha\beta}^h \eta_{\alpha\beta}^{v\dagger} \rangle \langle \eta_{\alpha\beta}^{h\dagger} \eta_{\alpha\beta}^v \rangle \right]. \end{aligned} \quad (11.14)$$

In general

$$\langle 0_{\alpha_1 \beta_1}^{(c_1)} 0_{\alpha_2 \beta_2}^{(c_2)} \dots 0_{\alpha_m \beta_m}^{(c_m)} \rangle = \text{the probability that sites} \quad (11.15)$$

(α_1, β_1) through (α_m, β_m) have configurations (c_1) through (c_m) .

Equation (11.15) is calculated using Eqs. (11.5)-(11.12), Eq. (II.6.3), and Eqs. (II.5.18)-(II.5.27). The result would be a sum of Pfaffians. A similar sum was encountered in Sec. VI of II in computing Ising model spin correlations [see Eqs. (II.6.9)-(II.6.11)]. There, it was possible to rewrite this sum as a single Pfaffian. The same trick works here. For example,

$$\langle 0_{\alpha\beta}^{(b)} \rangle = \langle b_h \eta_{\alpha\beta}^h \eta_{\alpha\beta}^{h\dagger} (1 - b_v \eta_{\alpha\beta}^v \eta_{\alpha\beta}^{v\dagger}) \rangle \quad (11.16)$$

$$= (-b_h b_v) (\text{Pf } M),$$

where

$$M_{34} = -M_{43} = \langle \eta_3 \eta_4 \rangle - \frac{1}{b_v}, \quad (11.17)$$

$$\text{all other } M_{ij} = \langle \eta_i \eta_j \rangle,$$

and the abbreviations

$$\eta_1 = \eta_{\alpha\beta}^h, \quad \eta_2 = \eta_{\alpha\beta}^{h\dagger}, \quad \eta_3 = \eta_{\alpha\beta}^v, \quad \eta_4 = \eta_{\alpha\beta}^{v\dagger}, \quad (11.18)$$

have been used. In other words the contraction between $\eta_{\alpha\beta}^v \eta_{\alpha\beta}^{v\dagger}$ in calculating Pf M (via Wicks theorem or Gaussian integration) gets an extra contribution of $-\frac{1}{b_v}$. A systematic set of rules can be developed to calculate Eq. (11.15) as a $4m$ by $4m$ Pfaffian.

Rules for Calculating Equation (11.15), the Vertex Correlations

1. Use the following abbreviations for anticommuting variables

$$\eta_{4\ell-3} = \eta_{\alpha_\ell \beta_\ell}^h, \quad \eta_{4\ell-2} = \eta_{\alpha_\ell \beta_\ell}^{h\dagger}, \quad \eta_{4\ell-1} = \eta_{\alpha_\ell \beta_\ell}^v, \quad \eta_{4\ell} = \eta_{\alpha_\ell \beta_\ell}^{v\dagger} \quad (11.19)$$

for $\ell = 1, 2, \dots, m$.

2. Equation (11.15) is

$$\langle 0_{\alpha_1 \beta_1}^{(c_1)} \dots 0_{\alpha_m \beta_m}^{(c_m)} \rangle = \left(\prod_{i=1}^m f^{(c_i)} \right) \text{Pf } M_{ij}, \quad (11.20)$$

where

$$M_{ij} = \langle \eta_i \eta_j \rangle + \Delta_{ij}. \quad (11.21)$$

It remains to define the f 's and Δ_{ij} 's:

3. The f 's are

$$\begin{aligned}
 f^{(a)} = f^{(h)} &= (b_h b_v - a_1 a_3 - a_2 a_4) \equiv f, \\
 f^{(b)} = f^{(c)} &= -b_h b_v, \\
 f^{(d)} = f^{(f)} &= +a_1 a_3, \\
 f^{(e)} = f^{(g)} &= +a_2 a_4.
 \end{aligned}
 \tag{11.22}$$

4. The Δ_{ij} 's are somewhat more awkward to define. Δ_{ij} is antisymmetric in i and j , that is $\Delta_{ij} = -\Delta_{ji}$, so that M in Eq. (11.21) is an antisymmetric matrix. Each of the m operators, $O_{\alpha_i \beta_i}^{(c_i)}$, involve the four anticommuting variables at (α_i, β_i) . It is useful to group these into "clusters". The cluster associated with $O_{\alpha_1 \beta_1}^{(c_1)}$ is η_1, η_2, η_3 , and η_4 , with $O_{\alpha_2 \beta_2}^{(c_2)}$ it is $\eta_5, \eta_6, \eta_7, \eta_8$, etc. If η_i and η_j are from different clusters then $\Delta_{ij} = 0$ (in fact most Δ_{ij} are zero). It is thus sufficient to define Δ_{ij} for i and j within the l^{th} cluster. This depends on (c_l) , the configuration associated with the l^{th} cluster. The results are tabulated as follows:

Configuration Type	Non-zero Δ_{ij}	i, j Values
(a)	all $\Delta_{ij} = 0$	
(b)	$\Delta_{ij} = -\frac{1}{b_v}$	for $i = 4l-1, j = 4l$
(c)	$\Delta_{ij} = -\frac{1}{b_h}$	for $i = 4l-3, j = 4l-2$,

(11.23) Continued on P. 104

Configuration Type	Non-zero Δ_{ij}	i, j Values
(d)	$\Delta_{ij} = \frac{1}{a_3}$	for $i = 4l-3, j = 4l$,
(e)	$\Delta_{ij} = \frac{1}{a_4}$	for $i = 4l-3, j = 4l-1$,
(f)	$\Delta_{ij} = -\frac{1}{a_1}$	for $i = 4l-2, j = 4l-1$,
(g)	$\Delta_{ij} = \frac{1}{a_2}$	for $i = 4l-2, j = 4l$,
(h)	$\Delta_{ij} = \frac{-b_h}{f}$	for $i = 4l-1, j = 4l$,
	$\Delta_{ij} = \frac{-b_v}{f}$	for $i = 4l-3, j = 4l-2$,
	$\Delta_{ij} = \frac{-a_1}{f}$	for $i = 4l-3, j = 4l$,
	$\Delta_{ij} = \frac{-a_2}{f}$	for $i = 4l-3, j = 4l-1$,
	$\Delta_{ij} = \frac{a_3}{f}$	for $i = 4l-2, j = 4l-1$,
	$\Delta_{ij} = \frac{-a_4}{f}$	for $i = 4l-2, j = 4l$,

(11.23)

where f is defined in Eq. (11.22). Equation (11.23) defines Δ_{ij} for $i < j$. For $i > j$, $\Delta_{ij} = -\Delta_{ji}$. All other Δ_{ij} are zero.

Equations (11.16), (11.17), and (11.18) form a simple example of these rules. As a more complicated example let us calculate the probability, $P_{\alpha_1\beta_1\alpha_2\beta_2\alpha_3\beta_3}^{(a)(c)(h)}$, of having simultaneously configurations (a), (c), and (h) at sites (α_1, β_1) , (α_2, β_2) , and (α_3, β_3) . Set

$$\begin{aligned} M_{5,6} &= \langle \eta_5 \eta_6 \rangle - \frac{1}{b_h}, \\ M_{9,10} &= \langle \eta_9 \eta_{10} \rangle - \frac{b_v}{f}, \\ M_{9,11} &= \langle \eta_9 \eta_{11} \rangle - \frac{a_2}{f}, \\ M_{9,12} &= \langle \eta_9 \eta_{12} \rangle - \frac{a_1}{f}, \\ M_{10,11} &= \langle \eta_{10} \eta_{11} \rangle + \frac{a_3}{f}, \\ M_{10,12} &= \langle \eta_{10} \eta_{12} \rangle - \frac{a_4}{f}, \\ M_{11,12} &= \langle \eta_{11} \eta_{12} \rangle - \frac{b_h}{f}, \end{aligned} \quad (11.24)$$

all other $M_{ij} = \langle \eta_i \eta_j \rangle$, ($i, j = 1$ to 12).

The η_i 's are defined via Eq.(11.19) for $\ell = 1, 2$, and 3 . The answer is

$$P_{\alpha_1\beta_1\alpha_2\beta_2\alpha_3\beta_3}^{(a)(c)(h)} = (-b_h b_v)(f)^2 \text{Pf } M_{ij}, \quad (11.25)$$

where f is given in Eq. (11.22). It is easy to calculate free-fermion vertex correlations using the above rules. If m configurations are specified the answer is a Pfaffian of a $4m$ by $4m$ matrix.

I conclude this section with a few remarks:

Remark (a): It is trivial to adapt the formalism to handle walls and vertex configurations simultaneously. Everything is calculable in terms of a Pfaffian. The probability of having a wall at (α, β) and a (b) vertex configuration at (α', β') is easily calculated and would be a Pfaffian of a 6×6 matrix.

Remark (b): When vacuum expectation values are taken, other operators work equally well. For example

$$\langle z_h b_v \eta_{\alpha-1\beta}^{h\dagger} \eta_{\alpha\beta}^h \eta_{\alpha\beta}^v \eta_{\alpha\beta}^{v\dagger} \rangle = \langle 0_{\alpha\beta}^{(c)} \rangle. \quad (11.26)$$

The reason for this is simple. $B_{\alpha-1\beta}^{h\dagger}$ which is $z_h \eta_{\alpha-1\beta}^{h\dagger} \eta_{\alpha\beta}^h$ produces a unit of wall which enters the (α, β) site from the left. Because $\eta_{\alpha\beta}^v \eta_{\alpha\beta}^{v\dagger}$ uses up the vertical variables at (α, β) this wall must continue straight through thus yielding configuration (c); it is impossible to use any of the corners at (α, β) .

In a sense the $0_{\alpha\beta}$'s are not unique; many operators will work. Those defined in Eqs. (11.5)-(11.12), however, have the advantage of using only those anticommuting variables at one site.

Remark (c): The matrix elements of M in Eq.(11.21) involve the anticommuting variable correlations. These, in turn, are given in integral form in Eqs.(II.5.18)-(II.5.27). In principle, the integrals in Eqs.(II.5.18)-(II.5.27) can be done in terms of elliptic functions. Appendix A demonstrates this for the case $(\alpha, \beta) = (\alpha', \beta')$. The method of Appendix A generalizes for the case when $(\alpha, \beta) \neq (\alpha', \beta')$ but is quite tedious. There appears to be no

simple analytic expression for the general case. For each (α, β) and (α', β') the integrals probably must be computed in the same laborious manner as for the $(\alpha, \beta) = (\alpha', \beta')$ case.

XII. THE EIGHT VERTEX MODEL: PERTURBATION THEORY

The eight vertex model is the most general closed non-overlapping polygon partition function on the two dimensional square lattice. At each site there are eight configurations (Fig. I.11), the weights of which can be assigned independently. Many models can be mapped into the eight vertex model. Examples are the usual two-dimensional Ising model, other Ising-like systems, the free-fermion model, ice-type models, the Baxter model, etc. All the above mentioned are exactly solvable. The most general vertex model, however, has not been solved. The ice-type and ferroelectric type models are obtainable from the polygon representation by converting to "arrow" notation in the standard way³⁴. Reference 34 summarizes many of the known results and has a good set of references on the eight vertex model. The large number of models contained in the eight vertex model make it a very interesting system.

The main philosophy of this paper has been the following: Given any unsolved model (i.e. the eight vertex model) find a model (i.e. the free-fermion model) which is exactly solvable via anticommuting variables and can approximate the unsolved model. The eight vertex model can be considered as a perturbation of the free fermion model. It is an interacting fermionic-like field theory. As such one can use the powerful mathematic methods bestowed to us from field theory.

This section contains two main results. The first is a set of Feynman graph rules. Using these one can compute the perturbation series for any action representable in anticommuting variable form. Because of their generality, these rules are somewhat abstract. The eight vertex model is used to exemplify them. This gives rise to the second main result. The eight vertex model is solved to second order in a free fermion breaking parameter, Δ . Equation (12.12) contains this result.

In the most general case, the interaction will be a product of an even number of anticommuting variables, i.e. $g_4 \eta_1 \eta_2 \eta_3 \eta_4$ or $g_6 \eta_1 \eta_2 \eta_3 \eta_4 \eta_5 \eta_6$ with g_4 and g_6 coupling constants. The Feynman graphs are constructed from vertices associated with these interactions. A $2n$ product of anticommuting variables corresponds to a vertex of degree $2n$. The $2n$ endpoints have labels to distinguish the different types of anticommuting variables (see Fig. 43). For $g_{2n} \eta_1 \eta_2 \dots \eta_{2n}$ the labels 1 to $2n$ correspond to the variables η_1 to η_{2n} . Vertices of this type will be called bare vertices. It is convenient to define another type of vertex. Group the anticommuting variables in pairs, i.e. $g_4 (\eta_1 \eta_2) (\eta_3 \eta_4)$ or $g_6 (\eta_1 \eta_2) (\eta_3 \eta_4) (\eta_5 \eta_6)$. Likewise group corresponding labels in pairs. Draw oriented lines between them to denote the order as discussed in I (see Fig. I.7). These vertices will be called "directed vertices" and graphs associated with them "directed graphs". Figure 43 also displays examples of directed vertices.

Feynman Graph Rules For Any Anticommuting Variable Action

(a) Graphs are constructed using directed vertices and drawing dotted lines between anticommuting variable labels (see Figs. 44, 45, and 46, for example). Draw all such topologically distinct directed graphs. In deciding whether graphs are topologically equivalent disregard the orientations of lines. Two graphs G_1 and G_2 are topologically equivalent if for each vertex (and anticommuting variable label) in G_1 , one can associate a vertex (and label) in G_2 , and dotted lines in G_2 are attached between anticommuting variable labels in precisely the same manner as in G_1 .

(b) For each vertex there is a coupling constant factor.

(c) The dotted and solid lines form closed loops. There is a (-1) for each closed loop.

(d) Transverse each closed loop in a particular direction. There is a (-1) for each arrow in the opposite directions.

(e) For each dotted line, oriented from labels α to β there is a factor of $G_{\alpha\beta} \equiv \langle \eta_\alpha \eta_\beta \rangle_0$, where G , the bare propagator, is the anticommuting variable correlation function when the interaction potential is dropped. It is the inverse of the quadratic piece of the action. [If the quadratic form is $\frac{1}{2} \sum_{\alpha\beta} \eta_\alpha H_{\alpha\beta} \eta_\beta$ then $HG = GH = 1$ (in matrix notation) defines G . G satisfies

$$G_{\beta\alpha} = -G_{\alpha\beta}]$$

(f) Form a bare graph by converting vertices to bare vertices, dropping labels and orientations, and converting dotted lines to solid lines (Figs. 44d, 45b, and 46b are examples). Let G be the point symmetry group of this bare graph. There is a factor of

[The order of $G]^{-1}$.

(g) $\Gamma \equiv \log Z = [\text{Pf}(H)] + \sum_{\text{connected graphs}} (\text{weigh of graph})$. Here H is the quadratic form in rule (e), so that $\log [\text{Pf}(H)]$ is Γ for the unperturbed system.

Consider a particular graph, G , with a particular labelling of anticommuting variables. Now consider all graphs obtainable from G by relabelling, that is, erase all the anticommuting labels and reassign them. These graphs all have the same bare graph. Their contribution can be lumped together by using the ϵ -symbol, $\epsilon_{\alpha_1 \alpha_2 \dots \alpha_{2n}}$, for each vertex of order $2n$. This corresponds to taking $V = \frac{g_{2n}}{(2n)!} \epsilon_{\alpha_1 \alpha_2 \dots \alpha_{2n}} \eta_{\alpha_1} \eta_{\alpha_2} \dots \eta_{\alpha_{2n}}$ (summation over repeated indices implied). As an example consider the graphs of one vertex of degree four. Figure 44 shows there are three of them. They have weights $g^4 G_{12} G_{34}$ (Fig. 44a), $g_4 G_{24} G_{31}$ (Fig. 44b), and $-g_4 G_{23} G_{41}$ (Fig. 44c). The sum of these is $\frac{g_4}{8} \epsilon_{i_1 i_2 i_3 i_4} G_{i_1 i_2} G_{i_3 i_4} = g_4 \text{Pf } G$. It is always possible to sum graphs with different oriented structure but the same bare structure:

Rules for Bare Graphs

(a') Draw all topologically distinct bare graphs. For each bare graph choose one directed graph associated with it (see Figs. 44e, 45a, and 46a for examples).

(b') For each vertex of order $2n$, use labels i_1 to i_{2n} . There is a factor of $\epsilon_{i_1 i_2 \dots i_{2n}}$ and a coupling constant factor.

(c'), (d'), (e'), (f'). Rules (c) and (d) still determine the overall sign. Rules (e) and (f) still hold. There are now two new statistical factors associated with bare graphs. Append to (f) the following: For each pair of vertices with ℓ lines between them (Fig. 15) there is a factor of $\frac{1}{\ell!}$. For each vertex with ℓ tadpoles (Fig. 28) there is a factor of $\frac{1}{2^{\ell} \ell!}$.

On a translationally invariant lattice anticommuting variables have a location label, \vec{x} , besides a type label, ℓ : $\eta_{\vec{x}}^{\ell}$. Daggered and undaggered labels can be absorbed into the index, ℓ . The propagator associated with a dotted line oriented from \vec{x} to \vec{y} between labels ℓ and m is $G_{\vec{x}\vec{y}}^{\ell m} = \langle \eta_{\vec{x}}^{\ell} \eta_{\vec{y}}^m \rangle_0$. For a translationally invariant lattice there is a sum over a vertex's location, \vec{x} . One can go to momentum space. The rules are similar to ordinary many body theory.

Momentum Space Rules For a Local Interaction

All the above rules hold except for (e). Replace (e) by (e') write propagators in the form

$$G_{\vec{x}\vec{y}}^{\ell m} = \int_{-\pi}^{\pi} \frac{d^d p}{(2\pi)^d} \exp[-i\vec{p} \cdot (\vec{x} - \vec{y})] G^{\ell m}(\vec{p}), \quad (12.1)$$

where d is the dimension of the space. Assign an independent set of loop momentum (the loops are determined by the bare graph). Associate a factor $\int_{-\pi}^{\pi} \frac{d^d k}{(2\pi)^d}$ for each loop. Determine the momentum in dotted lines by requiring momentum conservation at each vertex. If a momentum \vec{p} flows through a dotted line in the direction of the line orientation from label ℓ to label m there

is a factor $G^{\ell m}(\vec{p})$. Of course, if the orientation is opposite to the momentum flow there is a factor of $G^{\ell m}(-\vec{p}) = -G^{m\ell}(\vec{p})$.

Let us apply these rules to the general eight vertex model. This is the model in Fig. I.11 with all weights assigned arbitrarily. Except for certain subcases (the Baxter model and the free-fermion model) this system is unsolved. Let w_i be the weights shown in Fig. I.11(i). They satisfy one constraint known as the free-fermion constraint, which is

$$w^{(a)}w^{(h)} + w^{(b)}w^{(c)} = w^{(d)}w^{(f)} + w^{(e)}w^{(g)}. \quad (12.2)$$

Now add

$$v^{(a)} = \sum_{\alpha\beta} \Delta^{(a)} \eta_{\alpha\beta}^h \eta_{\alpha\beta}^{h\dagger} \eta_{\alpha\beta}^v \eta_{\alpha\beta}^{v\dagger}, \quad (12.3)$$

to the action in Eq. (I.44). This modifies the weight of configuration (a) in Fig. I.11 [$v^{(a)}$ is proportional to $\sum_{\alpha\beta} 0_{\alpha\beta}^{(a)}$ (Eq. 11.5)]. Weights (b) through (h) are unchanged while weight (a) becomes

$$(a_1 a_3 + a_2 a_4 - b_h b_v) - \Delta^{(a)}. \quad (12.4)$$

The minus in front of $\Delta^{(a)}$ is due to the $(-1)^N$ in Eq. (I.4.3).

Many potentials can be used to break the free-fermion constraint. Examples are

$$v^{(b)} = z_v \Delta^{(b)} \sum_{\alpha\beta} \eta_{\alpha\beta}^h \eta_{\alpha\beta}^{h\dagger} \eta_{\alpha\beta}^v \eta_{\alpha\beta+1}^{v\dagger},$$

$$U^{(b)} = z_v \Delta^{(b)} \sum_{\alpha\beta} \eta_{\alpha\beta}^h \eta_{\alpha\beta}^{h\dagger} \eta_{\alpha\beta-1}^v \eta_{\alpha\beta}^{v\dagger},$$

$$v^{(c)} = z_h \Delta^{(c)} \sum_{\alpha\beta} \eta_{\alpha\beta}^{h\dagger} \eta_{\alpha+1\beta}^h \eta_{\alpha\beta}^v \eta_{\alpha\beta}^{v\dagger},$$

(Eq.(12.5) cont. on p.113)

$$\begin{aligned}
U^{(c)} &= z_h \Delta^{(c)} \sum_{\alpha\beta} \eta_{\alpha-1\beta}^{h\dagger} \eta_{\alpha\beta}^h \eta_{\alpha\beta}^v \eta_{\alpha\beta}^{v\dagger}, \\
V^{(d)} &= z_h \Delta^{(d)} \sum_{\alpha\beta} \eta_{\alpha-1\beta}^{h\dagger} \eta_{\alpha\beta}^h \eta_{\alpha\beta}^{h\dagger} \eta_{\alpha\beta}^v, \\
U^{(d)} &= z_v \Delta^{(d)} \sum_{\alpha\beta} \eta_{\alpha\beta}^{h\dagger} \eta_{\alpha\beta}^v \eta_{\alpha\beta}^{v\dagger} \eta_{\alpha\beta+1}^v, \\
V^{(e)} &= z_v \Delta^{(e)} \sum_{\alpha\beta} \eta_{\alpha\beta-1}^{v\dagger} \eta_{\alpha\beta}^v \eta_{\alpha\beta}^{v\dagger} \eta_{\alpha\beta}^{h\dagger}, \\
U^{(e)} &= z_h \Delta^{(e)} \sum_{\alpha\beta} \eta_{\alpha-1\beta}^{h\dagger} \eta_{\alpha\beta}^h \eta_{\alpha\beta}^{v\dagger} \eta_{\alpha\beta}^{h\dagger}, \\
V^{(f)} &= z_h \Delta^{(f)} \sum_{\alpha\beta} \eta_{\alpha\beta}^{v\dagger} \eta_{\alpha\beta}^h \eta_{\alpha\beta}^{h\dagger} \eta_{\alpha+1\beta}^h, \\
U^{(f)} &= z_v \Delta^{(f)} \sum_{\alpha\beta} \eta_{\alpha\beta-1}^{v\dagger} \eta_{\alpha\beta}^v \eta_{\alpha\beta}^{v\dagger} \eta_{\alpha\beta}^h, \\
V^{(g)} &= z_h \Delta^{(g)} \sum_{\alpha\beta} \eta_{\alpha\beta}^v \eta_{\alpha\beta}^h \eta_{\alpha\beta}^{h\dagger} \eta_{\alpha+1\beta}^h, \\
U^{(g)} &= z_v \Delta^{(g)} \sum_{\alpha\beta} \eta_{\alpha\beta}^{v\dagger} \eta_{\alpha\beta+1}^v \eta_{\alpha\beta}^v \eta_{\alpha\beta}^h.
\end{aligned} \tag{12.5}$$

Adding $V^{(i)}$ (or $U^{(i)}$) to the action in Eq.(I.4.4) will break the free fermion constraint by adding $-\Delta^{(i)}$ to the weight of configuration (i). Although these interactions look non-local in the sense that all anticommuting variables are not multiplied at the same space point, a redefinition of one of the variable's location makes the interaction local. For example, for $V^{(b)}$ redefine $\eta_{\alpha\beta+1}^v$ as $\eta_{\alpha\beta}^v$; then a local interaction is obtained. It is also possible

to find interactions which modify two or more configuration weights.

For example $z_h z_v \Delta \sum_{\alpha\beta} \eta_{\alpha-1\beta}^{h\dagger} \eta_{\alpha\beta}^h \eta_{\alpha\beta}^{v\dagger} \eta_{\alpha\beta+1}^v$ adds $-a_1 \Delta$ to (d) and Δ to (h). All these interactions generate the general eight vertex model and hence they are equivalent. This means that a theory with $V^{(a)}$ for one value of $\Delta^{(a)}$, a_1, a_2, \dots is the same as a theory with $V^{(i)}$ for some corresponding values of $\Delta^{(i)}$, a_1, a_2, \dots .

However, they are not equivalent in the sense that some will yield better perturbation series (or Hartree-Fock series or $1/N$ expansions) for certain eight vertex models than others. Each will generate different perturbation, Hartree-Fock, and $1/N$ expansions. Many different series can be obtained from Eqs. (12.3) and (12.5). It is up to one's ingenuity to determine which is best. I know no simple way to decide this.

I will use $V^{(a)}$ as the interaction. The calculation will be done to second order in $\Delta \equiv \Delta^{(a)}$. It will be convenient to use numbers to label the different types of anticommuting variables:

$$1 \leftrightarrow h,$$

$$2 \leftrightarrow h^\dagger,$$

$$3 \leftrightarrow v,$$

$$4 \leftrightarrow v^\dagger,$$

so that $\eta_{\alpha\beta}^1 = \eta_{\alpha\beta}^h$, $\eta_{\alpha\beta}^2 = \eta_{\alpha\beta}^{h^\dagger}$, etc.

(12.6)

The lowest order diagrams are shown in Figs. 44a, 44b, and 44c. The corresponding bare graph is Fig. 44d and a "label blind" graph is shown in Fig. 44e from which one concludes

$$\begin{aligned} \Gamma^{(1)} &= \frac{\Delta}{8} \varepsilon_{i_1 i_2 i_3 i_4} \langle \eta_{\alpha\beta}^{i_1 i_2} \rangle \langle \eta_{\alpha\beta}^{i_3 i_4} \rangle \\ &= \Delta \left[\langle \eta_{\alpha\beta}^h \eta_{\alpha\beta}^{h\dagger} \rangle \langle \eta_{\alpha\beta}^v \eta_{\alpha\beta}^{v\dagger} \rangle + \langle \eta_{\alpha\beta}^v \eta_{\alpha\beta}^h \rangle \langle \eta_{\alpha\beta}^{h\dagger} \eta_{\alpha\beta}^{v\dagger} \rangle \right. \\ &\quad \left. - \langle \eta_{\alpha\beta}^{h\dagger} \eta_{\alpha\beta}^v \rangle \langle \eta_{\alpha\beta}^{v\dagger} \eta_{\alpha\beta}^h \rangle \right]. \end{aligned} \quad (12.7)$$

These anticommuting variable correlations are given in integral form in Eqs. (II.5.18) - (II.5.21), (II.5.24), and (II.5.27). In Appendix A they are computed in terms of elliptic functions.

In momentum space (with loop momentum as shown in Fig. 44d) Eq. (12.7) becomes

$$\Gamma^{(1)} = \Delta \int \frac{d^2 k_1}{(2\pi)^2} \int \frac{d^2 k_2}{(2\pi)^2} \frac{1}{8} \varepsilon_{i_1 i_2 i_3 i_4} \left(\frac{N_{i_1 i_2}(\vec{k}_1) N_{i_3 i_4}(\vec{k}_2)}{L(\vec{k}_1) L(\vec{k}_2)} \right), \quad (12.8)$$

where $L(p_x, p_y)$ and $N_{ij}(p_x, p_y)$ are the denominators and numerators in Eqs. (II.5.18) - (II.5.27), that is, $L(p_x, p_y)$ is given in Eq. (II.3.4) with Eq. (II.2.2). For Eqs. (II.5.18) - (II.5.24), the $N_{ij}(p_x, p_y)$ are precisely the numerators, i.e. $N_{12}(p_x, p_y) \equiv N_{hh}^{\dagger}(p_x, p_y) = [h(-p_x)v(p_y)v(-p_y) - a_1 a_3 v(p_y) - a_2 a_4 v(-p_y)]$, etc. The propagators must be put in the form of Eq. (12.1) so that for Eqs. (II.5.25) - (II.5.27) the $N_{ij}(p_x, p_y)$ are the numerators with opposite momentum flow: $N_{22}(p_x, p_y) \equiv N_{hh}^{\dagger}(p_x, p_y) \equiv a_3 a_4 [v(-p_y) - v(p_y)]$,

$N_{44}(p_x, p_y) \equiv N_{vv}^{\dagger}(p_x, p_y) = a_1 a_4 [h(p_x) - h(p_x)]$, and $N_{42}(p_x, p_y) \equiv N_{vh}^{\dagger}(p_x, p_y) \equiv a_4 [a_1 a_3 + a_2 a_4 - h(-p_x)v(p_y)]$. It is true that $N_{ji}(p_x, p_y) = -N_{ij}(-p_x, -p_y)$ for all i and j .

There are two bare graphs at second order. These are shown in Figs. 45 and 46. The result is

$$\Gamma^{(2)} = \Gamma_1^{(2)} + \Gamma_2^{(2)}, \quad (12.9)$$

where in coordinate space

$$\begin{aligned} \Gamma_1^{(2)} &= \left(\frac{\Delta^2}{2} \right) \frac{1}{8} \varepsilon_{i_1 i_2 i_3 i_4} \varepsilon_{j_1 j_2 j_3 j_4} \sum_{\alpha\beta} \\ &\quad \times \langle \eta_{\alpha\beta}^{i_1 i_2} \rangle \langle \eta_{\alpha\beta}^{i_3 i_4} \rangle \langle \eta_{\alpha\beta}^{j_1 j_2} \rangle \langle \eta_{\alpha\beta}^{j_3 j_4} \rangle, \\ \Gamma_2^{(2)} &= \left(\frac{\Delta^2}{2} \right) \frac{1}{4!} \varepsilon_{i_1 i_2 i_3 i_4} \varepsilon_{j_1 j_2 j_3 j_4} \sum_{\alpha\beta} \\ &\quad \times \langle \eta_{\alpha\beta}^{j_1 i_1} \rangle \langle \eta_{\alpha\beta}^{i_2 j_2} \rangle \langle \eta_{\alpha\beta}^{j_3 i_3} \rangle \langle \eta_{\alpha\beta}^{i_4 j_4} \rangle, \end{aligned} \quad (12.10)$$

and in momentum space (with loop momentum as in Figs. 45b and 46b)

$$\begin{aligned} \Gamma_1^{(2)} &= \left(\frac{\Delta^2}{2} \right) \frac{1}{8} \varepsilon_{i_1 i_2 i_3 i_4} \varepsilon_{j_1 j_2 j_3 j_4} \int \frac{d^2 k_1}{(2\pi)^2} \int \frac{d^2 k_2}{(2\pi)^2} \int \frac{d^2 k_3}{(2\pi)^2} \\ &\quad \times \left(\frac{N_{i_1 i_2}(\vec{k}_1)}{L(\vec{k}_1)} \right) \left(\frac{N_{i_3 i_4}(\vec{k}_2)}{L(\vec{k}_2)} \right) \left(\frac{N_{j_1 j_2}(\vec{k}_3)}{L(\vec{k}_3)} \right), \\ \Gamma_2^{(2)} &= \left(\frac{\Delta^2}{8} \right) \frac{1}{4!} \varepsilon_{i_1 i_2 i_3 i_4} \varepsilon_{j_1 j_2 j_3 j_4} \int \frac{d^2 k_1}{(2\pi)^2} \int \frac{d^2 k_2}{(2\pi)^2} \int \frac{d^2 k_3}{(2\pi)^2} \\ &\quad \times \left(\frac{N_{j_1 i_1}(\vec{k}_1)}{L(\vec{k}_1)} \right) \left(\frac{N_{i_2 j_2}(\vec{k}_1 + \vec{k}_2)}{L(\vec{k}_1 + \vec{k}_2)} \right) \left(\frac{N_{j_3 i_3}(\vec{k}_2 + \vec{k}_3)}{L(\vec{k}_2 + \vec{k}_3)} \right) \left(\frac{N_{i_4 j_4}(\vec{k}_3)}{L(\vec{k}_3)} \right). \end{aligned} \quad (12.11)$$

If $\Gamma^{(0)}$ is defined to be the Γ for the free fermion model [Eq. (II. 3.6)] then the general eight vertex model has been solved to second order in the free fermion breaking parameter, Δ :

$$\Gamma^{8\text{-vertex}} = \Gamma^{(0)} + \Gamma^{(1)} + \Gamma^{(2)} + \dots, \quad (12.12)$$

where $\Gamma^{(0)}$, $\Gamma^{(1)}$, and $\Gamma^{(2)}$ are given in Eqs. (II.3.6), (12.8), and (12.9). Equation (12.12) is a main result in this section.

XIII. THE HARTREE-FOCK APPROXIMATION FOR THE EIGHT VERTEX MODEL

This section presents the Hartree-Fock equations for the general eight vertex model. Not only is the Hartree-Fock approximation of interest by itself but it is the first step in obtaining the Hartree-Fock improved expansion or the $1/N$ expansion. Such expansions are expected to have a range of validity much greater than the perturbation theory of Sec. 12. Unfortunately the Hartree-Fock equations are formidable. This is not unexpected for such a general unsolved model in which there are seven coupling constants. The system is six algebraic non-linear equations involving elliptic integrals. Because of their formidability no attempt is made to solve them. Instead, this section simply presents the equations. They can be the starting point for future work. Given a particular model computers can be used to find solutions. The important equations are Eqs. (13.4) and (13.5).

The Hartree-Fock equations for the 8-vertex model are easy to write down. To solve them is a more difficult matter. The interaction in Eq. (12.3) will be used. The Hartree-Fock approximation consists of the replacement

$$\begin{aligned} & \Delta n_{\alpha\beta}^h n_{\alpha\beta}^{h\dagger} n_{\alpha\beta}^v n_{\alpha\beta}^{v\dagger} + \Delta \left[n_{\alpha\beta}^h n_{\alpha\beta}^{h\dagger} \langle n_{\alpha\beta}^v n_{\alpha\beta}^{v\dagger} \rangle_H + \langle n_{\alpha\beta}^h n_{\alpha\beta}^{h\dagger} \rangle_H n_{\alpha\beta}^v n_{\alpha\beta}^{v\dagger} \right. \\ & - n_{\alpha\beta}^{v\dagger} n_{\alpha\beta}^h \langle n_{\alpha\beta}^{h\dagger} n_{\alpha\beta}^h \rangle_H - \langle n_{\alpha\beta}^{v\dagger} n_{\alpha\beta}^h \rangle_H n_{\alpha\beta}^{h\dagger} n_{\alpha\beta}^h \\ & \left. - n_{\alpha\beta}^v n_{\alpha\beta}^h \langle n_{\alpha\beta}^{v\dagger} n_{\alpha\beta}^{h\dagger} \rangle_H - \langle n_{\alpha\beta}^v n_{\alpha\beta}^h \rangle_H n_{\alpha\beta}^{v\dagger} n_{\alpha\beta}^{h\dagger} \right] \\ & + \Delta \left[- \langle n_{\alpha\beta}^h n_{\alpha\beta}^{h\dagger} \rangle_H \langle n_{\alpha\beta}^v n_{\alpha\beta}^{v\dagger} \rangle_H + \langle n_{\alpha\beta}^{v\dagger} n_{\alpha\beta}^h \rangle_H \langle n_{\alpha\beta}^{h\dagger} n_{\alpha\beta}^v \rangle_H \right. \\ & \left. + \langle n_{\alpha\beta}^v n_{\alpha\beta}^h \rangle_H \langle n_{\alpha\beta}^{v\dagger} n_{\alpha\beta}^{h\dagger} \rangle_H \right]. \end{aligned} \quad (13.1)$$

More precisely, the first four terms represent Hartree-Fock. In this model all contractions must be made. Equation (13.1) might be more appropriately called the Hartree-Fock BCS approximation. This replacement makes the anticommuting variable action quadratic. The Hartree-Fock expectations, $\langle \rangle_H$, are determined self-consistently. This leads to six non-linear equations. They involve the functions in Equations (II. 5.18) - (II. 5.21), (II.5.24), and (II.5.27) at $(\alpha', \beta') = (\alpha, \beta)$. It is important to make explicit their functional dependence on b_h, b_v, a_1, a_2, a_3 , and a_4 . Write

$$f_{ij}(b_h, b_v, a_1, a_2, a_3, a_4) = \langle n_{\alpha\beta}^i n_{\alpha\beta}^j \rangle \quad (13.2)$$

where (i,j) take on the six values (h, h^\dagger) , (v, v^\dagger) , (h^\dagger, v) , (v^\dagger, h^\dagger) , (v^\dagger, h) , and (v, h) and the six anticommuting variable correlations are given in Eqs. (II.5.18) - (II.5.21), (II.5.24), and (II.5.27).

In these equations all functional dependence on $b_h, b_v, a_1, a_2, a_3,$ and a_4 must be made manifest including the dependence of $h(p_x), v(p_y),$ and $L(p_x, p_y)$ on these parameters. Set

$$\begin{aligned}
 b_h' &= b_h + \Delta \langle n_{\alpha\beta}^v n_{\alpha\beta}^{v\dagger} \rangle_H, \\
 b_v' &= b_v + \Delta \langle n_{\alpha\beta}^h n_{\alpha\beta}^{h\dagger} \rangle_H, \\
 a_1' &= a_1 - \Delta \langle n_{\alpha\beta}^{v\dagger} n_{\alpha\beta}^h \rangle_H, \\
 a_2' &= a_2 - \Delta \langle n_{\alpha\beta}^v n_{\alpha\beta}^h \rangle_H, \\
 a_3' &= a_3 - \Delta \langle n_{\alpha\beta}^{h\dagger} n_{\alpha\beta}^v \rangle_H, \\
 a_4' &= a_4 - \Delta \langle n_{\alpha\beta}^{v\dagger} n_{\alpha\beta}^{h\dagger} \rangle_H,
 \end{aligned} \tag{13.3}$$

where the Hartree-Fock expectations are

$$\langle n_{\alpha\beta}^i n_{\alpha\beta}^j \rangle_H = f_{ij}(b_h', b_v', a_1', a_2', a_3', a_4'), \tag{13.4}$$

and the indices (i, j) take on the same six values as above.

Because of Eqs. (13.3) the Hartree-Fock correlations appear on both sides of Eq. (13.4).

In Appendix A the f_{ij} functions are explicitly computed in terms of elliptic integrals. Equation (13.4) represents six algebraic non-linear equations involving elliptic functions. In general, they are difficult to solve. Perhaps, at low temperatures, at high temperatures, and at critical points approximate solutions

can be found by using the asymptotic forms for elliptic integrals. For a particular model in which many of the constants, $b_h, b_v, a_1, a_2, a_3, a_4,$ and Δ have numerical values, approximate solutions can be obtained via computers. The bootstrap technique can be applied: Guess a solution, plug into the right hand side of Eq. (13.4), calculate a new set of $\langle \rangle_H$'s as input. Hopefully the process converges to a fixed point solution.

Equations (13.4) along with Appendix A represent the system to be solved to obtain the Hartree-Fock approximation. They are the key equations.

Given such a solution, $\Gamma^{H.F.}$, the Hartree-Fock approximation to $\frac{1}{N} \log Z$, is

$$\begin{aligned}
 \Gamma^{H.F.}(b_h, b_v, a_1, a_2, a_3, a_4) &= \Gamma^{f.f.}(b_h', b_v', a_1', a_2', a_3', a_4') \\
 &+ \Delta \left[- \langle n_{\alpha\beta}^h n_{\alpha\beta}^{h\dagger} \rangle_H \langle n_{\alpha\beta}^v n_{\alpha\beta}^{v\dagger} \rangle_H + \langle n_{\alpha\beta}^{v\dagger} n_{\alpha\beta}^h \rangle_H \langle n_{\alpha\beta}^{h\dagger} n_{\alpha\beta}^v \rangle_H \right. \\
 &\left. + \langle n_{\alpha\beta}^v n_{\alpha\beta}^h \rangle_H \langle n_{\alpha\beta}^{v\dagger} n_{\alpha\beta}^{h\dagger} \rangle_H \right], \tag{13.5}
 \end{aligned}$$

where $\Gamma^{f.f.}$, the free-fermion solution given in Eq.(II.3.6), is computed using the values, $b_h', b_v', a_1', a_2', a_3,$ and a_4 in Eqs. (13.3).

Corrections to the Hartree-Fock approximation can systematically be computed in the same manner as in Sec. IV: Use the parameters, $b_h', b_v', a_1', a_2', a_3,$ and a_4 in the anticommuting variable correlation functions, use the Feynman rules of Sec. XII, but ignore all graphs with self energy tadpoles.

XIV. OTHER TECHNIQUES

This section briefly discusses other approximation methods. Paragraph (b) studies the effects of explicitly doing some of the anticommuting integrals. The two-dimensional dimer problem is used as an example. Paragraph (c) discusses methods of obtaining upper bounds on the free energy. Equation (14.17) displays result for the three-dimensional close-packed dimer model. Finally paragraph (d) explains how correlation functions can be computed via the methods of this paper.

(a) Standard Many Body Theory. Although many approximation methods have been considered in this paper there are still others. All the standard techniques in many body theory²⁴ can be adapted. For example, there is the Bethe-Salpeter equation which sums the ladder diagrams. This method would be particularly good for bound state problems. The closed polygons in the general eight vertex model can be thought of as particle trajectories. For certain values of Δ a two particle bound state will form. Even if bound states do not occur, the ladder diagrams may still be a good approximation scheme.

(b) Partial Integration and the Renormalization Group.

This method should be useful near critical points. There are two approaches. The first is to use the renormalization group equations to sum leading infrared diverges. Consider the eight vertex model as a perturbation of the free-fermion model. Some free fermion correlation functions diverge logarithmically at the critical point. When perturbation theory is used these infrared logarithms will manifest themselves. The renormalization group equations sum the leading logarithmic behavior and calculate, for example, critical

indices. This approach should be particularly useful in understanding critical phenomenon. The other approach is to do a subset of anticommuting variable integrals. This can lead to many interesting transformations, insights, and techniques.

Take the two dimensional dimer model (in the isotropic case $z_h = z_v = z$ for simplicity) and integrate out every other site, i.e. the odd sites. Each anticommuting integral at (α, β) ($\alpha + \beta =$ an odd integer) results in the factor

$$1 + z B_{\alpha\beta} \quad (14.1)$$

$$B_{\alpha\beta} = N_{\alpha+1\beta} + N_{\alpha-1\beta} + N_{\alpha\beta+1} + N_{\alpha\beta-1}$$

where $N_{\alpha\beta}$ is the monomer operator at (α, β) : $n_{\alpha\beta} n_{\alpha\beta}^\dagger$. $B_{\alpha\beta}$ is the sum of the four nearest neighbor [to (α, β)] monomer operators. The factor in Eq. (14.1) can be exponentiated to yield

$$\exp \left[\ln(1 + z B_{\alpha\beta}) \right] = \exp \left[z B_{\alpha\beta} - \frac{z^2}{2} (B_{\alpha\beta})^2 + \frac{z^3}{3} (B_{\alpha\beta})^3 - \frac{z^4}{4} (B_{\alpha\beta})^4 \right] \quad (14.2)$$

Higher powers in $B_{\alpha\beta}$ are absent from Eq. (14.2) because squares of anticommuting variables are zero. After the integration over odd sites is done, variables are located at only even sites. A diamond type lattice is obtained. By rotating it 45° and rescaling the lattice spacing by a factor of $\frac{1}{\sqrt{2}}$ a square lattice is obtained just like the original one except that there are half as many sites. Equation (14.2) generates polymers on this new lattice: They are

nearest neighbor dimers, next nearest neighbor dimers, right angle trimers, and square quadrimers. Monomers are also generated and when combined with the original monomers at even sites a factor of

$$(1 + 4z), \quad (14.3)$$

multiplies these operators. Rescaling $\eta \rightarrow \frac{1}{\sqrt{1+4z}} \eta$ and $\eta^\dagger \rightarrow \frac{1}{\sqrt{1+4z}} \eta^\dagger$ returns this factor to 1. The conclusion is

$$z^{2\text{-dimer}}(z, N) = (1 + 4z)^{N/2} z^{\text{polymer}}(\omega_2^{\text{NN}}, \omega_2^{\text{NNN}}, \omega_3, \omega_4, \frac{N}{2}), \quad (14.4)$$

where N is the number of sites, ω_2^{NN} , ω_2^{NNN} , ω_3 , and ω_4 are the new weights for nearest neighbor dimers, next nearest neighbor dimers, right angle trimers, and square quadrimers. These polymers are shown in Fig. 47. There are two kinds of each of the two types of dimers corresponding to the two directions they can point. There are four kinds of right angle trimers. The weights in Eq. (14.4) are

$$\begin{aligned} \omega_2^{\text{NN}} &= \frac{-2z^2}{(1+4z)^2}, \\ \omega_2^{\text{NNN}} &= \frac{-z^2}{(1+4z)^2}, \\ \omega_3 &= \frac{2z^3}{(1+4z)^3}, \\ \omega_4 &= \frac{-6z^4}{(1+4z)^4}. \end{aligned} \quad (14.5)$$

Notice that the ω 's are now at most of intermediate magnitude. This seems to happen often for models which I have looked at: After integrating out sites, even a strong coupling problem gets mapped into a model with an intermediate (less than unity) coupling. The magnitudes of the ω 's are bounded by $\frac{1}{8}$, $\frac{1}{16}$, $\frac{1}{32}$, and $\frac{3}{128}$. Perturbative methods will now work better.

The action corresponding to Fig. 47 is easily written down. To save space it is omitted. By now the reader should have no problem transcribing pictures into equations. For example, the first trimer in Fig. 47(e) corresponds to an action of

$$\omega_3 \sum_{\alpha\beta} N_{\alpha-1\beta} N_{\alpha\beta} N_{\alpha\beta+1} \quad \text{where} \quad N_{\alpha\beta} \equiv \eta_{\alpha\beta} \eta_{\alpha\beta}^\dagger.$$

There are several continuations to the representation of the two dimensional dimer model as a polymer system in Eq. (14.4):

(i) One can try to integrate out more sites. Unfortunately because of the next nearest neighbor interactions, integrals over only one fourth of the new sites can be done. This will lead to even more complicated polymer structures.

(ii) Because the couplings in Eq. (14.5) are small low temperature expansions should work. Rushbrooke, Scoins, and Wakefield²⁰ have adapted the Mayer cluster expansion to lattice polymer systems. Their method is amenable to Eq. (14.4). For z sufficiently small Eq. (14.4) will be an ideal gas:

$$\Gamma^{2\text{-d dimer}}(z) \sim \frac{1}{2} \log(1+4z) + \omega_2^{\text{NN}} + \omega_3^{\text{NNN}} + 2\omega_3 + \frac{1}{2}\omega_4. \quad (14.6)$$

(iii) The Hartree approximation can be applied. This consists of the replacements

$$N_1 N_2 = :N_1 N_2: + \langle N_1 \rangle_H N_2 + N_1 \langle N_2 \rangle_H - \langle N_1 \rangle_H \langle N_2 \rangle_H,$$

$$\begin{aligned} N_1 N_2 N_3 &= :N_1 N_2 N_3: + (:N_1 N_2: \langle N_3 \rangle_H + :N_1 N_3: \langle N_2 \rangle_H + :N_2 N_3: \langle N_1 \rangle_H) \\ &+ (N_1 \langle N_2 \rangle_H \langle N_3 \rangle_H + N_2 \langle N_1 \rangle_H \langle N_3 \rangle_H + N_3 \langle N_1 \rangle_H \langle N_2 \rangle_H) \\ &- 2 \langle N_1 \rangle_H \langle N_2 \rangle_H \langle N_3 \rangle_H, \end{aligned} \quad (14.7)$$

$$\begin{aligned} N_1 N_2 N_3 N_4 &= :N_1 N_2 N_3 N_4: + (:N_1 N_2 N_3: \langle N_4 \rangle_H + \text{permutations}) \\ &+ (:N_1 N_2: \langle N_3 \rangle_H \langle N_4 \rangle_H + \text{permutations}) \\ &+ (N_1 \langle N_2 \rangle_H \langle N_3 \rangle_H \langle N_4 \rangle_H + \text{permutations}) \\ &- 3 \langle N_1 \rangle_H \langle N_2 \rangle_H \langle N_3 \rangle_H \langle N_4 \rangle_H, \end{aligned}$$

where N_i stands for any of the monomer operators, the colons denote normal ordering, meaning that contractions are not allowed within the colons, and $\langle \rangle_H$ denotes the Hartree expectation to be determined self-consistently. The Hartree approximation ignores the normal order interaction terms and uses the action linearized by Eqs. (14.7). The self-consistent equations are

$$\langle N_{\alpha\beta} \rangle_H = [1 + 4(\omega_2^{NN} + \omega_2^{NNN}) \langle N_{\alpha\beta} \rangle_H + 12\omega_3 \langle N_{\alpha\beta} \rangle_H^2 + 4\omega_4 \langle N_{\alpha\beta} \rangle_H^3]^{-1}. \quad (14.8)$$

Equation (14.8) is a fourth order polynomial in $\langle N_{\alpha\beta} \rangle_H$ and can be solved algebraically. Given the solution, the Hartree approximation is

$$\begin{aligned} \Gamma^{\text{2-dimer H.A.}}(z) &= \frac{1}{2} \log(1 + 4z) + \frac{1}{2} \log[1 + 4(\omega_2^{NN} + \omega_2^{NNN}) \langle N_{\alpha\beta} \rangle_H \\ &+ 12\omega_3 \langle N_{\alpha\beta} \rangle_H^2 + 4\omega_4 \langle N_{\alpha\beta} \rangle_H^3] - \langle N_{\alpha\beta} \rangle_H^2 (\omega_2^{NN} + \omega_2^{NNN}) \\ &- 4\omega_3 \langle N_{\alpha\beta} \rangle_H^3 - \frac{3}{2} \omega_4 \langle N_{\alpha\beta} \rangle_H^4. \end{aligned} \quad (14.9)$$

There are factors of $\frac{1}{2}$ in Eq. (14.9) due to the fact that there are only $\frac{N}{2}$ sites. Corrections can systematically be computed using the normal ordered interactions in a manner similar to Sec. IV.

(iv) One can try to approximate the polymer system by a dimer system and then use the renormalization group method³⁵. Unfortunately the process of approximating a polymer system is rather arbitrary. Its success depends on the ingenuity of the approximation. Furthermore, there is no systematic way to calculate corrections. These are great disadvantages to this approach.

Let us replace the monomer operators in the next nearest neighbor dimers, in the trimers, and in the quadrimers by c-numbers, c, so that they become a linear combination of nearest neighbor dimers, monomers, and constants. The process is shown in Fig. 48. The next nearest neighbor dimer replacement is, as indicated in Fig. 48a, $N_{\alpha\beta} N_{\alpha+1\beta+1} \rightarrow c N_{\alpha\beta} + c N_{\alpha+1\beta+1} - c^2$, and so on for the other polymers. The constant, c, represents a rough approximation to the vacuum expectation of $\langle N_{\alpha\beta} \rangle$. In lowest order perturbation theory $c = 1$.

A better approximation might be to set $c = \langle \eta_{\alpha\beta} \eta_{\alpha\beta}^+ \rangle_H$ determined from Eq. (14.8). When the replacements in Fig. 48 are done the following renormalization group equation is obtained:

$$Z(z, N) = (1 + 4z)^{N/2} (1 + 4c\omega_2^{NNN} - 4c^2\omega_3 - 4c^3\omega_4)^{N/2} \times \exp \frac{N}{2} (-c^2\omega_2^{NNN} + c^4\omega_4) Z(z', \frac{N}{2}), \quad (14.10)$$

where

$$z' = \frac{\omega_2^{NN} + 4c\omega_3 + 2c^2\omega_4}{(1 + 4c\omega_2^{NNN} - 4c^2\omega_3 - 4c^3\omega_4)^2}. \quad (14.11)$$

Let us consider the case $c = 1$ which is at least valid at a low temperatures. The only fixed point of Eq. (14.1) is $z = 0$. Under Eq.(14.1) the z' 's which are generated occur between 0 and $\frac{-48}{529}$ for z ranging from to infinity. The positive real axis is mapped onto a small negative interval below 0. Successive transformations move transformed z' 's closer to zero so that the flow is up the negative axis towards zero. No phase transition is indicated in accord with reference 12.

(c) Lower Bounds. The methods used in I and II to exactly solve models in two dimensions do not extend to three dimensions. A prime example is the close-packed dimer model on the simple cubic lattice. The solvability condition in Sec. IV of II is not satisfied because of non-planarity. In terms of anticommuting variables, extension of the method of solution in IV to three dimensions doesn't work because of minus signs due to reordings of variables. Instead

of calculating

$$Z = \sum_{\text{configurations}} (\text{Boltzmann factor of configuration}), \quad (14.12)$$

anticommuting variable integrals calculate

$$Z' = \sum_{\text{configurations}} \pm (\text{Boltzmann factor}), \quad (14.13)$$

so that some configurations have negative weight. Equations (14.12) and (14.13) imply that

$$Z \geq Z', \quad (14.14)$$

so that a lower bound on Z can be calculated. This method of calculating lower bounds works for many three dimensional unsolved systems (i.e., the three dimensional Ising model). I will use the three dimensional close-packed dimer model as an example.

Let us apply the techniques in Sec. IV of II. First arrange bond orientations so that all elementary polygons are clockwise odd. Choose bonds in the z direction to point in the z direction unless the bond's location is $(2\ell, 2m, z)$ (with ℓ and m integers and z half-integer), in which case the orientation points in the negative z direction. The midpoint of a bond specifies its location. Likewise choose bonds in the x direction (respectively y direction) to point in the positive x direction (respectively y direction)

unless the bond's position is $(x, 1 + 2\ell, 1 + 2m)$ [respectively $(1 + 2\ell, y, 2m)$] where ℓ and m are integers and x and y are half-integers. Now use the Graphical Rules When Condition C Holds (Sec. IV of II). A unit consists of an elementary lattice cube of eight sites. Within the cube there are twelve [type (a)] bonds (see Fig. 49a) and contingent are twelve type (b) bonds which go to a neighboring site (see Fig. 49b). A standard configuration is shown in Fig. 49c. When type (b) bonds are "folded" back into the elementary cube, the weights indicated in Fig. 50 are obtained. Here

$$\begin{aligned} h(p_x) &= z_x [1 - \exp(ip_x)] , \\ v(p_y) &= z_y [1 - \exp(ip_y)] , \\ u(p_z) &= z_z [1 - \exp(ip_z)] , \end{aligned} \quad (14.15)$$

and $z_x, z_y,$ and z_z are the Boltzmann factors for dimers in each of the three directions. The nine coverings of the miniature dimer problem are easily found. They sum to

$$L(p_x, p_y, p_z) = [h(p_x)h(-p_x) + v(p_y)v(-p_y) + u(p_z)u(-p_z)]^2, \quad (14.16)$$

so that

$$\Gamma_{3\text{-d pure dimer}}(z_x, z_y, z_z) \geq \frac{1}{4} \int_{-\pi}^{\pi} \frac{dp_x}{2\pi} \int_{-\pi}^{\pi} \frac{dp_y}{2\pi} \int_{-\pi}^{\pi} \frac{dp_z}{2\pi} \quad (14.17)$$

$$\times \ln [2z_x^2(1 - \cos p_x) + 2z_y^2(1 - \cos p_y) + 2z_z^2(1 - \cos p_z)] .$$

Figure 51 shows an example of a configuration with a negative weight so that the inequality in Eq. (14.17) is strict unless one of the z 's vanishes in which case the right hand side becomes exact. The right hand side of Eq. (14.17) is analytic in $z_x, z_y,$ and z_z . If it were a good approximation to the exact answer it would indicate the absence of a phase transition.

This method of obtaining lower bounds on the free-energy is applicable to many systems. As an approximation to the exact partition function it suffers from the same disadvantage as the real space renormalization method: corrections are either difficult or impossible to calculate. All configurations of negative weight must be found and compensated for.

(d) The Calculation of Correlation Functions. Because statistical systems have been rewritten as fermionic-like field theories, the approximation methods use to calculate partition functions can be applied to correlation functions. The free energy is the sum of vacuum bubble diagrams. Anticommuting variable correlation functions are calculated by using Feynman graphs with external legs. When physical correlation are related to anticommuting variable ones, a perturbative computation of physical correlations is possible. More sophisticated approaches can also be incorporated including the Hartree-improved perturbative and $1/N$ techniques. The same systematic methods work for correlation functions.

XV. CONCLUSION

These papers have demonstrated the power of anticommuting variables. Models, which are solvable, are trivially solved. For models which are unsolvable there are powerful approximation methods.

I have tried to choose simple but interesting models to exemplify the techniques. However, the anticommuting variable method is applicable to a wide range of systems. Whenever there is a constraint that objects can overlap (be it polygons, polymers, or surfaces) the anticommuting variables will be useful.

Although many many new results have been obtained, much more can be done: the Ising model in three-dimensions has been expressed in anticommuting variable form and is thus amenable to new approximation schemes. The eight vertex Hartree-Fock equations beckon a solution. Perhaps the two-dimensional dimer model can be exactly solved using Sec. VIII results. Polymer (instead of dimer) systems can be treated. Computer work needs to be done so that physical quantities for several expansion series can be calculated. And so on. The most important progress, however, can be made in the area of critical phenomenon. This paper, for the most part, has avoided the critical region. I felt it was best to develop and check the techniques where they are simplest to apply. What is needed is an adaptation of renormalization group methods. In short, this large body of work is a small piece of what can be done with anticommuting variables.

I would like to conclude with what I call "The Optimistic Philosophy." Reality demands that most systems be unsolvable. The Optimistic Philosophy accepts the reality of unsolvability but postulates the existence of a model which is, in an abstract sense, not far away from the system of interest. The physics of the model approximates that of the actual system. A few correction orders then yields an even better approximation. It requires great ingenuity

to find the right model. The relevant degrees of freedom must be extracted. But once found, perturbative or semi-perturbative methods yield a "physicist's solution", that is, not an exact answer but a good answer. Systems are almost solvable because they are stable, and stability, in some sense, means a quadratic action. Hartree-Fock attempts to find better quadratic actions than those given in perturbation theory. In the dimer models, the Hartree approximation searches for a good monomer approximation. Of course, one model is not expected to reproduce the physics in the entire physical region. Different models are required in different areas. In QCD perturbation theory is good at short distances in processes like deep inelastic scattering but a string or bag model is required for large distance phenomena. The latter is an example of when the model differs vastly from the underlying fundamental theory. The Landau-Ginsberg theory of superconductivity is another example. This paper has been written in the spirit of "The Optimistic Philosophy." It has found "fermionic" approximations to interesting physical systems.

ACKNOWLEDGMENTS

I would like to thank Harry Morrison for reading the manuscript and making useful suggestions, Eliezer Rabinovici for some initial assistance with the computer work, Luanne Neumann for the typing, and Antoinette Czerwinski for assistance with the figures.

APPENDIX A

This Appendix calculates the anticommuting variable correlations (Sec. V of II) when $(\alpha', \beta') = (\alpha, \beta)$. Although needed for first order perturbation theory (Eq. 12.7), they are even more important for the Hartree-Fock approximation (Sec. 13).

Related quantities have been computed in Section 8.4 of reference 4. Unfortunately, there are a number of misprints and mistakes. Reference 36 has done the computations when $\epsilon = 0$ [see Eq. (A.4) for the definition of ϵ]. Only the corrected results are presented since the calculational technique is described in detail in reference 4. I have kept to the notation of reference 4 except that η_+ and η_- used here are $-\lambda$ and $-\mu$, and v_+ and v_- correspond to v_2 and v_3 . The corrected results are contained in Eqs. (A.7) through (A.11). The anticommuting variable correlations are related to these via Eqs. (A.5) and (A.6). The calculation technique can be extended to anticommuting variation correlations for $(\alpha', \beta') \neq (\alpha, \beta)$. One must decompose $\cos(np)$ and $\sin(np)$ type factors into products of sine's and cosine's, do some polynomial long division, and follow reference 4.

Define

$$I = \int_{-\pi}^{\pi} \frac{dp_x}{2\pi} \int_{-\pi}^{\pi} \frac{dp_y}{2\pi} \ln L(p_x, p_y), \quad (\text{A.1})$$

so that I is twice the quantity in Eq. (II.3.6). Write the function $L(p_x, p_y)$ [Eq. (II.3.4)] as

$$L(p_x, p_y) = \alpha + 2\beta \cos p_x + 2\gamma \cos p_y + 2(\delta + \epsilon) \cos p_x \cos p_y + 2(\delta - \epsilon) \sin p_x \sin p_y \quad (\text{A.2})$$

The constants $\alpha, \beta, \gamma, \delta$, and ϵ can be computed in terms of b_h , b_v , a_1, a_2, a_3, a_4, z_h , and z_v , however they take on a simpler form when expressed in terms of the vertex weights of Fig. I.11. Let w_1, w_2, \dots, w_8 be the weight in Fig. I.11 with Boltzmann factors z_h and z_v included:

$$\begin{aligned} w_1 &= (a_1 a_3 + a_2 a_4 - b_v b_h), \\ w_2 &= -b_h z_v, \\ w_3 &= -b_v z_h, \\ w_4 &= -a_1 \sqrt{z_h z_v}, \\ w_5 &= -a_2 \sqrt{z_h z_v}, \\ w_6 &= -a_3 \sqrt{z_h z_v}, \\ w_7 &= -a_4 \sqrt{z_h z_v}, \\ w_8 &= z_h z_v. \end{aligned} \quad (\text{A.3})$$

The w 's satisfy the constraint in Eq. (12.2). Then

$$\alpha = w_1^2 + w_2^2 + w_3^2 + w_8^2,$$

$$\beta = -w_1 w_3 + w_2 w_8,$$

$$\gamma = -w_1 w_2 + w_3 w_8,$$

$$(\delta + \epsilon) = w_2 w_3 - w_1 w_8,$$

$$(\delta - \epsilon) = w_4 w_6 - w_5 w_7.$$

In terms of the integral, I , in Eq. (A.1)

$$\langle n_{\alpha\beta}^h n_{\alpha\beta}^{h\dagger} \rangle = \frac{1}{2} \frac{\partial I}{\partial b_h},$$

$$\langle n_{\alpha\beta}^v n_{\alpha\beta}^{v\dagger} \rangle = \frac{1}{2} \frac{\partial I}{\partial b_v},$$

$$\langle n_{\alpha\beta}^{h\dagger} n_{\alpha\beta}^v \rangle = \frac{1}{2} \frac{\partial I}{\partial a_1},$$

$$\langle n_{\alpha\beta}^v n_{\alpha\beta}^{h\dagger} \rangle = \frac{1}{2} \frac{\partial I}{\partial a_2},$$

$$\langle n_{\alpha\beta}^{v\dagger} n_{\alpha\beta}^h \rangle = \frac{1}{2} \frac{\partial I}{\partial a_3},$$

$$\langle n_{\alpha\beta}^v n_{\alpha\beta}^h \rangle = \frac{1}{2} \frac{\partial I}{\partial a_4}.$$

(A.5)

By using the chain rule

$$\frac{\partial I}{\partial c} = \frac{\partial \alpha}{\partial c} \frac{\partial I}{\partial \alpha} + \frac{\partial \beta}{\partial c} \frac{\partial I}{\partial \beta} + \frac{\partial \gamma}{\partial c} \frac{\partial I}{\partial \gamma} + \frac{\partial(\delta + \epsilon)}{\partial c} \frac{\partial I}{\partial(\delta + \epsilon)}$$

$$+ \frac{\partial(\delta - \epsilon)}{\partial c} \frac{\partial I}{\partial(\delta - \epsilon)},$$

(A.6)

where c stands for b_h , b_v , a_1 , a_2 , a_3 , or a_4 , it is sufficient to calculate $\frac{\partial I}{\partial \alpha}$, $\frac{\partial I}{\partial \beta}$, $\frac{\partial I}{\partial \gamma}$, $\frac{\partial I}{\partial(\delta + \epsilon)}$, and $\frac{\partial I}{\partial(\delta - \epsilon)}$:

$$\frac{\partial I}{\partial \alpha} = \frac{2}{\pi f} K(k), \quad (A.7)$$

$$\frac{\partial I}{\partial \beta} = \frac{4}{\pi f} \left\{ \left(\frac{1 + \eta_+}{1 - \eta_-} \right) K(k) - \left(\frac{2\eta_+}{1 - \eta_+} \right) \Pi_1(\eta_+, -1, k) \right\}, \quad (A.8)$$

$$\frac{\partial I}{\partial \gamma} = \frac{2g}{\pi f} \left\{ \left(\frac{v_+ - v_4}{v_+ - v_-} \right) \left(\frac{v_+ - v_5}{v_+} \right) \Pi_1 \left(\frac{k^2}{v_+}, k \right) + \left(\frac{v_- - v_4}{v_- - v_+} \right) \left(\frac{v_- - v_5}{v_-} \right) \Pi_1 \left(\frac{k^2}{v_-}, k \right) - K(k) \right\}, \quad (A.9)$$

$$\begin{aligned} \frac{\partial I}{\partial(\delta + \epsilon)} &= \frac{2g}{\pi f} \left\{ \left(\frac{v_1 - v_6}{v_1 - v_+} \right) \left(\frac{v_1 - v_4}{v_1 - v_-} \right) \left(\frac{v_1 - v_5}{v_1} \right) \Pi_1 \left(\frac{k^2}{v_1}, k \right) \right. \\ &+ \left. \left(\frac{v_+ - v_6}{v_+ - v_-} \right) \left(\frac{v_+ - v_4}{v_+ - v_1} \right) \left(\frac{v_+ - v_5}{v_+} \right) \Pi_1 \left(\frac{k^2}{v_+}, k \right) \right. \\ &+ \left. \left(\frac{v_- - v_6}{v_- - v_+} \right) \left(\frac{v_- - v_4}{v_- - v_1} \right) \left(\frac{v_- - v_5}{v_-} \right) \Pi_1 \left(\frac{k^2}{v_-}, k \right) - K(k) \right. \\ &+ \left. \left(\frac{v_1 - v_4}{v_1 - v_+} \right) \left(\frac{v_1 - v_6}{v_1 - v_-} \right) \left[\frac{f \sqrt{\eta_+}}{\alpha + 2\beta} - \left(\frac{v_1 - v_5}{v_1} \right) \right] \right. \\ &\times \left. \sqrt{\frac{v_1}{k^2 + v_1}} \right\}, \quad (A.10) \end{aligned}$$

$$\begin{aligned}
\frac{\partial I}{\partial(\delta - \epsilon)} = & \frac{8\eta_+(\delta - \epsilon)g}{\pi(\gamma + \delta + \epsilon)f} \left\{ - \frac{(\nu_+ + 1) \dots}{(\nu_+ - \nu_1)(\nu_+ - \nu_-)} \left(\frac{\nu_+ - \nu_5}{\nu_+} \right) \Pi_1 \left(\frac{k^2}{\nu_+}, k \right) \right. \\
& - \frac{(\nu_- + 1) \dots}{(\nu_- - \nu_1)(\nu_- - \nu_+)} \left(\frac{\nu_- - \nu_5}{\nu_-} \right) \cdot \Pi_1 \left(\frac{k^2}{\nu_-}, k \right) \\
& - \frac{(\nu_1 + 1) \dots}{(\nu_1 - \nu_+)(\nu_1 - \nu_-)} \left(\frac{\nu_1 - \nu_5}{\nu_1} \right) \Pi_1 \left(\frac{k^2}{\nu_1}, k \right) - K(k) \\
& \left. - \frac{\pi \sqrt{1 + \nu_1}}{2(\nu_1 - \nu_+)(\nu_1 - \nu_-)} \left[\frac{f\sqrt{\eta_+}}{(\alpha + 2\beta)} - \frac{\nu_1 - \nu_5}{\sqrt{\nu_1(k^2 + \nu_1)}} \right] \right\}, \quad (A.11)
\end{aligned}$$

where

$$f = \sqrt{\eta_-(a - 2b + c)}, \quad (A.12)$$

$$g = \frac{\alpha + 2\beta}{\gamma + \delta + \epsilon}$$

$$a = \alpha^2 - 4(\gamma^2 + (\delta - \epsilon)^2), \quad (A.13)$$

$$b = 2\alpha\beta - 4\gamma(\delta + \epsilon),$$

$$c = 4(\beta^2 - 4\delta\epsilon).$$

$$\eta_{\pm} = - \frac{(c - a) \pm 2\sqrt{b^2 - ac}}{a - 2b + c}. \quad (A.14)$$

$$k = \frac{\eta_- - \eta_+}{\eta_-}. \quad (A.15)$$

$$\nu_{\pm} = -1 + \eta_{\pm} \left(\frac{(\delta - \epsilon) \pm \sqrt{\gamma^2 - 4\delta\epsilon}}{\gamma + \delta + \epsilon} \right)^2,$$

$$\nu_1 = \eta_+ - 1,$$

$$\nu_4 = -1 + \eta_+ \left(\frac{\gamma - \delta - \epsilon}{\gamma + \delta + \epsilon} \right) \quad (A.16)$$

$$\nu_5 = -1 + \eta_+ \left(\frac{\alpha - 2\beta}{\alpha + 2\beta} \right),$$

$$\nu_6 = -1 - \eta_+.$$

$K(k)$ and $\Pi_1(\nu, k)$ are complete elliptic integrals of the first and third kind:

$$K(k) \equiv \int_0^{\pi/2} (1 - k^2 \sin^2 \phi)^{-1/2} d\phi, \quad (A.17)$$

$$\Pi_1(\nu, k) \equiv \int_0^{\pi/2} (1 - k^2 \sin^2 \phi)^{-1/2} (1 + \nu \sin^2 \phi)^{-1} d\phi.$$

Using the fact that the partition function is invariant under interchange of horizontal and vertical directions, there is an alternative formula for $\frac{\partial I}{\partial \gamma}$ obtained from using $\frac{\partial I}{\partial \beta}$:

$$\frac{\partial I}{\partial \gamma} = \frac{4}{\pi f} \left\{ \left(\frac{1 + \eta_+^*}{1 - \eta_+^*} \right) K(k) - \left(\frac{2\eta_+^*}{1 - \eta_+^*} \right) \Pi_1(\eta_+^* - 1, k) \right\} \quad (A.18)$$

where

$$\eta_+^* = \left(\frac{\alpha - 2\beta + 2\gamma - 2\delta - 2\epsilon}{\alpha + 2\beta - 2\gamma - 2\delta - 2\epsilon} \right) \eta_+. \quad (A.19)$$

TABLES

Table I:	The Hartree Approximation for the One Dimensional Dimer Model.
Table II:	Molecular Freedoms at Close-Packing as Computed in the $1/q$ Expansion for Various Lattices.
Table III:	Molecular Freedoms at Close-Packing as Computed by the Hartree Series With a Comparison to Other Methods.
Table IV:	An Order by Order Comparison of Nagle's Series to the Hartree Series for Molecular Freedoms on the Hypercubic Lattices.
Table V:	The Density, ρ , and the Entropy, S , of the Simple Quadratic and Tetrahedral Dimer Lattice Models.
Table VI:	The Density and Entropy for the Dimer Models on the Triangular and Simple Cubic Lattices.
Table VII:	The Density and Entropy for the Dimer Models on the Body-Centered Cubic and Face-Centered Cubic Lattices.
Table VIII:	A Comparison of the Exact Density and Entropy to the Hartree Estimated Density and Entropy for the One-Dimensional Dimer Model.

FIGURE CAPTIONS

- Fig. 1: (a) Intersecting Polyhedrons. Such intersections are allowed. (b) Overlapping Polyhedrons. Such overlaps are forbidden. This configuration would be drawn as in (c).
- Fig. 2: The Three Different Types of Faces. (a) An x-face or a face in the x-direction. (b) A y-face. (c) A z-face.
- Fig. 3: A Cube of the Dual Lattice. The spin, σ , sits in the middle of the cube at (α, β, γ) . The twelve surrounding edges and the cartesian coordinates of their midpoints are shown. The three bolder lines show the three types of edges.
- Fig. 4: A_{face} .
- Fig. 5: Linking. (a) The faces of Figure 4(a) can form larger area elements. Here five faces link. (b) But a face in the x-direction is unable to link with a face in the z-direction. The object in Figure (c) is needed.
- Fig. 6: A_{corner} . To the left is the edge and its coordinates. In the middle are the possible anticommuting variables which could enter. These variables come from A_{face} . To the right are the four types of corners needed to link faces.
- Fig. 7: The Minus Sign Problem. (a) A cube of polyhedron. (b) The anticommuting variables used to construct the cube trace out this object. (b) By breaking quartics into products of bilinears, the object factorizes into a product

of three planar polygons. Reordering minus factors reduce to the planar case.

- Fig. 8: The z_3 Factor. When drawing polyhedrons around regions of down spin z_3 enters twice for each down spin.
- Fig. 9: Redundant Quartic Terms. Figure (a) shows how the anticommuting variables construct a polyhedron. It is not necessary to "gift wrap" so lavishly. Figure (b) shows a simpler way to "gift wrap." This simplification of quartic terms also applies to the three dimensional $H = 0$ Ising model representation treated in Sec. II.
- Fig. 10: A Plaquette. Here is a "square" of the lattice. The anticommuting variables sit at lattice sites, the U's sit on the links (or edges), and the spins sit in the middle of plaquettes. The action in Eq. (3.12) is a sum over plaquettes (like this one) of a product of U's around the square (the U's shown here).
- Fig. 11: The Dimer Potential.
- Fig. 12: Simple Perturbation Theory to Third Order.
- Fig. 13: Figure 11 in Contracted Form.
- Fig. 14: A Vertex, α , With ℓ Lines Attached.
- Fig. 15: Two Vertices With ℓ Lines Between Them
- Fig. 16: Explanation of the $(\ell - 1)!$ in Feynman Rule (c)
- Fig. 17: A Typical Bubble Tree Graph Included in the Hartree Approximation.
- Fig. 18: The Hartree-Improved Perturbation Theory Graphs and Their Statistical Weights to Sixth Order.

- Fig. 19: The Embeddings of Figure 12 Graphs for the Two-Dimensional Lattice.
- Fig. 20: Diagrams to Third Order for the Two-Dimensional Dimer Model.
- Fig. 21: How Two Graphs Can Have Identical Embeddings
- Fig. 22: The Embedding Graphs.
- Fig. 23: The Weight of an Embedding Graph is the Sum of Contributing Figure 18 Graphs.
- Fig. 24: The Embeddings of Figure 22 Graphs for the Two-Dimensional Lattice. This Figure shows the Hartree expansion computation to fifth order.
- Fig. 25: The Superpropagator. The bolder line on the left denotes the superpropagator, $G_{\alpha\alpha}^S$.
- Fig. 26: The One Loop Graphs.
- Fig. 27: The Two Loop Graphs.
- Fig. 28: Tadpoles. Here is a vertex with ℓ tadpoles attached. The $1/N$ Feynman Rules (c) and (e) give rise to a factor of $\{(-1)(m + 2\ell - 1)!\} [1/(2^\ell \ell!)]$.
- Fig. 29: The Dimer Breakup Trick. The bilinears in figure (a) generate the wanted dimer operators in figure (b), but they also generate those typified in figure (c). The latter occur, for example, when the bilinear $\eta_\alpha^\dagger \eta_{\alpha+1}$ "links" up with the bilinear, $\eta_{\alpha+1}^\dagger \eta_{\alpha+2}$, in the adjacent site. The form of these terms is a set of θ 's with an "o" at one end and an "x" at the other end. The leftover "o" or "x" means that these terms do not contribute. An

exception occurs when periodic boundary conditions are used as in figure (d).

Fig. 30: One-Dimensional Polymers. On the left are a trimer spanning sites α , $\alpha + 1$ and $\alpha + 2$ and a quadrimer spanning sites α through $\alpha + 3$. Such polymers are produced by the anticommuting variable operators

$$z_3 n_{\alpha}^{\dagger} n_{\alpha+1}^{\dagger} n_{\alpha+2}^{\dagger} \quad \text{and} \quad z_4 n_{\alpha}^{\dagger} n_{\alpha+1}^{\dagger} n_{\alpha+2}^{\dagger} n_{\alpha+3}^{\dagger}$$

and there would be a piece of the action with these operators. Similar type operators can produce polymers of arbitrary shape in higher dimensions.

Fig. 31: The Set-up for the Transfer Matrix Elements.

Fig. 32: The Potential.

Fig. 33: The Lowest Order Graph.

Fig. 34: Second Order Graphs

Fig. 35: Third Order Graphs.

Fig. 36: Illustration of Rule (f).

Fig. 37: The Fermion Propagator.

Fig. 38: The Loop Momentum Assignments for the Graph of Figure 34a.

Fig. 39: The One Loop $1/N$ Graphs.

Fig. 40: The Staircase Approximation. The dimer breakup trick of Sec. VII is applied to those dimers lying on the solid lines.

Fig. 41: A Configuration Generated by the Breakup in Equation (9.34) Which Is Not Contained in the Partition Function.

Fig. 42: The Eight Different Types of Corners.

Fig. 43: Vertices. At the left are bare vertices and at the right are the corresponding directed vertices.

Fig. 44: First Order Graphs. Figures (a), (b), and (c) are the first order graphs corresponding to the bare graph in (d). Graphs (a), (b), and (c) can be organized into the single graph in (e).

Fig. 45: (a) One of the Second Order Graphs. (b) The Bare Version of (a).

Fig. 46: (a) The Other Second Order Graph. (b) The Bare Version of (a).

Fig. 47: The Polymers Generated From the Two-Dimensional Dimer Model. The nine kinds of polymers and their weights (the w factors) are shown here.

Fig. 48: Reduction of the Polymer System to Nearest Neighbor Dimers by Replacing Operators by c-Numbers.

Fig. 49: Dimers. (a) The Type (a) Dimers, (b) the Type (b) Dimers, and (c) a Standard B-Dimer Configuration

Fig. 50: The Weights of the Miniature Dimer Problem.

Fig. 51: A Configuration with Negative Weight. Except for the eight dimers shown in (a), all A-dimers are put in the standard positions. The latter dimers do not generate any minus signs. The other eight when combined with standard B-dimers create the closed polygon in (b). Fig. I.8 sign rules reveal that this polygon has negative weight.

REFERENCES

1. S. Samuel, The Use of Anticommuting Integrals in Statistical Mechanics I, LBL preprint 8217 (Sept., 1978). References to the figures and equations of this paper are prefaced by a I.
2. S. Samuel, The Use of Anticommuting Integrals in Statistical Mechanics II, LBL preprint 8300 (Oct., 1978). References to the figures and equations of this paper are prefaced by a II.
3. T. D. Schultz, D. C. Mattis, E. H. Lieb, *Rev. Mod. Phys.* 36, 856 (1964).
4. H. S. Green and C. A. Hurst, Order-Disorder Phenomena (Interscience, New York, 1964).
5. C. A. Hurst, *J. Math. Phys.* 7, 305 (1966).
6. See, for example, E. W. Montroll, Brandeis University Summer Institute in Theoretical Physics, 1966, edited by M. Chretien, E. P. Gross, and S. Deser (Bordon and Breach, New York, 1968). E. W. Montroll, Chapter IV in Applied Combinatorial Mathematics, ed. E. F. Beckenbach (Wiley, New York, 1964).
7. R. F. Dashen, B. Hasslacher, and A. Neveu, *Phys. Rev.* D10, 4114 (1974); *Phys. Rev.* D10, 4138 (1974); *Phys. Rev.* D11, 3424 (1975).
8. R. F. Dashen, B. Hasslacher, and A. Neveu, *Phys. Rev.* D10, 4130 (1974).
9. R. Balian, J. M. Drouffe, and C. Itzykson, *Phys. Rev.* D11, 2098 (1975); *Phys. Rev.* D11, 2104 (1975); E. Fradkin and S. H. Shenker, SLAC-PUB-2238 (Nov., 1978).

10. F. J. Wegner, *J. Math. Phys.* 12, 2259 (1971).
11. J. K. Roberts, *Proc. Roy. Soc. (London) A* 152, 469 (1935).
See also the references in reference 12.
12. O. J. Hellmann and E. H. Lieb, *Comm. Math. Phys.* 25, 190 (1972).
13. R. H. Fowler and G. S. Rushbrooke, *Trans. Farad. Soc.* 33, 1272 (1937).
F. H. Ree and D. A. Chestnut, *Phys. Rev. Lett.* 18, 5 (1967).
A. Bellemans and R. K. Nigam, *J. Chem. Phys.* 46, 2922 (1967).
J. Urban and A. Bellemans, *J. Chem. Phys.* 49, 363 (1968).
14. J. K. Roberts, *Proc. Roy. Soc. (London) A* 161, 141 (1937); *Proc. Cambridge Phil. Soc.* 34, 399 (1938).
P. A. Readhead, *Trans. Farad. Soc.* 57, 641 (1961).
D. R. Rossington and R. Bost, *Surface Sci.* 3, 202 (1965).
15. E. H. Lieb, *J. Math. Phys.* 8, 2339 (1967).
R. J. Baxter, *J. Math. Phys.* 9, 650 (1968).
L. K. Runnels, *J. Math. Phys.* 11, 842 (1970).
16. T. S. Chang, *Proc. Cambridge Phil. Soc.* 35, 265 (1939);
J. K. Roberts and A. R. Miller, *Proc. Cambridge Phil. Soc.* 35, 293 (1939).
17. R. D. Kaye and D. M. Burley, *Physica* 87A, 499 (1977).
18. J. F. Nagle, *Phys. Rev.* 152, 190 (1966).
19. C. Gruber and H. Kunz, *Comm. Math. Phys.* 22, 133 (1971).
20. G. S. Rushbrooke, H. I. Scoins, and A. J. Wakefield, *Discussions Farad. Soc.* 15, 57 (1953).
21. D. S. Gaunt, *Phys. Rev.* 179, 174 (1969).
22. L. Degreve, *Physica* 66, 395 (1973).

23. J. Van Craen and A. Bellemans, J. Chem. Phys. 56, 2041 (1972).
24. A. L. Fetter and J. D. Walecka, Quantum Theory of Many-Particle Systems, (Mc Graw-Hill, San Francisco, 1971).
D. Pines, The Many-Body Problem (W. A. Benjamin, New York, 1961).
25. H. N. V. Temperley and M. E. Fisher, Phil. Mag. 6, 1061 (1960);
M. E. Fisher, Phys. Rev. 124, 1664 (1961).
26. A typical example is D. J. Gross and A. Neveu, Phys. Rev. D10,
3247 (1974).
27. H. N. V. Temperley, Phys. Rev. 103, 1 (1956).
28. T. H. Berlin and M. Kac, Phys. Rev. 86, 821 (1952).
29. E. H. Lieb (see Reference 15).
30. M. E. Fisher and J. Stephenson, Phys. Rev. 132, 1411 (1963).
31. M. Bander, Phys. Rev. D13, 1566 (1975).
32. J. Hubbard, Phys. Rev. Lett. 3, 77 (1959);
R. L. Stratonovich, Doklady Akad. S. S. S. R. 115, 1097 (1957),
English translation: Soviet Phys. Doklady 2, 416 (1958).
33. See, for example, E. S. Abers and B. W. Lee, Phys. Rep. 9C,
1 (1973) or S. Coleman, Secret Symmetry, published in Proceedings
of the 1973 International School of Physics "Ettore Majorana"
(1973).
34. See Phase Transitions and Critical Phenomenon, volume 1,
Exact Results, ed. by C. Domb and M. S. Green (Academic Press,
New York, 1972).
35. For a review, see H. J. Maris and L. P. Kadanoff, Am. J. Phys. 46,
652 (1977).
36. C. Fan and F. Y. Wu, Phys. Rev. B2, 723 (1970).

TABLE I

z	Exact Γ	Hartree Γ	% Error	Expansion Parameter
$10^{-2} = 01$	0.0099	0.0098	0.48 %	0.010
$10^{-1.5} \approx .032$	0.0302	0.0298	1.36 %	0.028
$10^{-1} = .1$	0.0877	0.0848	3.30 %	0.073
$10^{-.5} \approx .316$	0.2251	0.2116	6.01 %	0.153
$10^0 = 1$	0.4812	0.4431	7.91 %	0.250
$10^{.5} \approx 3.16$	0.8532	0.7829	8.24 %	0.337
10	1.3088	1.2094	7.59 %	0.400
$10^{1.5} \approx 31.62$	1.8157	1.6954	6.63 %	0.441
$10^2 = 100$	2.3526	2.2186	5.69 %	0.466
$10^{2.5} \approx 316.2$	2.9063	2.7642	4.89 %	0.481
$10^3 = 1000$	3.4697	3.3227	4.24 %	0.489
$10^{3.5} \approx 3162$	4.0384	3.8886	3.71 %	0.494
$10^4 = 10000$	4.6102	4.4588	3.28 %	0.496
10^{10}	11.5129	11.3595	1.33 %	0.500

TABLE II

model	q	$\frac{1}{q}$ estimate	exact or best estimate	% error
1-d	2	.94	1	6 %
sq	4	1.67	1.79	6.5 %
t	4	1.67	1.70	2 %
sc	6	2.40	2.45	2 %
bcc	8	3.13	3.19	2 %
pt	6	2.21	2.36	6.5 %
fcc	12	4.41	4.57	3.5 %

TABLE III

	sq	pt	t	sc	bcc	fcc
Exact	1.7916	2.3565	-----	-----	-----	-----
Bethe Approximation	1.69	2.41	1.69	2.41	3.14	4.61
Nagle's Series Truncated	1.769	2.352	1.701	2.442	-----	4.564
Nagle's Series Extended by Gaunt, Truncated	1.773	2.360	1.701	2.451	3.189	4.565
Gaunt's Padé Improved	1.78-1.80	2.356	1.702	2.449	3.198	4.570
Hartree Approximation	1.47	2.21	1.47	2.21	2.94	4.41
Hartree Series at Sixth Order	1.75 ± .03	2.37 ± .06	1.70 ± .02	2.44 ± .01	3.17 ± .01	4.56 ± .03
Hartree Series, Truncated	1.776 ± .009	2.347 ± .015	1.700 ± .003	2.449 ± .005	3.187 ± .003	4.574 ± .004

TABLE IV

order	1 - d	2 - d Simple quadratic		3 - d simple cubic	
	Hartree Series	Hartree Series	Nagle's Series	Hartree Series	Nagle's Series
1	0.7358	1.4715	1.6875	2.2073	2.4113
2	0.9447	1.6674	1.6875	2.3991	2.4113
3	1.1161	1.7384	1.6875	2.4439	2.4113
4	1.0162	1.6783	1.7297	2.4019	2.4345
5	0.9428	1.7235	1.7297	2.4445	2.4345
6	0.9932	1.7518	1.7392	2.4402	2.4414
7	1.0385	1.7292	1.7520	2.4353	2.4459
8	1.0036	1.7437	1.7501	2.4519	2.4455
9	0.9736	1.7629	1.7644	2.4457	2.4506
10	0.9978	1.7534	1.7618	2.4466	2.4488
11	1.0204	1.7586	1.7696	2.4540	2.4527
12	1.0014	1.7720	1.7704	2.4493	2.4515
13	0.9842	1.7671	1.7712		
14	0.9990	1.7671	1.7750		
15	1.0131	1.7759	1.7728		
16	1.0007				
exact	1.	1.7916			

TABLE V

$\frac{w}{w_{\max}}$	w	Simple Quadratic Lattice	Tetrahedral Lattice		
		P_{15}	S_{15}	P_{16}	S_{16}
0.1	0.025	0.025534345332921949 ± (15)	0.116814864054067036 ± (37)	0.02553353977813695063 ± (60)	0.1168118264806264350 ± (21)
0.2	0.050	0.05180380074377 ± (41)	0.1949643466614 ± (12)	0.051790983870680 ± (32)	0.194927214968692 ± (84)
0.3	0.075	0.07838101424 ± (14)	0.25349328917 ± (39)	0.078318571157 ± (17)	0.253349894577 ± (34)
0.4	0.100	0.1049369153 ± (85)	0.295353081 ± (12)	0.1047525671 ± (13)	0.2950219984 ± (19)
0.5	0.125	0.13122827 ± (19)	0.32135808 ± (17)	0.130819262 ± (37)	0.320810503 ± (33)
0.6	0.150	0.1570755 ± (22)	0.33132011 ± (73)	0.15632504 ± (52)	0.33064735 ± (16)
0.7	0.175	0.182330 ± (16)	0.3240767 ± (45)	0.1811370 ± (42)	0.3235364 ± (13)
0.8	0.200	0.206800 ± (73)	0.296955 ± (74)	0.205148 ± (23)	0.296918 ± (23)
0.9	0.225	0.22998 ± (20)	0.24426 ± (38)	0.228209 ± (71)	0.24440 ± (14)

TABLE VI

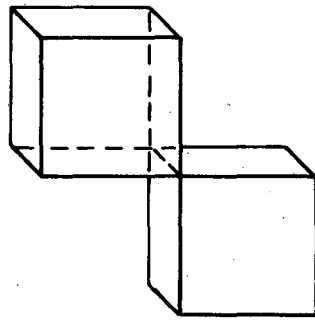
$\frac{w}{w_{\max}}$	w	Planar Triangular Lattice		Simple Cubic Lattice	
		ρ_{10}	S_{10}	ρ_{12}	S_{12}
0.1	$\frac{1}{60}$	0.01689214299601 ± (89)	0.0841945595015 ± (36)	0.0169006865736503 ± (31)	0.084231124247639 ± (12)
0.2	$\frac{2}{60}$	0.03405266733 ± (74)	0.1422176561 ± (23)	0.034114158049 ± (10)	0.142428661957 ± (32)
0.3	$\frac{3}{60}$	0.051266315 ± (34)	0.187111775 ± (85)	0.0514487921 ± (10)	0.1876342661 ± (27)
0.4	$\frac{4}{60}$	0.06838822 ± (49)	0.22104537 ± (94)	0.068760241 ± (27)	0.221940351 ± (51)
0.5	$\frac{5}{60}$	0.0853296 ± (35)	0.2446703 ± (49)	0.08594040 ± (31)	0.24589635 ± (42)
0.6	$\frac{6}{60}$	0.102041 ± (16)	0.257883 ± (14)	0.1029054 ± (21)	0.25930907 ± (66)
0.7	$\frac{7}{60}$	0.118500 ± (54)	0.259825 ± (17)	0.1195810 ± (93)	0.2612807 ± (20)
0.8	$\frac{8}{60}$	0.13470 ± (13)	0.248409 ± (39)	0.135880 ± (29)	0.249809 ± (13)
0.9	$\frac{9}{60}$	0.15069 ± (20)	0.21841 ± (16)	0.151661 ± (57)	0.220254 ± (63)

TABLE VII

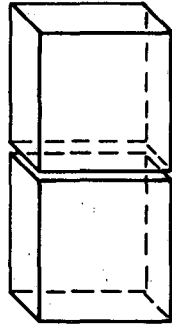
$\frac{w}{w_{\max}}$	Body-Centered Cubic Lattice		Face-Centered Cubic Lattice	
	ρ_{12}	S_{12}	ρ_8	S_8
0.1	0.0126308078545463 \pm (13)	0.0666064413803685 \pm (54)	0.0083890254360 \pm (42)	0.047655678485 \pm (20)
0.2	0.0254353696746 \pm (42)	0.113584413678 \pm (14)	0.01684367298 \pm (88)	0.0821056143 \pm (34)
0.3	0.03830861920 \pm (44)	0.1508592102 \pm (12)	0.025312649 \pm (18)	0.110062846 \pm (59)
0.4	0.051173247 \pm (11)	0.180052915 \pm (24)	0.03376250 \pm (14)	0.13266446 \pm (39)
0.5	0.06397071 \pm (13)	0.20157738 \pm (21)	0.04217243 \pm (67)	0.1502187 \pm (15)
0.6	0.07665304 \pm (75)	0.21524997 \pm (92)	0.0505306 \pm (22)	0.1626165 \pm (36)
0.7	0.0891737 \pm (38)	0.2203287 \pm (19)	0.0588309 \pm (53)	0.1693450 \pm (60)
0.8	0.101475 \pm (12)	0.2152042 \pm (20)	0.067070 \pm (10)	0.1692448 \pm (59)
0.9	0.113467 \pm (23)	0.196182 \pm (19)	0.075243 \pm (12)	0.1595724 \pm (42)

TABLE VIII

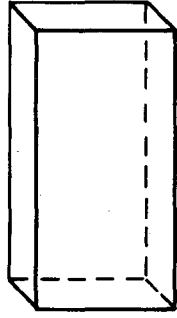
$\frac{w}{w_{\max}}$	w	ρ_{16}	ρ_{exact}	S_{16}	S_{exact}
0.1	0.05	0.0522332644055048897 ± (81)	0.0522332644055048890	0.202159043168350649 ± (23)	0.202159043168350647
0.2	0.10	0.10776772972370 ± (43)	0.10776772972363	0.32877414039132 ± (83)	0.32877414039119
0.3	0.15	0.16476080022 ± (23)	0.16476080017	0.41476557223 ± (30)	0.41476557217
0.4	0.20	0.221456997 ± (18)	0.221456993	0.464874051 ± (13)	0.464874048
0.5	0.25	0.27639331 ± (50)	0.27639320	0.481211845 ± (94)	0.481211825
0.6	0.30	0.3285028 ± (70)	0.3285014	0.4652904 ± (25)	0.4652909
0.7	0.35	0.377125 ± (58)	0.377115	0.417789 ± (58)	0.417798
0.8	0.40	0.42195 ± (31)	0.42191	0.33720 ± (53)	0.33726
0.9	0.45	0.46291 ± (97)	0.46284	0.2158 ± (25)	0.2159



(a)



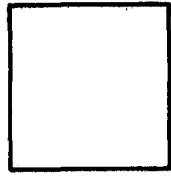
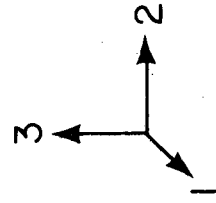
(b)



(c)

XBL 796 - 1710

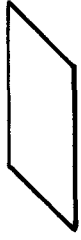
Figure 1



(a)



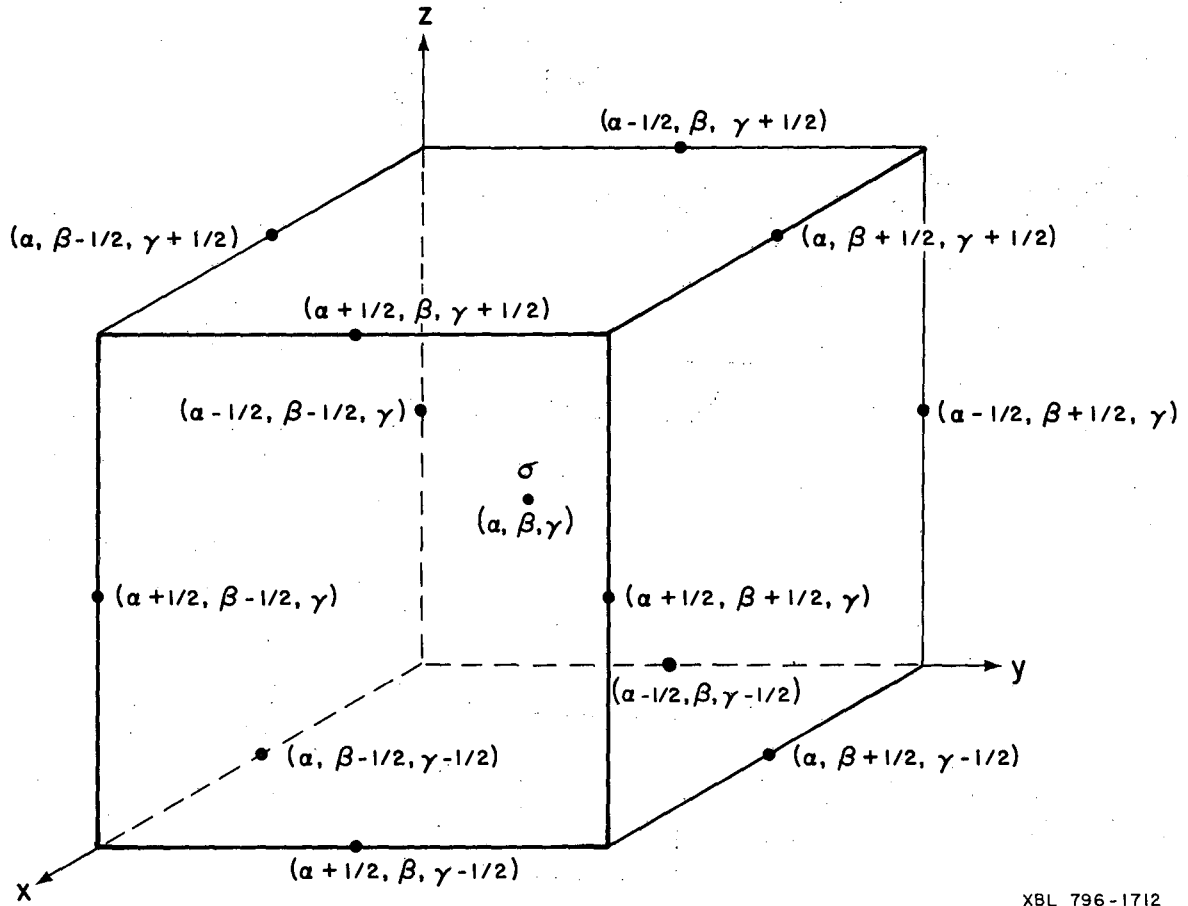
(b)



(c)

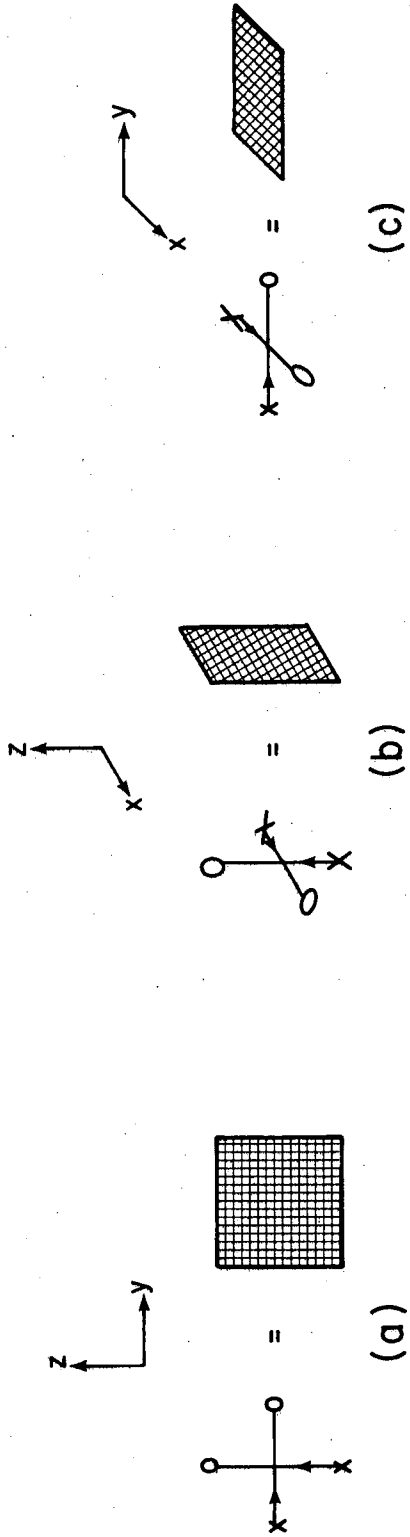
XBL 796-1711

Figure 2



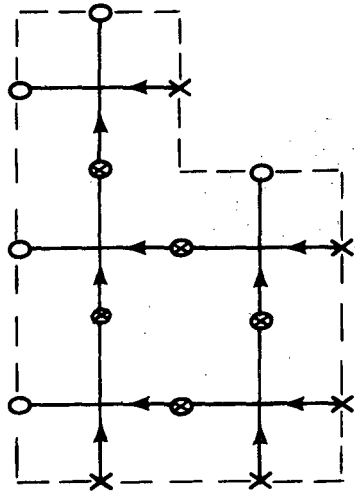
XBL 796-1712

Figure 3



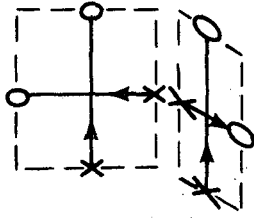
XBL 796-1713

Figure 4



Linked
(a)

but



Unlinked
(b)

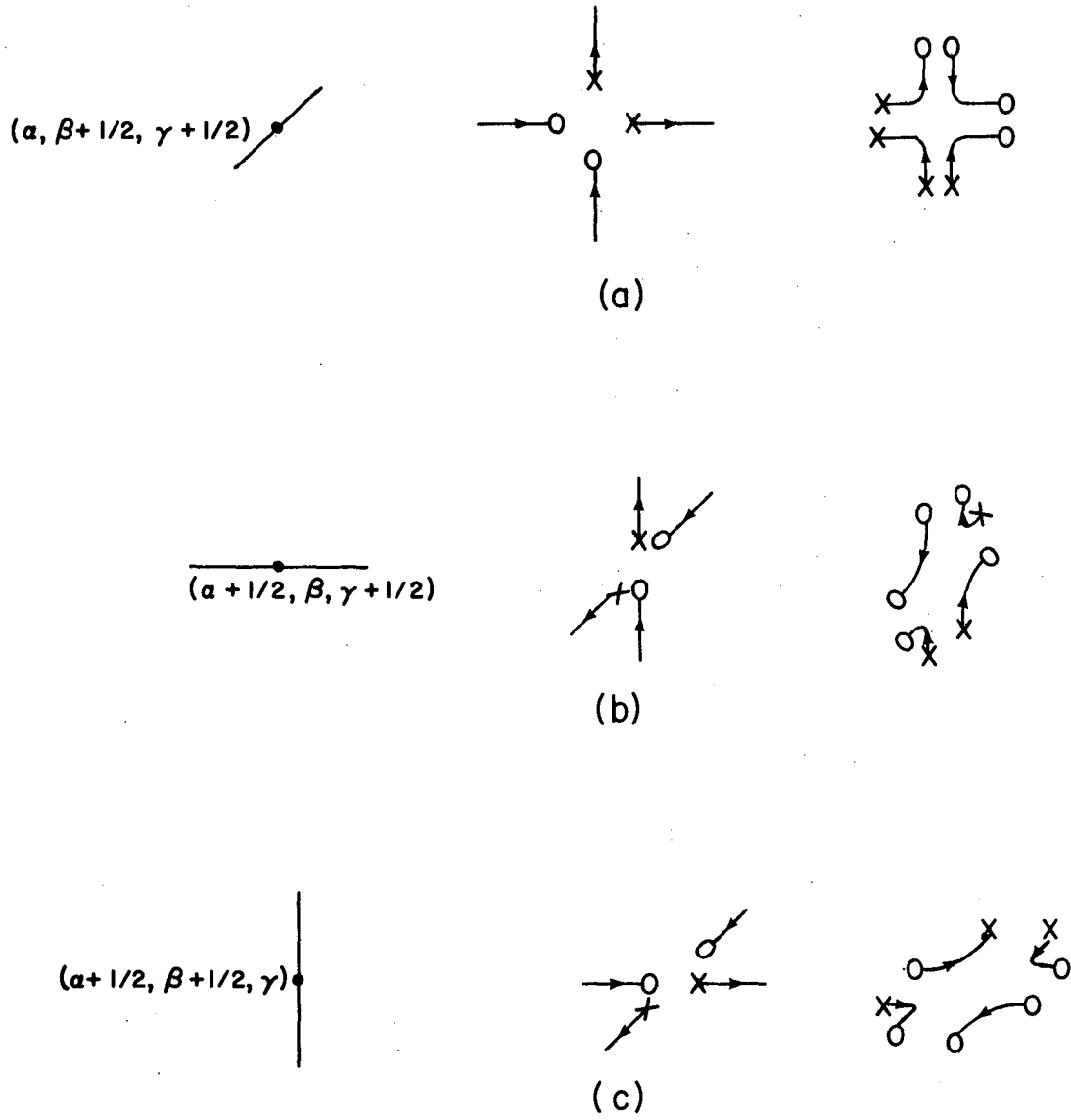
need



(c)

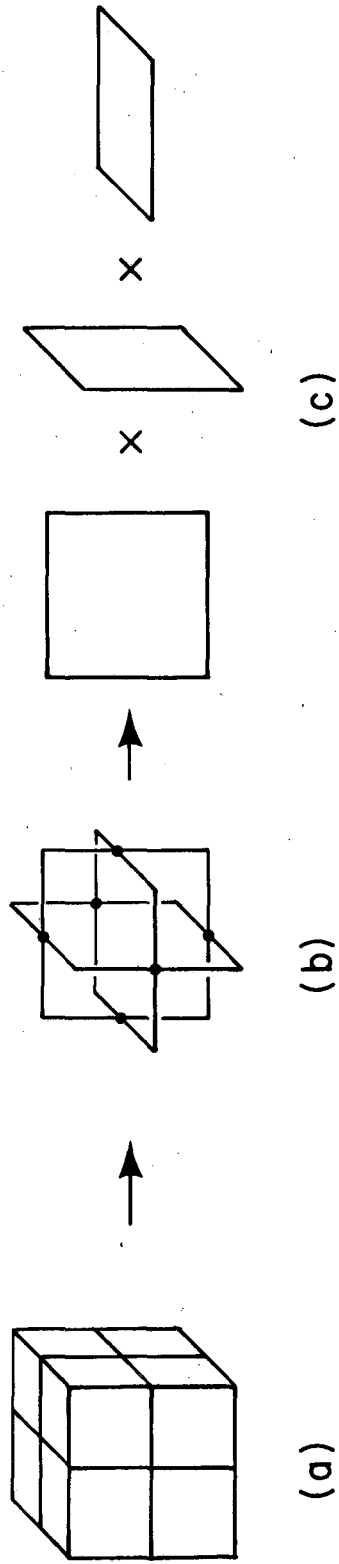
XBL 796-1714

Figure 5



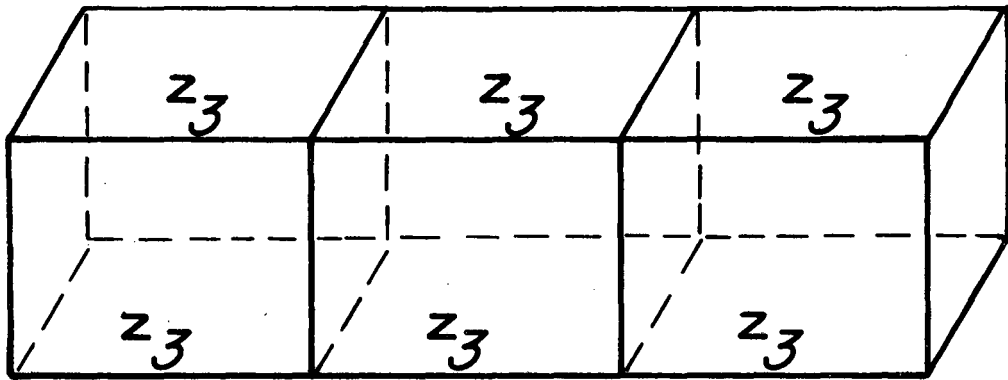
XBL 796-1724

Figure 6



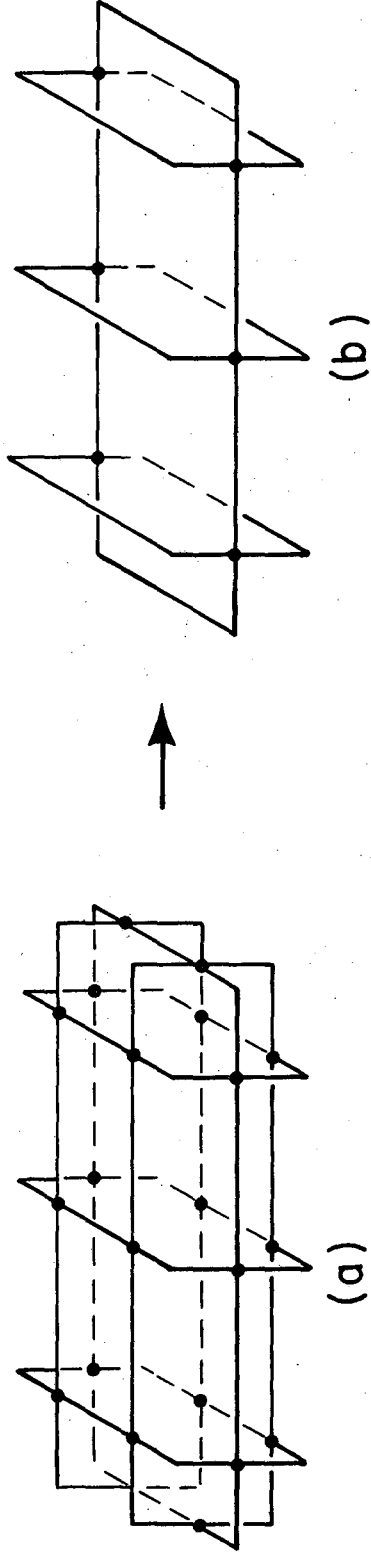
XBL 796-1715

Figure 7



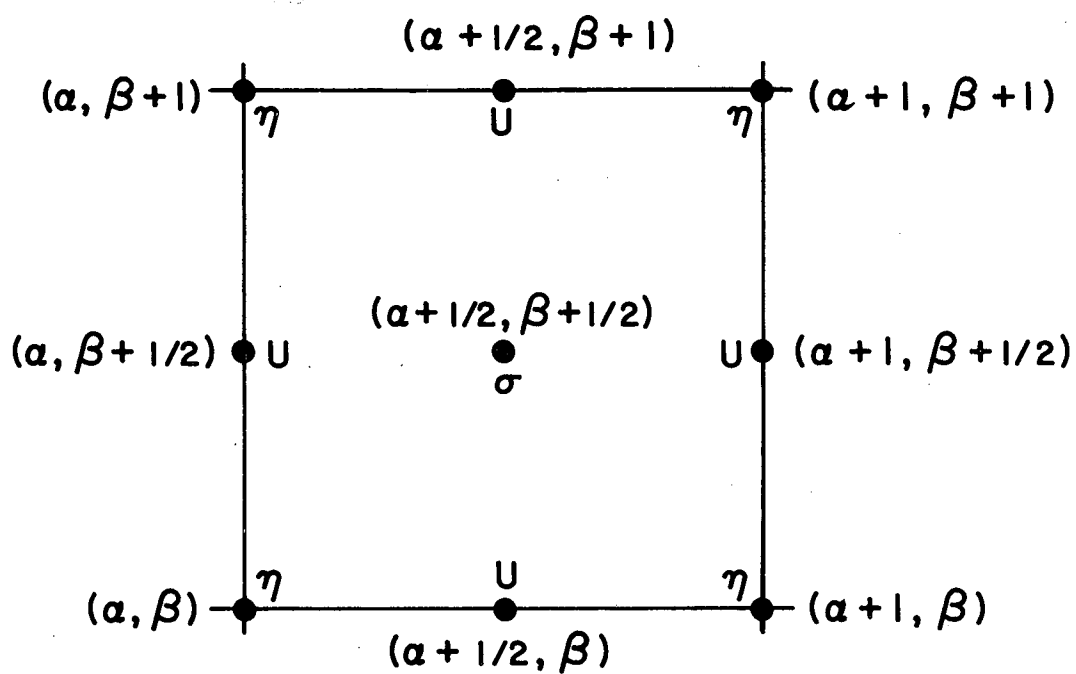
XBL 796-1721

Figure 8



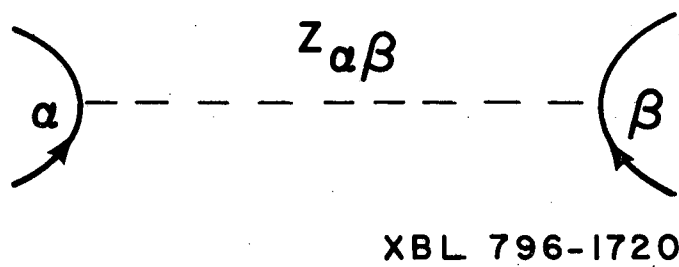
XBL 796-1716

Figure 9



XBL 796 - 1719

Figure 10



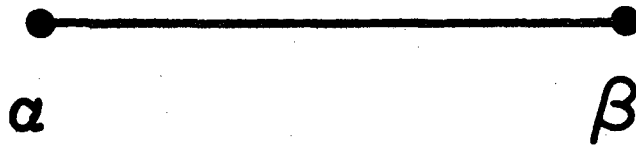
XBL 796-1720

Figure 11

	Graph	Contracted graph	Factors from rule (b)	Factor from rule (c)	Factor from rule (d)	Factor from rule (e)	Weight of graph
(a)			$\sum_{a\beta} Z_{a\beta}$	$(-1)^2$	$\frac{1}{2}$	1	$\frac{1}{2} \sum_{a\beta} Z_{a\beta}$
(b)			$\sum_{a\beta\gamma} Z_{a\beta} Z_{\beta\gamma}$	$(-1)^3$	$\frac{1}{2}$	1	$-\frac{1}{2} \sum_{a\beta\gamma} Z_{a\beta} Z_{\beta\gamma}$
(c)			$\sum_{a\beta} Z_{a\beta}^2$	$(-1)^2$	$\frac{1}{2}$	$\frac{1}{2}$	$\frac{1}{4} \sum_{a\beta} Z_{a\beta}^2$
(d)			$\sum_{a\beta\gamma\delta} Z_{a\beta} Z_{\beta\gamma} Z_{\gamma\delta}$	$(-1)^4$	$\frac{1}{2}$	1	$\frac{1}{2} \sum_{a\beta\gamma\delta} Z_{a\beta} Z_{\beta\gamma} Z_{\gamma\delta}$
(e)			$\sum_{a\beta\gamma\delta} Z_{\beta a} Z_{\gamma a} Z_{\delta a}$	$(-1)^3 (-2)$	$\frac{1}{6}$	1	$\frac{1}{3} \sum_{a\beta\gamma\delta} Z_{\beta a} Z_{\gamma a} Z_{\delta a}$
(f)			$\sum_{a\beta\gamma} Z_{a\beta} Z_{\beta\gamma} Z_{\gamma a}$	$(-1)^3$	$\frac{1}{6}$	1	$-\frac{1}{6} \sum_{a\beta\gamma} Z_{a\beta} Z_{\beta\gamma} Z_{\gamma a}$
(g)			$\sum_{a\beta\gamma} Z_{a\beta}^2 Z_{\beta\gamma}$	$(-1)^2 (-2)$	1	$\frac{1}{2}$	$-\sum_{a\beta\gamma} Z_{a\beta}^2 Z_{\beta\gamma}$
(h)			$\sum_{a\beta} Z_{a\beta}^3$	$(-2)^2$	$\frac{1}{2}$	$\frac{1}{6}$	$\frac{1}{3} \sum_{a\beta} Z_{a\beta}^3$

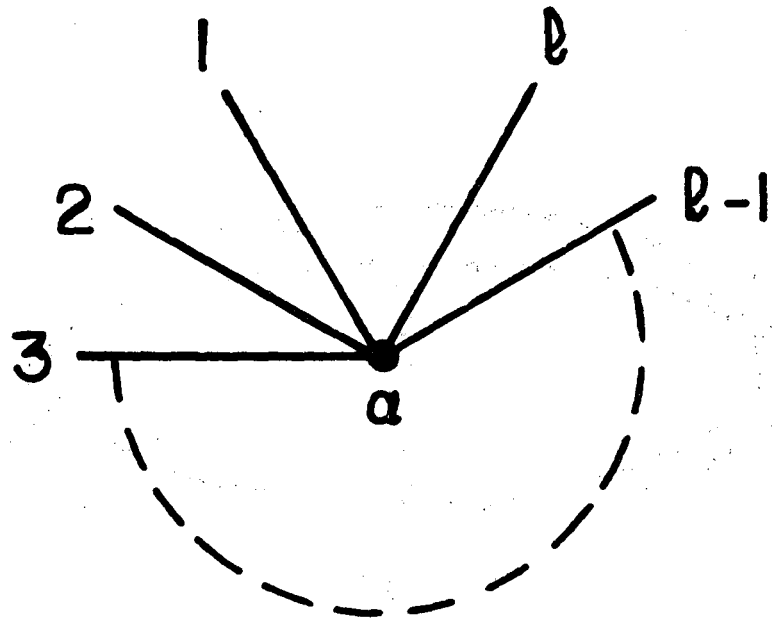
XBL 796-1723

Figure 12



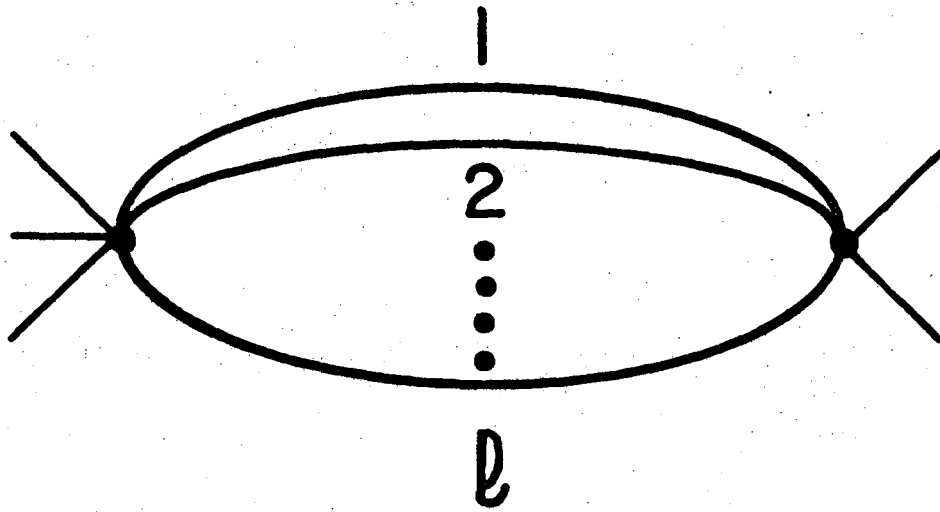
XBL 796 - 1923

Figure 13



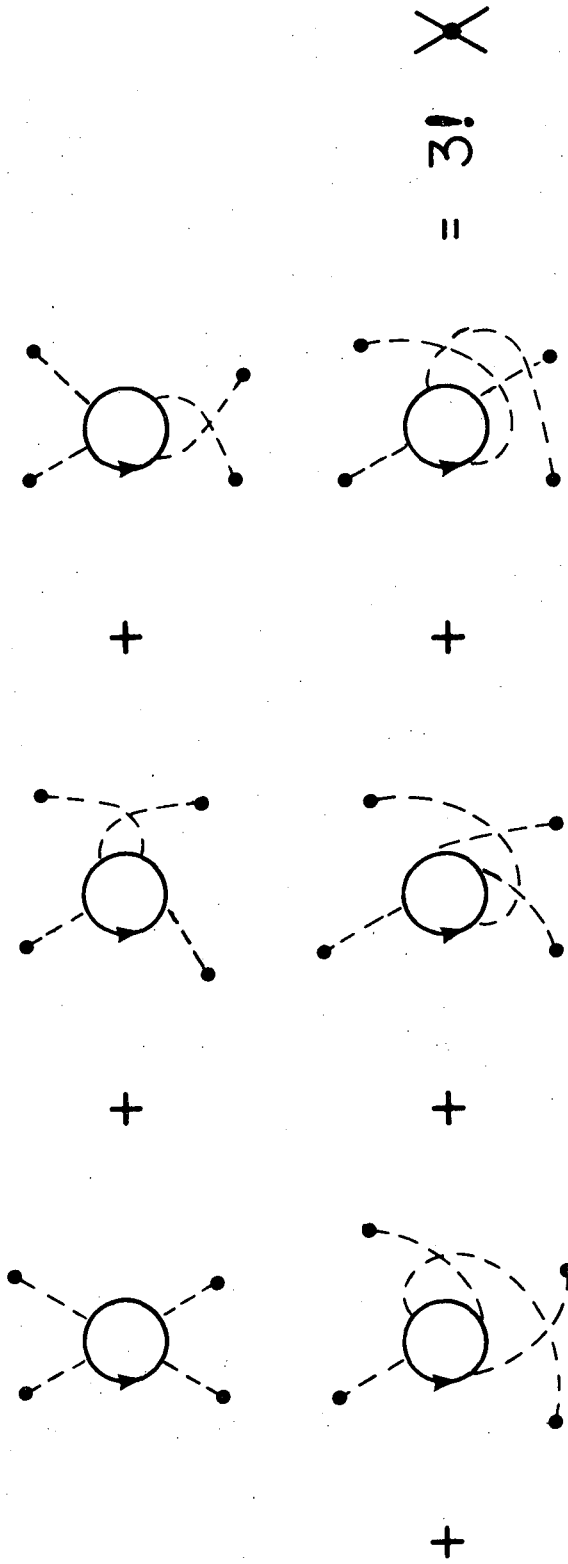
XBL 796 - 1924

Figure 14



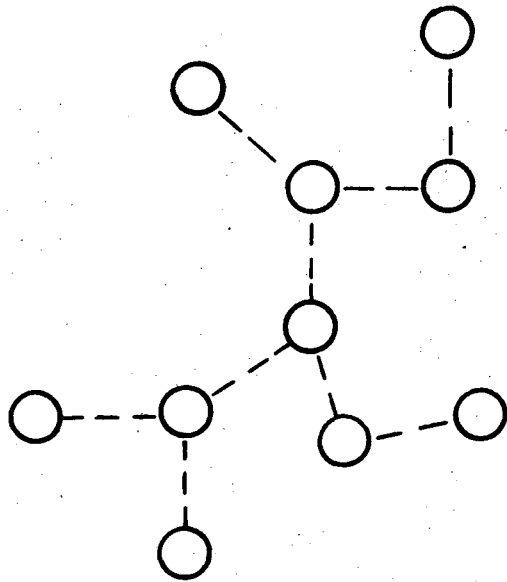
XBL 796 - 1925

Figure 15



XBL 796-1718

Figure 16



XBL 796-1717

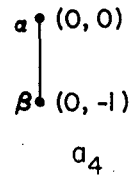
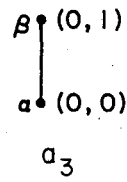
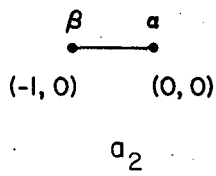
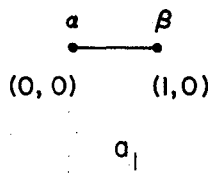
Figure 17

	Graph	(c) Vertex attaching factor	(d) Point symmetry factor	(e) Line symmetry factor	Graph	(c) Vertex attaching factor	(d) Point symmetry factor	(e) Line symmetry factor
1		1	$\frac{1}{2}$	$\frac{1}{2!}$	22	-2! 2!	$\frac{1}{2}$	$\frac{1}{2!}$
2		-1	$\frac{1}{6}$	1	23	-3!	$\frac{1}{8}$	1
3		2! 2!	$\frac{1}{2}$	$\frac{1}{3!}$	24	-2! 2!	$\frac{1}{2}$	$\frac{1}{2!} \frac{1}{2!}$
4		-2! 2!	$\frac{1}{2}$	$\frac{1}{2!}$	25	3! 3!	$\frac{1}{2}$	$\frac{1}{3!}$
5		-3!	$\frac{1}{2}$	$\frac{1}{2!} \frac{1}{2!}$	26	2! 2! 3!	1	$\frac{1}{2!}$
6		1	$\frac{1}{8}$	1	27	2! 2! 3!	$\frac{1}{2}$	$\frac{1}{2!} \frac{1}{2!}$
7		3! 3!	$\frac{1}{2}$	$\frac{1}{4!}$	28	2! 2! 2! 2!	$\frac{1}{4}$	$\frac{1}{2!} \frac{1}{2!}$
8		-1	$\frac{1}{10}$	1	29	3! 3!	$\frac{1}{4}$	$\frac{1}{2!}$
9		-2! 2! 3!	$\frac{1}{2}$	$\frac{1}{2!} \frac{1}{2!}$	30	2! 2! 2! 2!	$\frac{1}{24}$	1
10		-3! 3!	$\frac{1}{2}$	$\frac{1}{3!}$	31	2! 4!	$\frac{1}{2}$	$\frac{1}{3!}$
11		3!	$\frac{1}{2}$	$\frac{1}{2!}$	32	2! 2! 3!	$\frac{1}{2}$	$\frac{1}{2!} \frac{1}{2!}$
12		2! 2!	$\frac{1}{4}$	1	33	2! 4!	1	$\frac{1}{2!} \frac{1}{2!}$
13		2! 2!	$\frac{1}{2}$	$\frac{1}{2!}$	34	3! 3!	$\frac{1}{2}$	$\frac{1}{2!} \frac{1}{2!} \frac{1}{2!}$
14		2! 2!	$\frac{1}{2}$	$\frac{1}{2!} \frac{1}{2!}$	35	2! 2! 3!	1	$\frac{1}{2!} \frac{1}{3!}$
15		4! 4!	$\frac{1}{2}$	$\frac{1}{5!}$	36	5!	$\frac{1}{6}$	$\frac{1}{2!} \frac{1}{2!} \frac{1}{2!}$
16		-2! 4!	1	$\frac{1}{2!} \frac{1}{3!}$	37	-4! 4!	$\frac{1}{2}$	$\frac{1}{4!}$
17		1	$\frac{1}{12}$	1	38	-2! 3! 4!	1	$\frac{1}{2!} \frac{1}{3!}$
18		-2! 2!	$\frac{1}{2}$	$\frac{1}{2!}$	39	-3! 3! 3!	$\frac{1}{6}$	$\frac{1}{2!} \frac{1}{2!} \frac{1}{2!}$
19		-2! 2!	$\frac{1}{2}$	1	40	-3! 5!	1	$\frac{1}{2!} \frac{1}{4!}$
20		-3!	$\frac{1}{2}$	$\frac{1}{2!}$	41	-2! 2! 5!	$\frac{1}{2}$	$\frac{1}{3!} \frac{1}{3!}$
21		-2! 2!	$\frac{1}{12}$	1	42	5! 5!	$\frac{1}{2}$	$\frac{1}{6!}$

XBL 796-1722

Figure 18

(a)



(b)

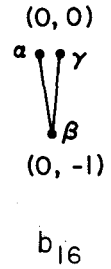
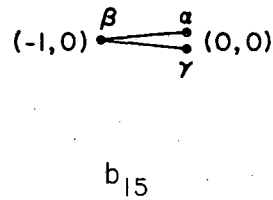
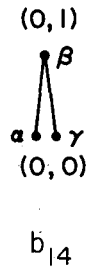
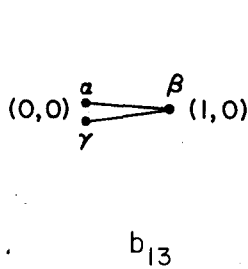
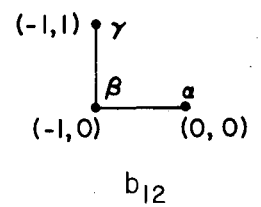
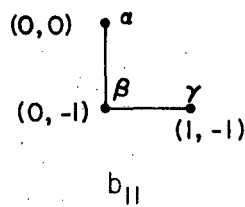
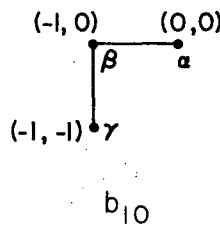
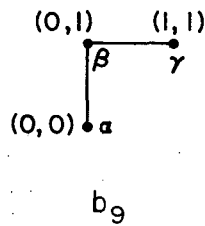
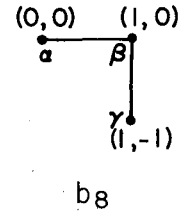
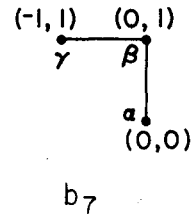
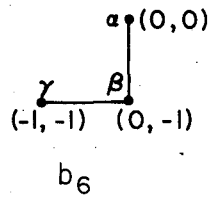
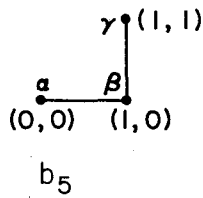
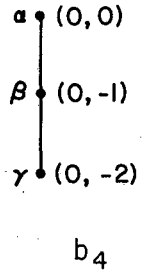
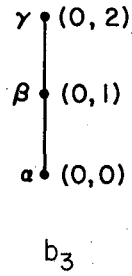
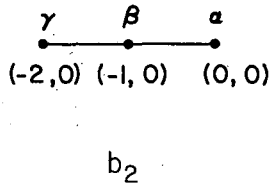
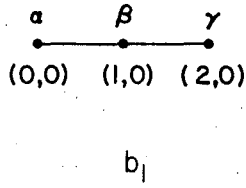
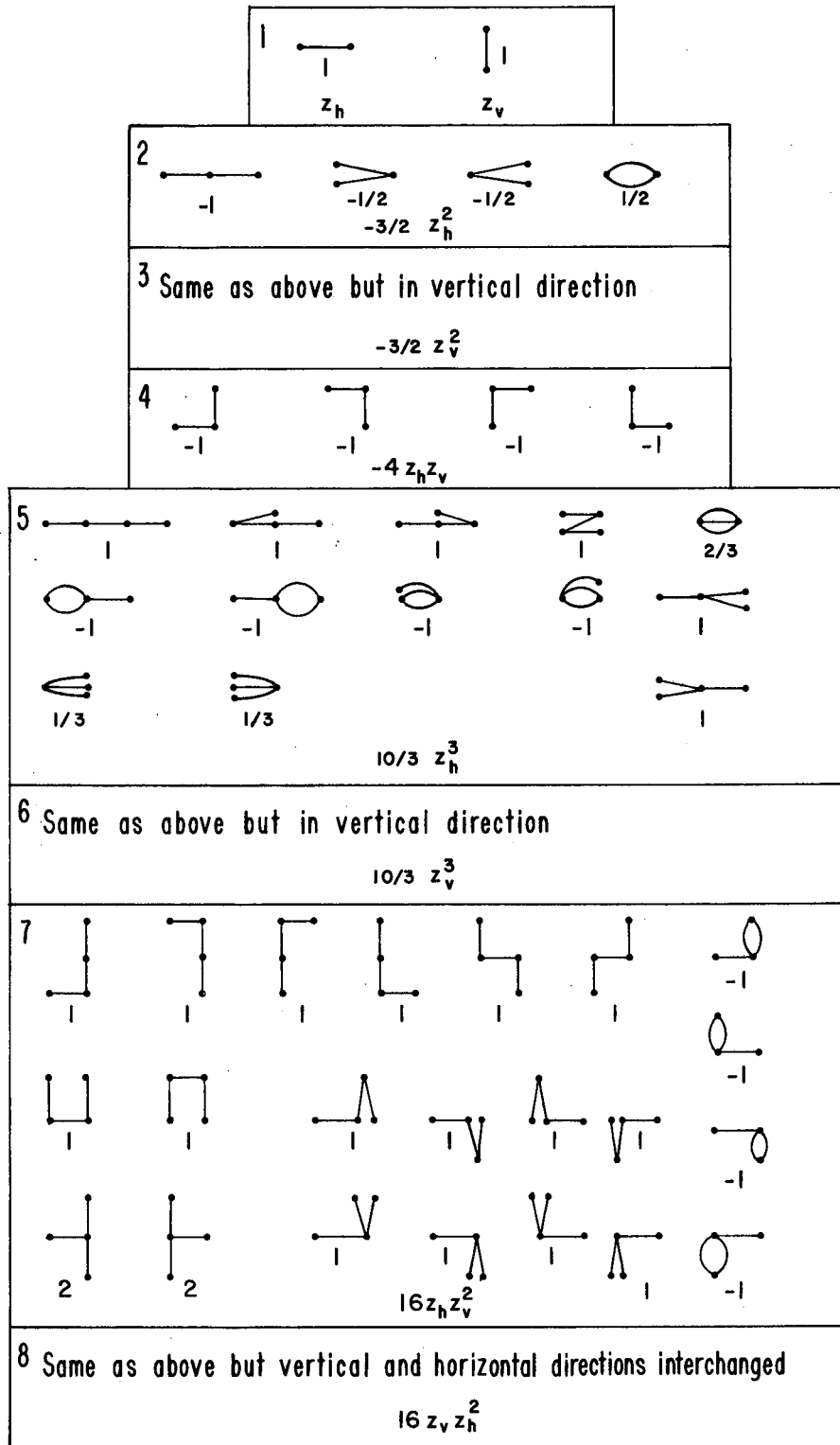
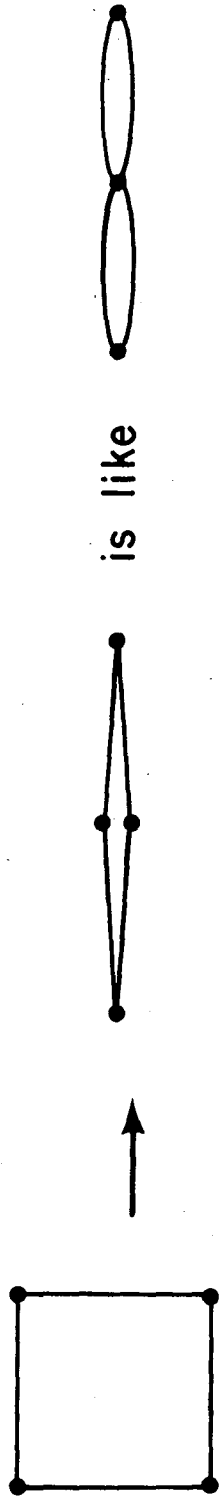


Figure 19



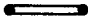



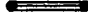
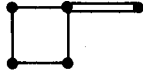






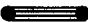








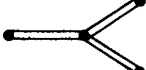







XBL 797-1947

Figure 20



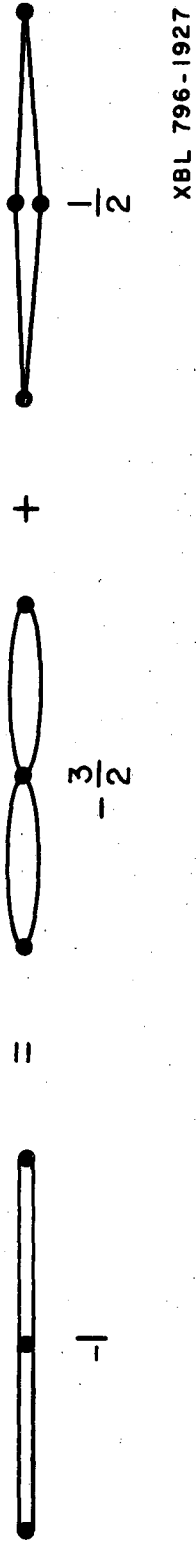
XBL 796-1926

Figure 21

1		$\frac{1}{2}$	16		-1
2		-1	17		1
3		$\frac{2}{3}$	20		-2
4		-2	21		-4
5		-1	24		-1
6		1	25		1
7		$\frac{1}{4}$	27		3
8		-1	28		4
9		-3	34		2
10		-1	35		1
11		2	36		2
12		4	40		0
13		2	41		-1
14		1	42		$-\frac{1}{3}$
15		$-\frac{1}{5}$			

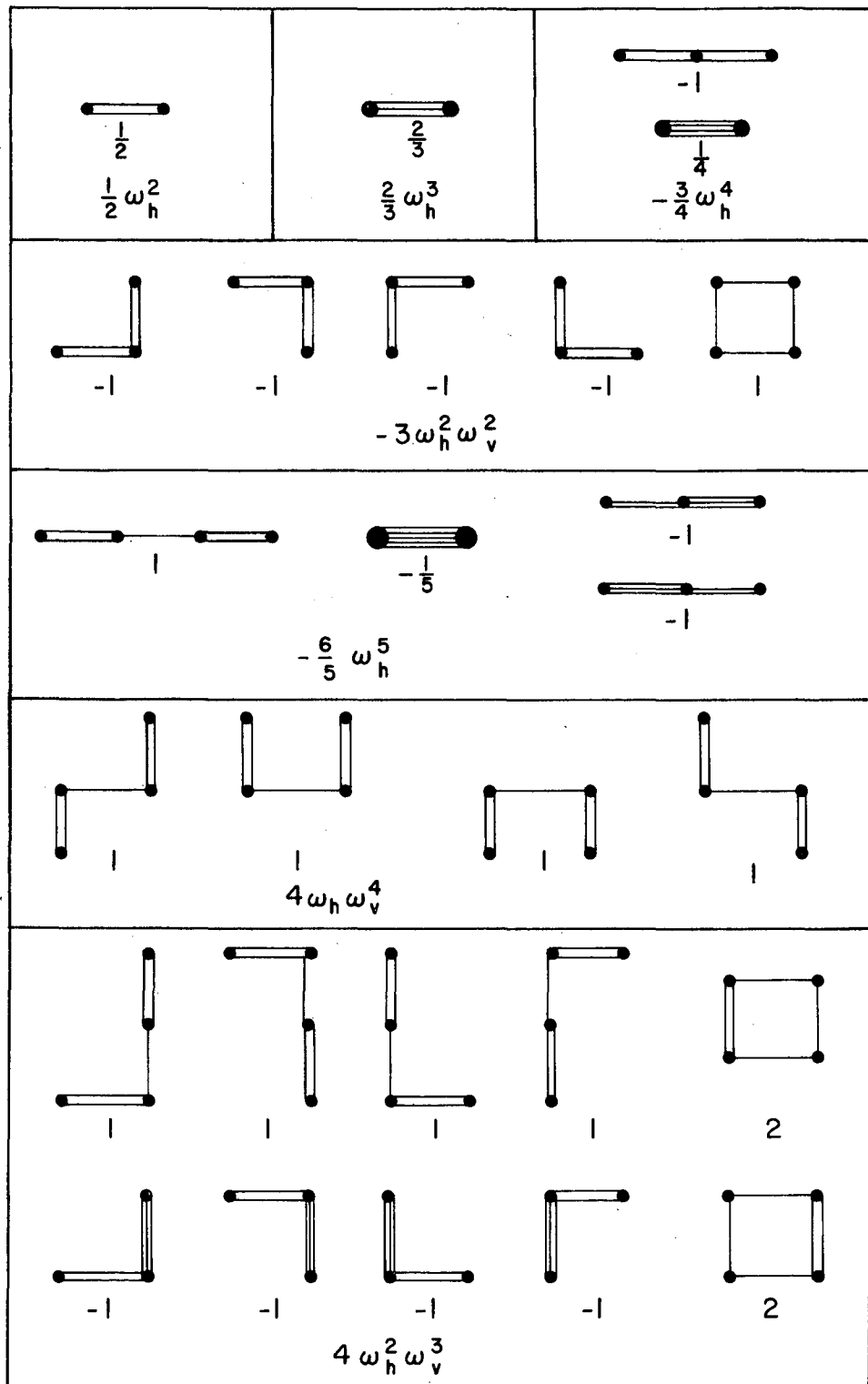
XBL 797-1960

Figure 22



XBL 796-1927

Figure 23



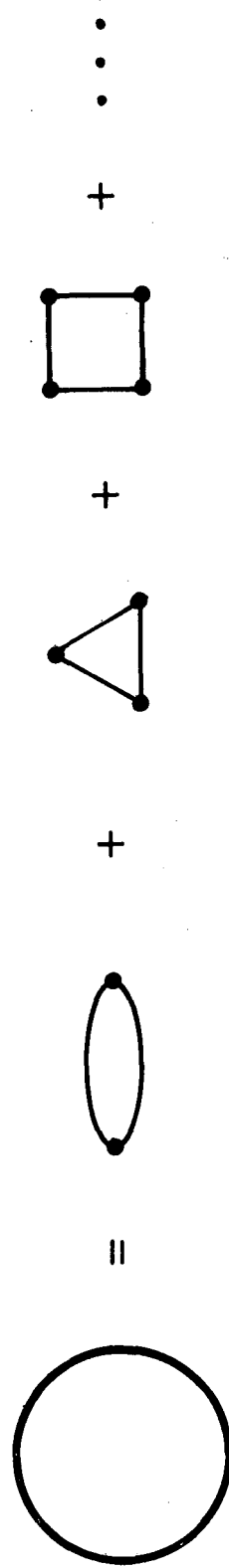
XBL 797-1946

Figure 24

$$\begin{array}{c} \bullet \\ \hline \bullet \end{array} \begin{array}{c} a' \\ \hline a \end{array} = \begin{array}{c} \bullet \\ \hline \bullet \end{array} \begin{array}{c} a' \\ \hline a \end{array} + \begin{array}{c} \bullet \\ \hline \bullet \end{array} \begin{array}{c} \beta \\ \hline \alpha \end{array} \begin{array}{c} a' \\ \hline a \end{array} + \begin{array}{c} \bullet \\ \hline \bullet \end{array} \begin{array}{c} \beta \\ \hline \alpha \end{array} \begin{array}{c} \gamma \\ \hline a \end{array} \begin{array}{c} a' \\ \hline a \end{array} + \dots$$

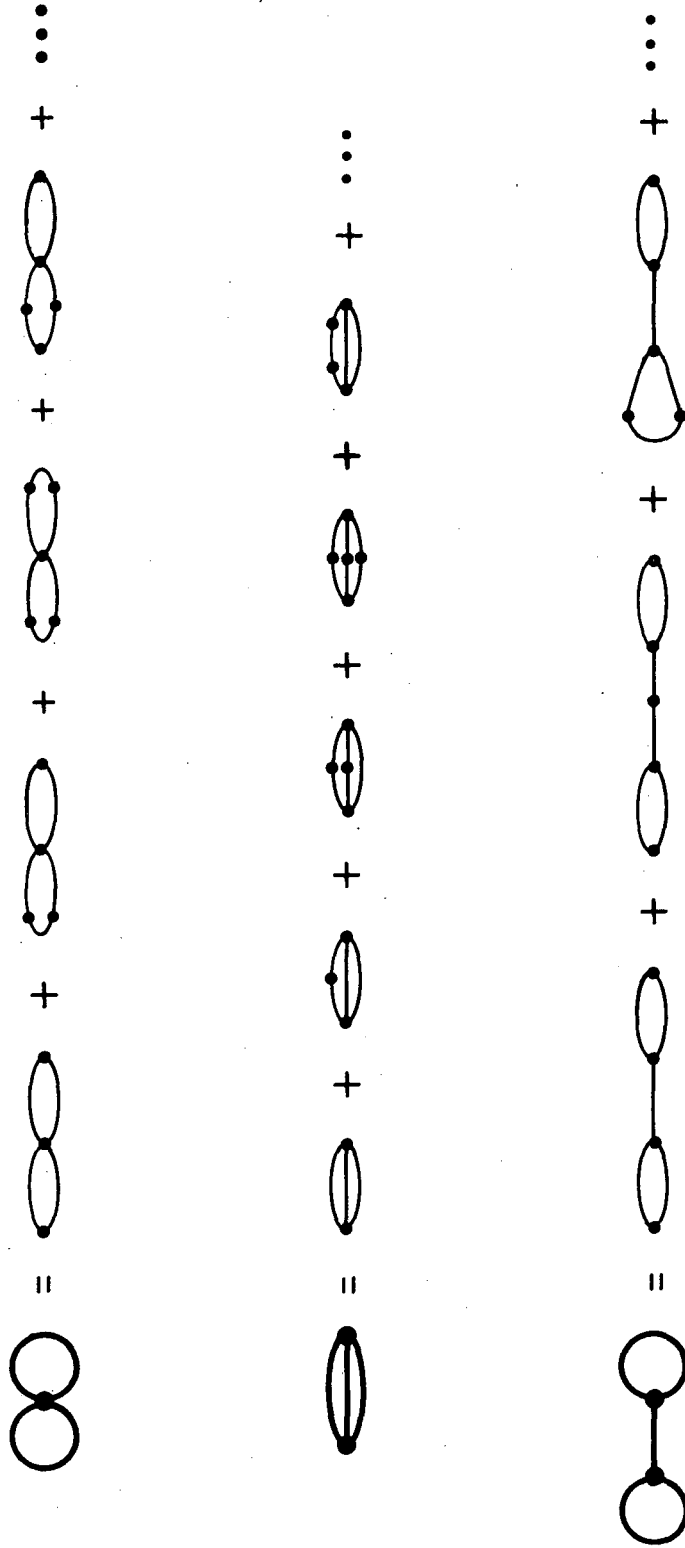
XBL 797-1941

Figure 25



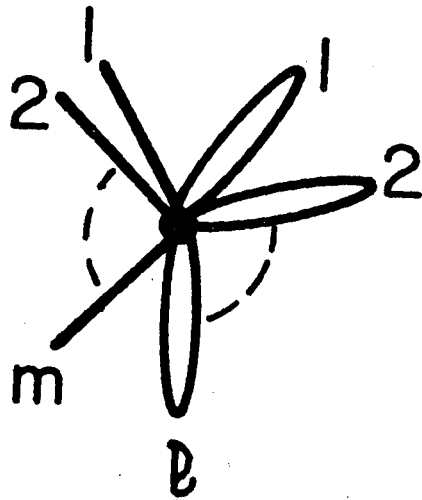
XBL 796 - 1928

Figure 26



XBL 797-1956

Figure 27



XBL 796-1934

Figure 28

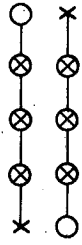
exp (X → O + O → X)

(a)

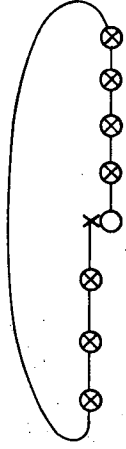
and



(b)



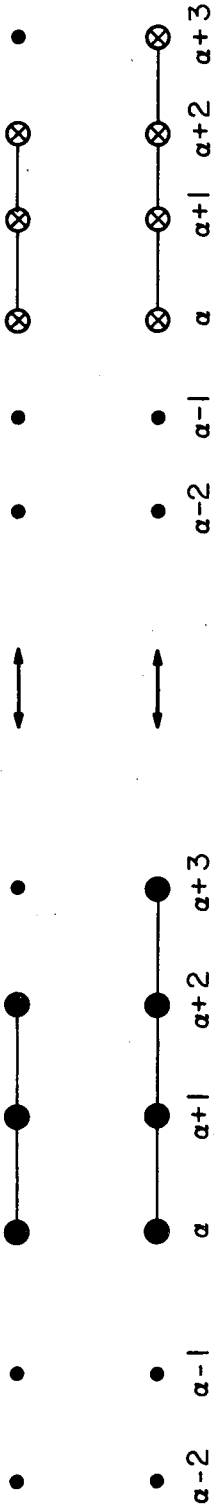
(c)



(d)

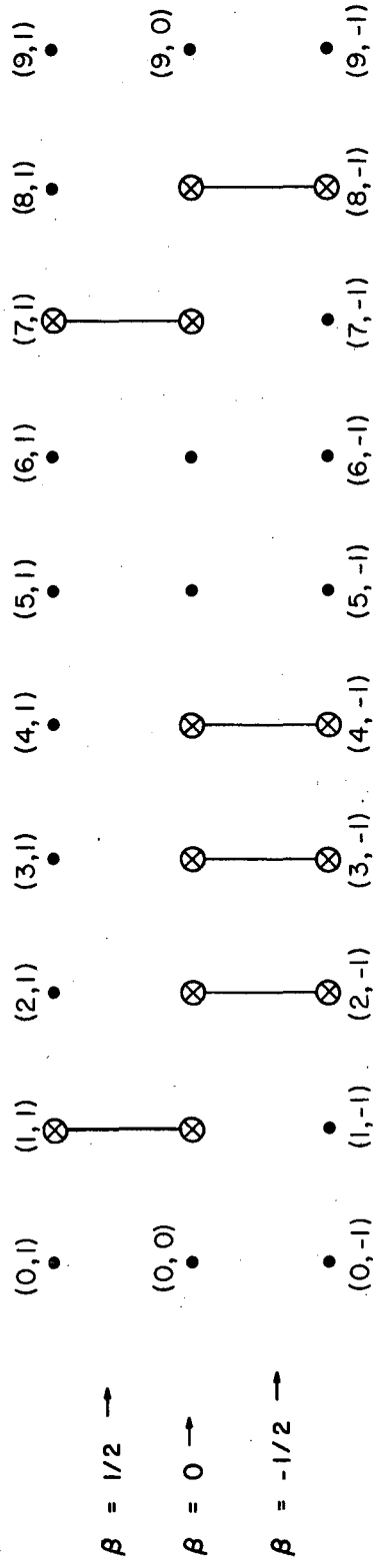
XBL 797-1945

Figure 29



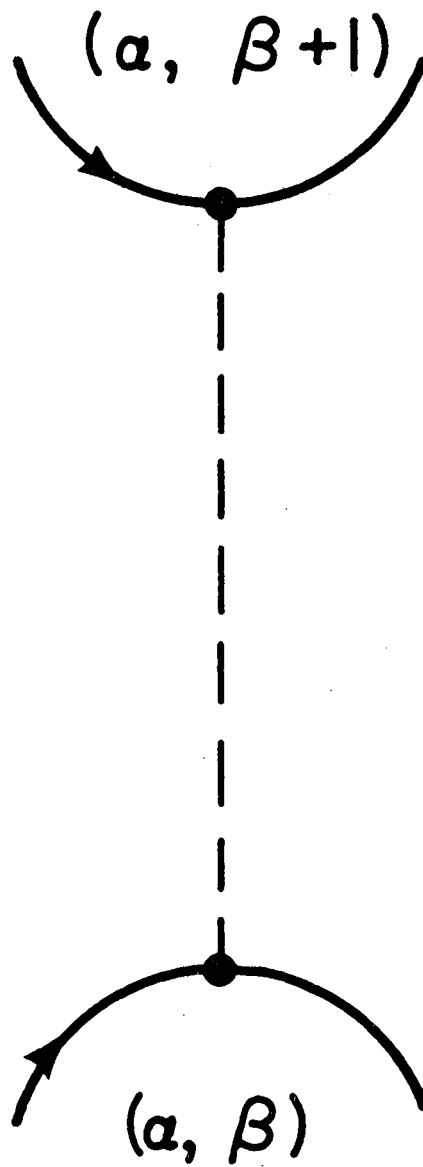
XBL 797-1944

Figure 30



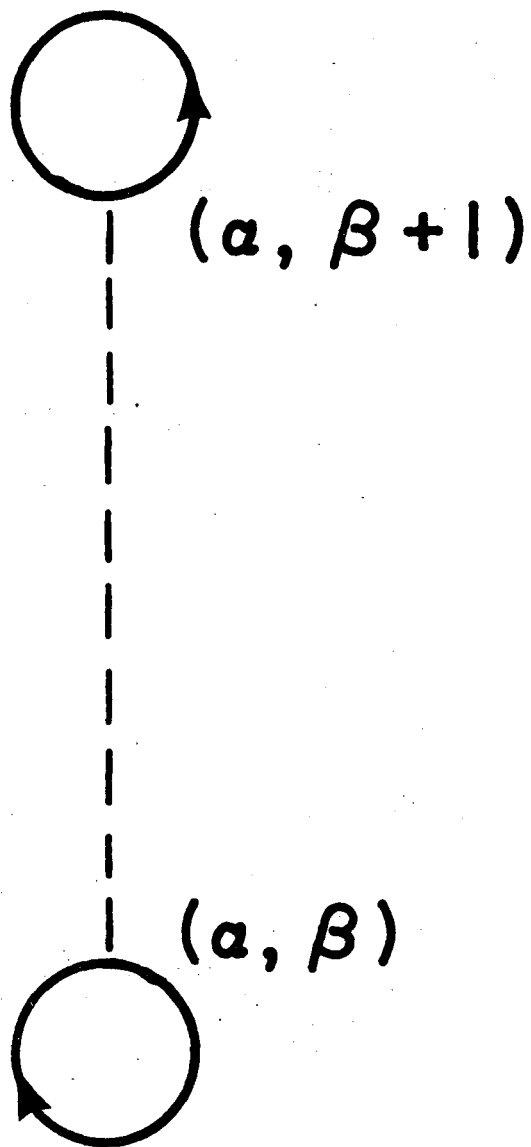
XBL 797-1943

Figure 31



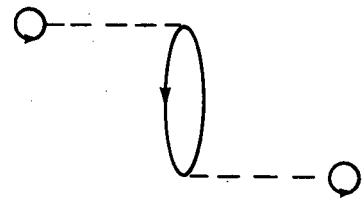
XBL 796-1929

Figure 32

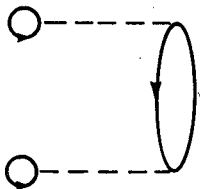


XBL 796-1932

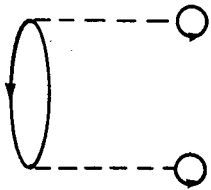
Figure 33



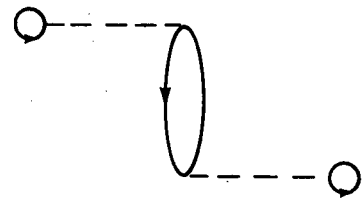
(a)



(b)



(c)



(d)

XBL 797-1940

Figure 34

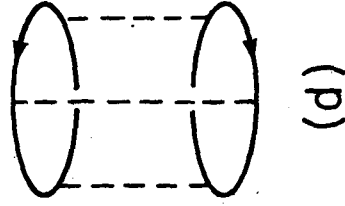
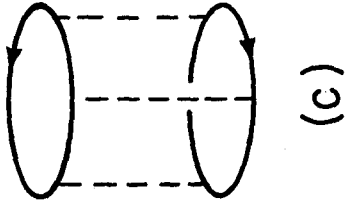
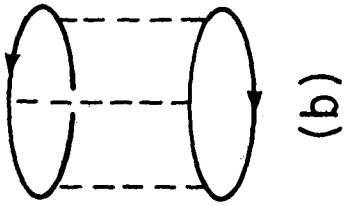
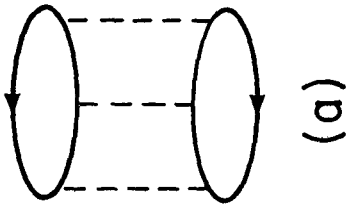
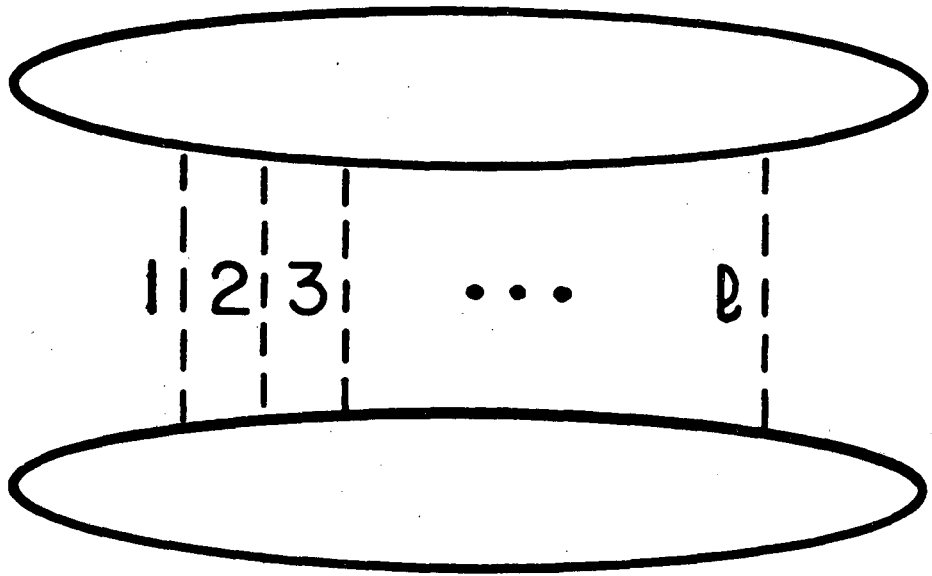


Figure 35

XBL 796 - 1936



XBL 796-1933

Figure 36

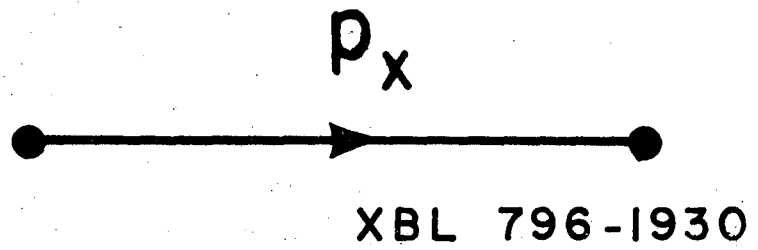
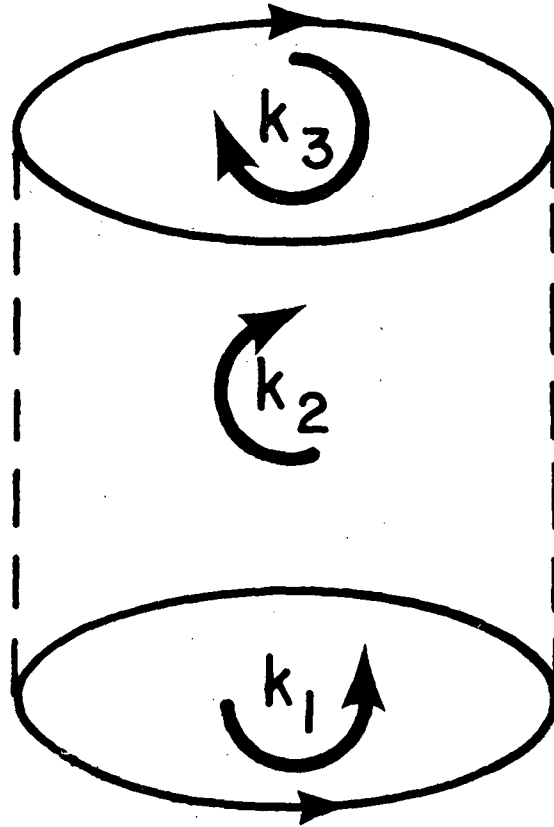
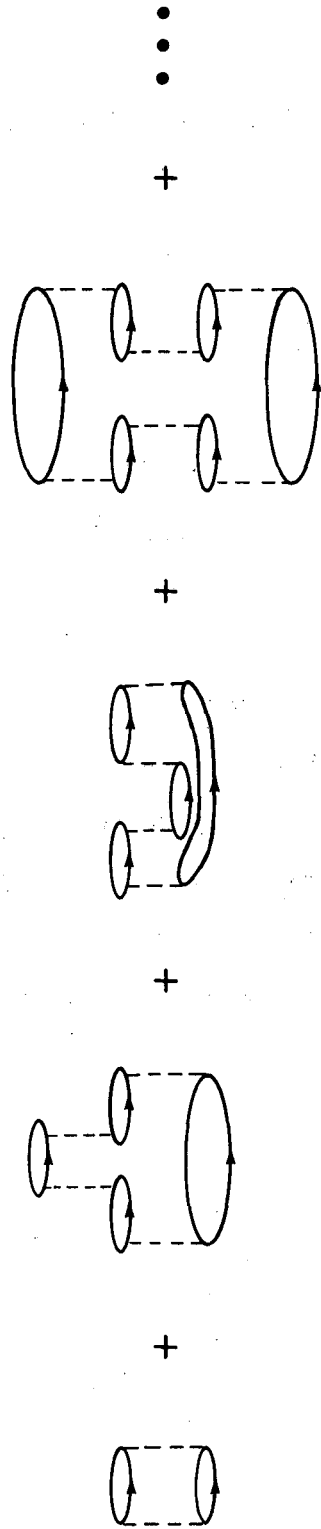


Figure 37



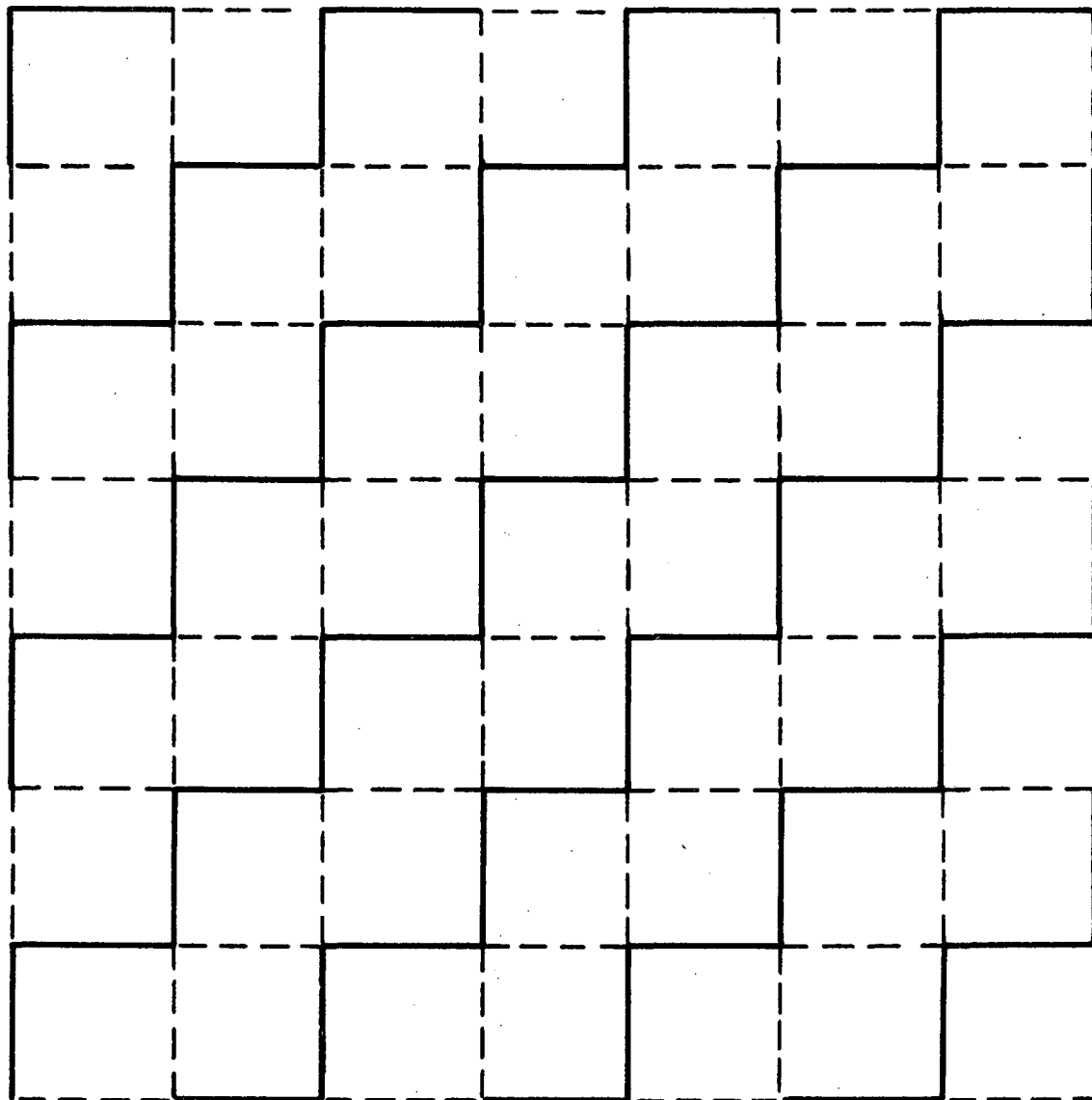
XBL 797-1938

Figure 38



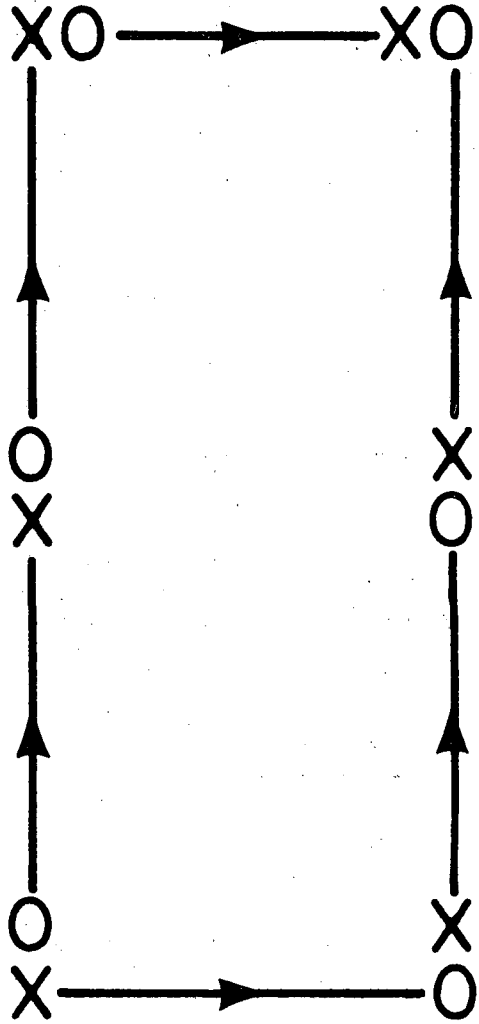
XBL 797-1939

Figure 39



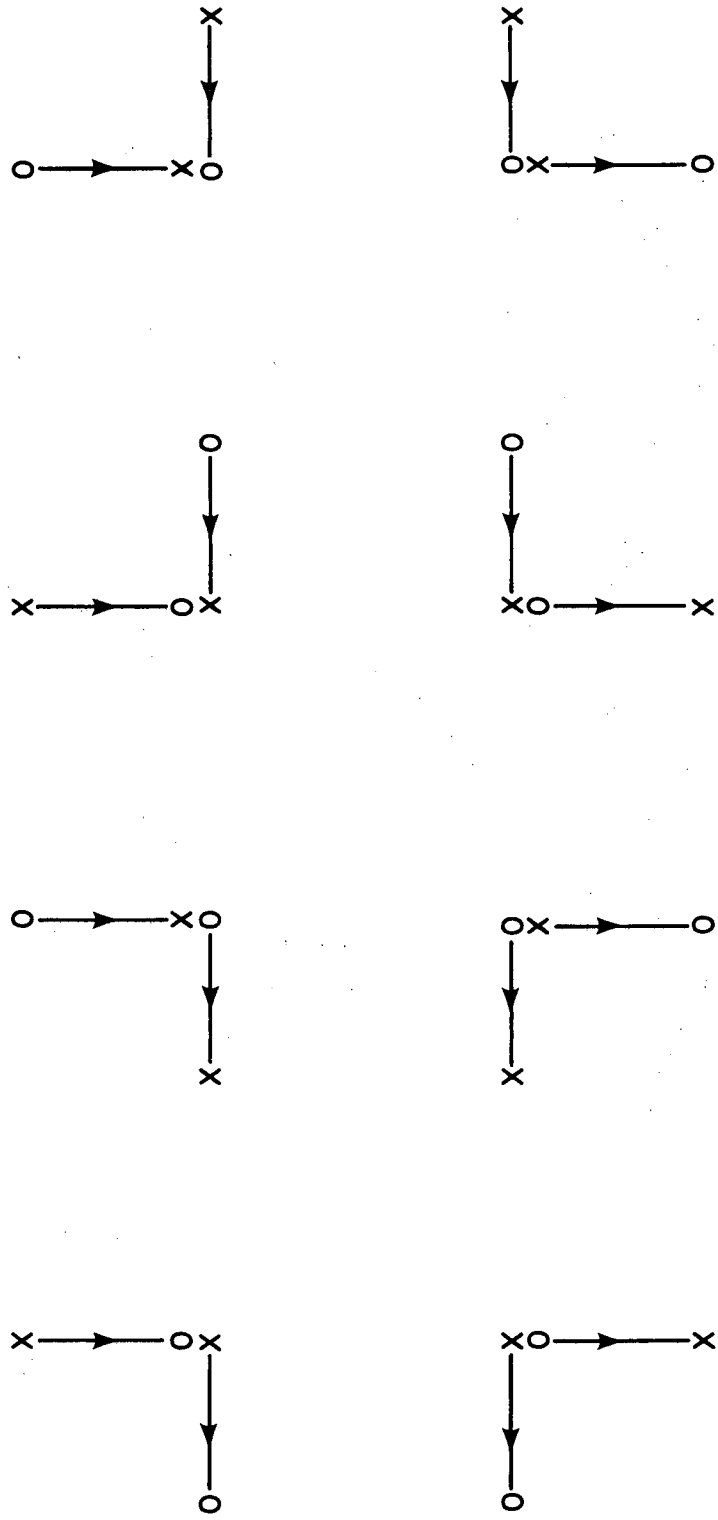
XBL 796-1935

Figure 40



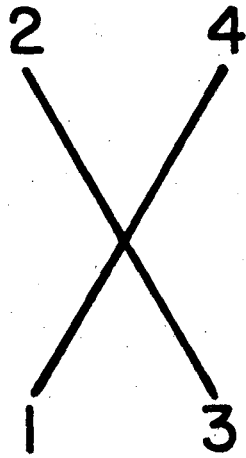
XBL 796 -1931

Figure 41

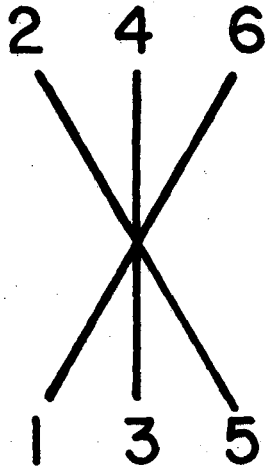
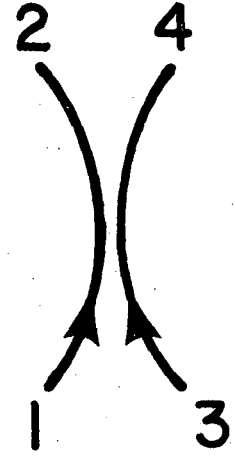


XBL 797-1937

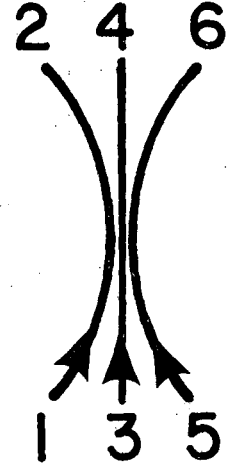
Figure 42



~

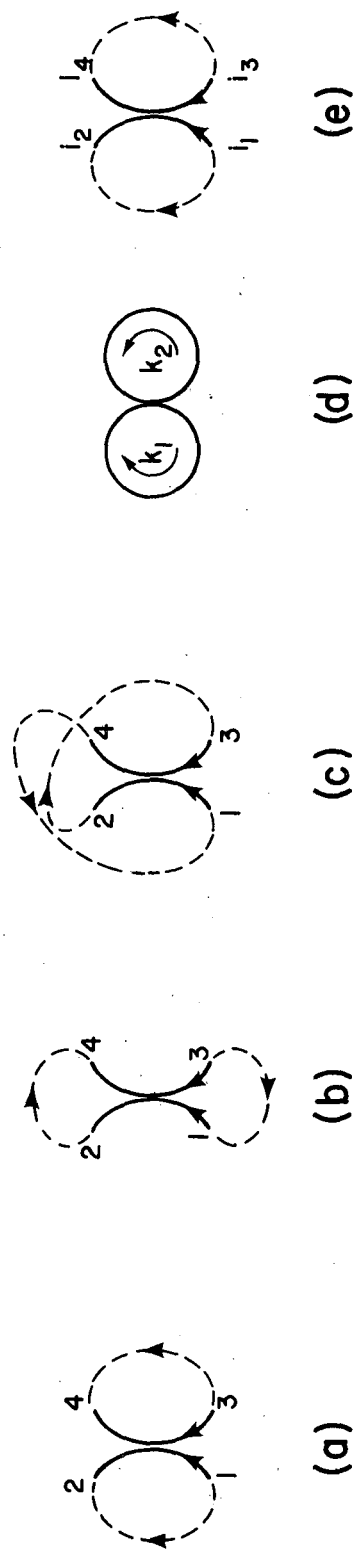


~



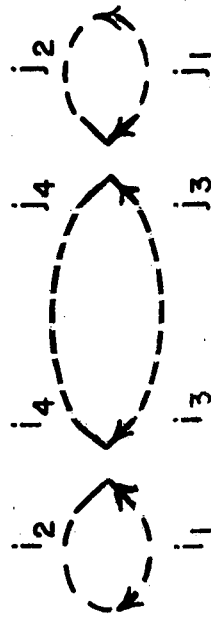
XBL 797-1957

Figure 43



XBL 797-1956A

Figure 44



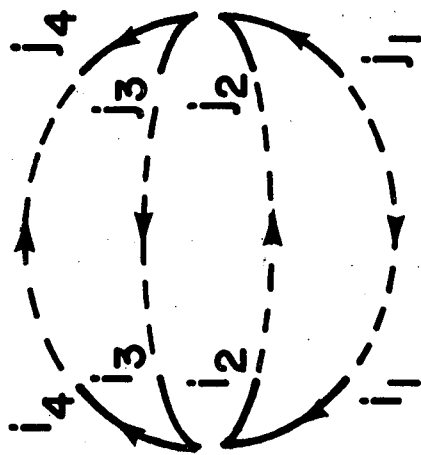
(a)



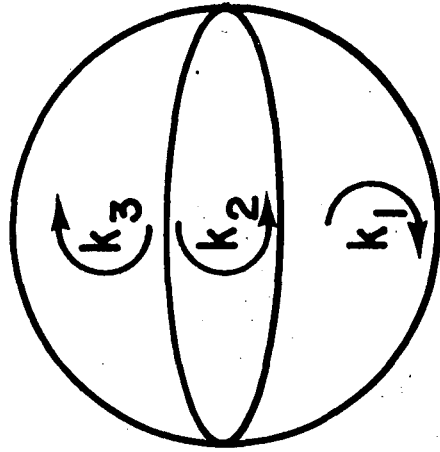
(b)

XBL 797 - 1960A

Figure 45



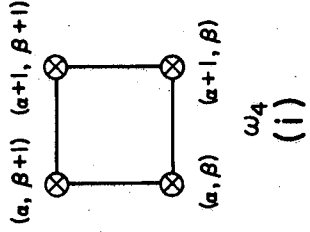
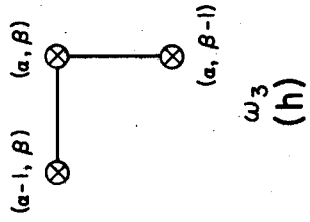
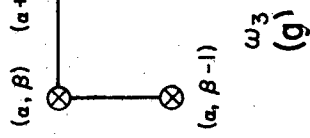
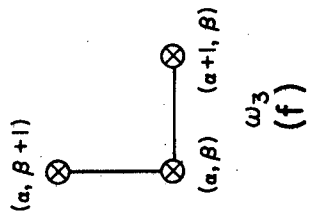
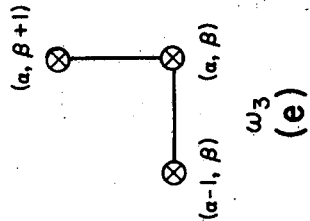
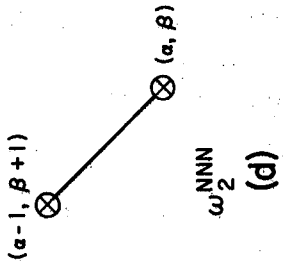
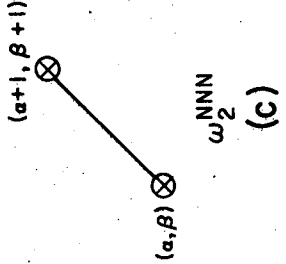
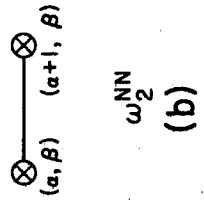
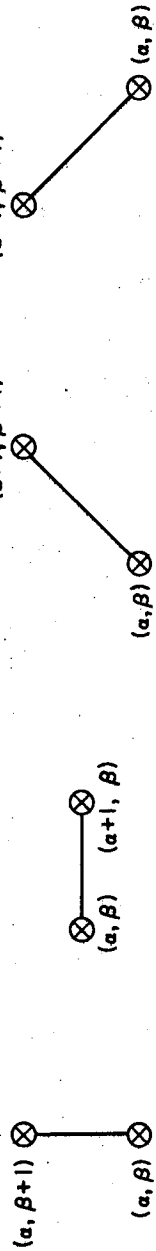
(a)



(b)

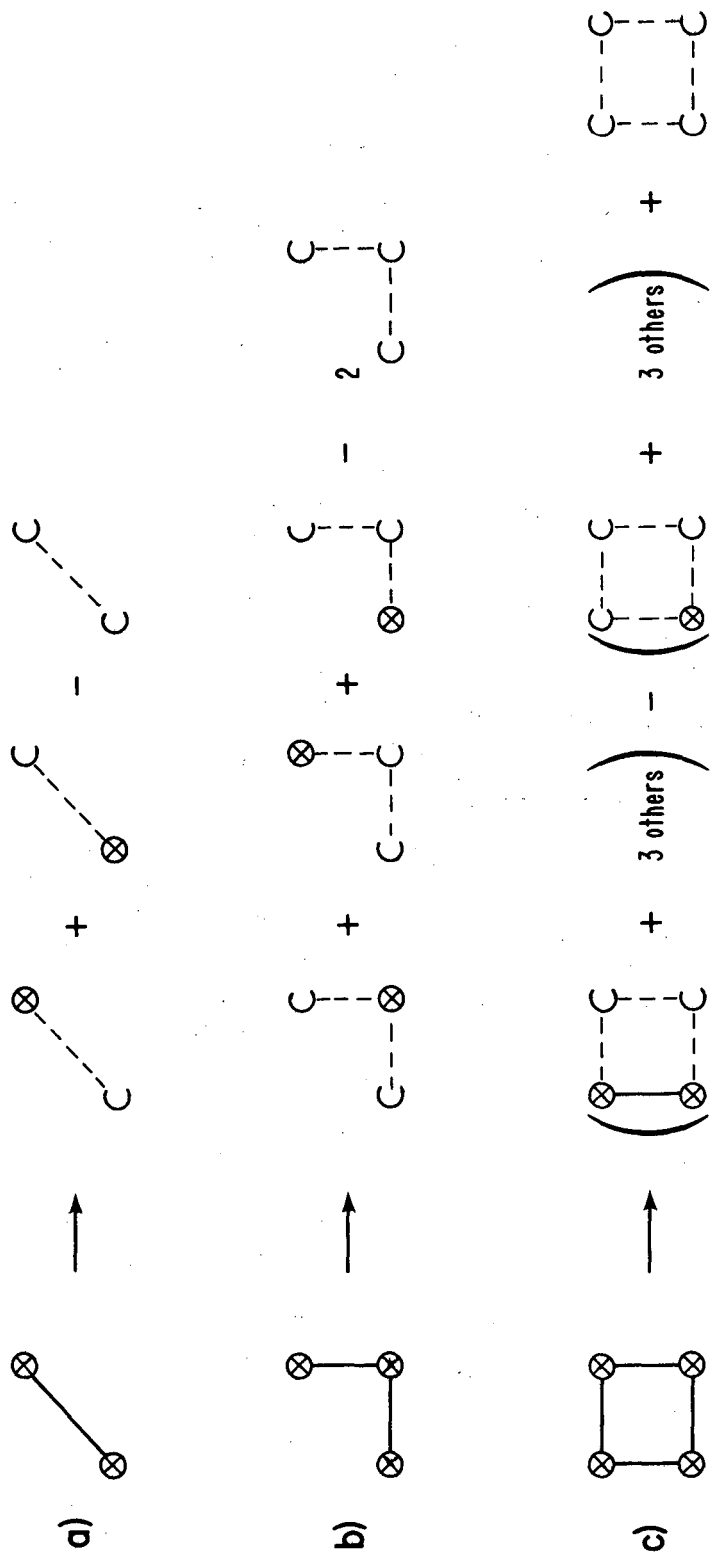
Figure 46

XBL 797-1942



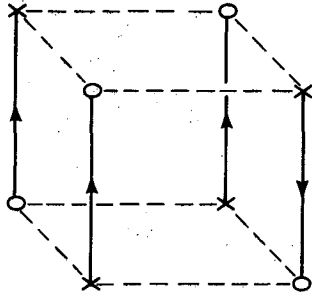
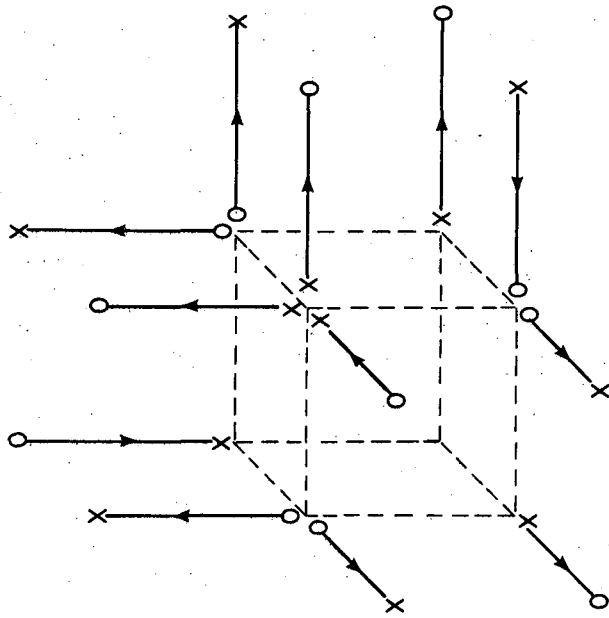
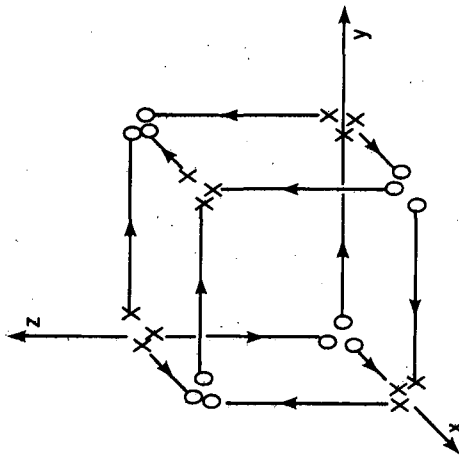
XBL 797-1959

Figure 47



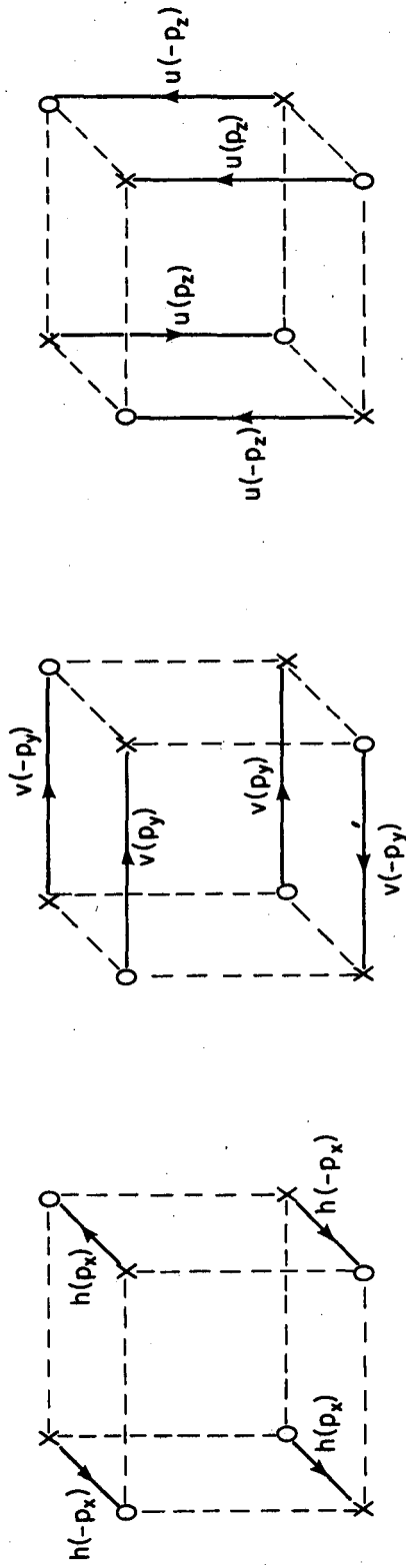
XBL 797-1958

Figure 48



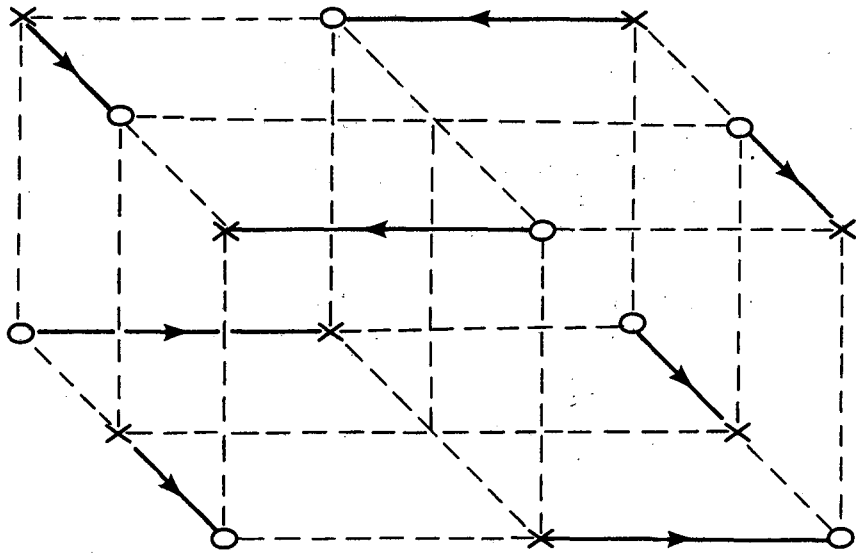
XBL 797-1955A

Figure 49

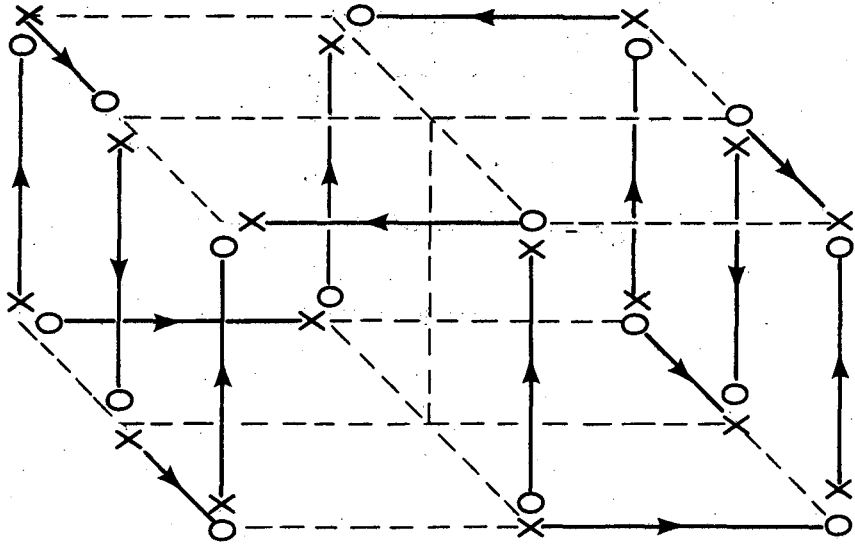


XBL 797-1953

Figure 50



(a)



(b)

XBL 797-1952

Figure 51

This report was done with support from the Department of Energy. Any conclusions or opinions expressed in this report represent solely those of the author(s) and not necessarily those of The Regents of the University of California, the Lawrence Berkeley Laboratory or the Department of Energy.

Reference to a company or product name does not imply approval or recommendation of the product by the University of California or the U.S. Department of Energy to the exclusion of others that may be suitable.

TECHNICAL INFORMATION DEPARTMENT
LAWRENCE BERKELEY LABORATORY
UNIVERSITY OF CALIFORNIA
BERKELEY, CALIFORNIA 94720